UNIVERSITY OF CALIFORNIA, SAN DIEGO

Synthesis and Applications of Quinazoline-Based Fluorescent Nucleoside Analogues

A dissertation submitted in partial satisfaction of the requirements for the degree Doctor of Philosophy

in

Chemistry

by

Yun Xie

Committee in Charge:

Professor Yitzhak Tor, Chair
Professor Michael Burkart
Professor Jeffery Esko
Professor Thomas Hermann
Professor William Trogler

2010

The Dissertation of Yun Xie is approved, and it is acceptable in quality and form for publication on microfilm and electronically:

_____

_____

_____

_____

_____
Chair

University of California, San Diego

2010

DEDICATION

For my parents, Yimei Li and Yichun Xie,

and Eric Watt.

TABLE OF CONTENTS

LIST OF FIGURES

LIST OF SCHEMES

LIST OF TABLES

ACKNOWLEDGEMENTS

I would like to acknowledge Professor Yitzhak Tor for providing an excellent educational experience in his lab. With the rare combination of an unerring editorial eye and remarkable patience, he has taught me to pursue research both thoughtfully and critically. I learned that hard work and perseverance are truly the keys to success.

I would also like to acknowledge Professor Thomas Hermann for discussions related to RNA–ligand interactions and binding studies. His clear instructions have saved me many hours of needless work.

I would like to acknowledge Dr. Seergazhi G. Srivatsan, Dr. Nicholas Greco and Dr. Victor Tam for showing me the way when I first began my PhD studies. In addition, I acknowledge Mary Noé, Andro Rios, Andrew Dix and Tucker Maxson for intellectual discussions that greatly enhanced my education. Finally, I thank Andrew Dix and Tucker Maxson for helping me complete projects with greater expediency.

The introduction contains sections of text and figures that are reprinted from: Xie, Y.; Tam, V. K.; Tor, Y. In *The Chemical Biology of Nucleic Acids*; G, M., Ed.; John Wiley & Sons, Ltd: Chichester, UK, 2010. The dissertation author is the main author and researcher for this work.

Chapter 1 is in full a reprint from: Xie, Y.; Dix, A. V.; Tor, Y. *J. Am. Chem. Soc.* **2010**, *131*, 17605–17614. The dissertation author is the main author and researcher for this work.

Chapter 2 is in full a reprint of: Xie, Y.; Dix, A. V.; Tor, Y. *Chem. Commun*. **2010**, *64*, 5542–5544. The dissertation author is the main author and researcher for this work.

Chapter 3 is in full a reprint of: Xie, Y.; Maxson, T.; Tor, Y. Fluorescent ribonucleoside as a FRET acceptor for tryptophan in native proteins. *J. Am. Chem. Soc.* **2010**, In Press. The dissertation author is the main author and researcher for this work.

Chapter 4 is in full a reprint of: Xie, Y.; Maxson, T.; Tor, Y. Fluorescent nucleoside analogue displays enhanced emission upon pairing with guanine. Submitted. The dissertation author is the main author and researcher for this work.

Chapter 5 contains sections from: Xie, Y.; Tor, Y. Synthesis and Applications of Quinazoline-Based Fluorescent Nucleoside Analogues. In Preparation. The dissertation author is the main author and researcher for this work.

VITA

2003–2005	Teaching Assistant, University of Michigan, Ann Arbor
2005	Bachelor of Science, University of Michigan, Ann Arbor
2005–2007	Teaching Assistant, University of California, San Diego
2008–Present	Science Writer, Ars Technica
2010	Doctor of Philosophy, University of California, San Diego

PUBLICATIONS

Xie, Y.; Tam, V. K.; Tor, Y. In *The Chemical Biology of Nucleic Acids*; G, M., Ed.; John Wiley & Sons, Ltd: Chichester, UK, 2010.

Xie, Y.; Dix, A. V.; Tor, Y. *J. Am. Chem. Soc.* **2009**, *131*, 17605–17614.

Xie, Y.; Dix, A. V.; Tor, Y. *Chem. Commun*. **2010**, *64*, 5542–5544.

Xie, Y.; Maxson, T.; Tor, Y. *J. Am. Chem. Soc.* **2010**, In Press.

Xie, Y.; Maxson, T.; Tor, Y. Fluorescent nucleoside analogue displays enhanced emission upon pairing with guanine, Submitted.

Xie, Y.; Tor, Y. Synthesis and Applications of Quinazoline-Based Fluorescent Nucleoside Analogues, In Preparation.

Tor, Y. & Xie, Y. *New fluorescent nucleosides for real-time exploration of nucleic acids.* SPIE Newsroom: Biomedical Optics & Medical Imaging, 2009.

McCoy, L., Xie, Y. & Tor, Y. WIREs RNA, **2010**, In Press.

ABSTRACT OF THE DISSERTATION

Synthesis and Applications of Quinazoline-Based Fluorescent Nucleoside Analogues

by

Yun Xie

Doctor of Philosophy

University of California, San Diego, 2010

Professor Yitzhak Tor, Chair

A family of quinazoline-based fluorescent nucleoside analogues is synthesized for photophysical studies and applications in probing nucleic acid structure, dynamics, and recognition. These size-expanded U analogues exhibit fluorescent emission wavelengths that span 155 nm, from 335 to 490 nm. Each nucleoside has unique characteristic response to changes in its microenvironment. These distinct features lead to a variety of applications in biological assays, many of which have been explored.

The fluorescent nucleoside analogues are useful in Förster Resonance Energy Transfer (FRET) experiments. The 5-methoxyquinazoline-2,4(1*H*,3*H*)-dione based nucleoside acts as the donor fluorophore to commercially available 7-

diethylaminecoumarin. The FRET pair is used in a robust analysis and discovery platform for antibiotics targeting the bacterial ribosomal RNA A-site. The emissive U surrogate is incorporated into a model RNA construct of the A-site and the aminoglycosides are labeled with the 7-diethylaminecoumarin fluorescence acceptor. Titrating the coumarin labeled aminoglycosides into the emissive A-site construct shows a decrease in donor emission and concurrent increase of the acceptor emission. Titration curves faithfully generate EC_{50} values. Titration of unlabeled ligands into the pre-formed FRET complex yields valuable data regarding competitive displacement of aminoglycosides. Furthermore, an orthogonal FRET assembly reports antibiotic affinities to two different RNA targets. A binder was labeled with a fluorophore that acts both as an acceptor for the emissive nucleoside on the bacterial A-site and a donor fluorophore for the terminally-labeled human A-site. Unlabeled drugs were used to dissociate the labeled antibiotic.

The nucleoside based on 5-aminoquinazoline-2,4(1*H*,3*H*)-dione makes a good FRET acceptor to tryptophan, one of the most infrequently occurring amino acids in proteins. The FRET pair facilitates the study of RNA–protein interactions, which is demonstrated in studying the binding of the Rev peptide to the RRE. Additionally, upon incorporation into a RNA oligonucleotide, 5-aminoquinazoline-2,4(1*H*,3*H*)-dione detects the presence of a RNA bulge by fluorescence enhancement and hypsochromic wavelength shift. In another single fluorophore experiment, the fluorescent U-analogue 7-aminoquinazoline-2,4(1*H*,3*H*)-dione detects mismatch G upon incorporation into a DNA oligonucleotide by displaying G-specific fluorescence enhancement.

INTRODUCTION

Nucleic acids are key factors in the central dogma of biology. DNA, often referred to as the genetic blueprint of life, undergoes transcription to produce RNA, which is involved in translation to manufacture proteins in the ribosome. Besides being crucial components in the flow of biological information, nucleic acids are active in many other processes. RNA, in the form of ribozymes, has catalytic properties that rival the functions of proteins.[1–3] In addition, RNA can form a variety of secondary structures outside of a typical double helix, such as hairpin loops, junctions, and symmetric and asymmetric bulges.[4–7] DNA is also capable of forming complex structures like triplexes and quadruplexes.[8–12] Fluorescence spectroscopy can be a valuable tool for biophysical studies aimed at elucidating the multitude of dynamics, structure, and recognition events involving nucleic acids.[13] However, nucleic acids are weakly emissive with picoseconds scale lifetimes and fluorescence quantum yields of 0.03 %, or less.[14,15] Such features are beneficial for the photochemical stability of our genetic material, but present a challenge for biophysical studies. One answer to this challenge is the development of fluorescent nucleoside analogues that are isomorphic and isosteric to their native counterparts, but are endowed with favorable photophysical properties.[13, 16–18] Fluorescent nucleoside analogues have been used in both single fluorophore and Forster Resonance Energy Transfer techniques to study a variety of biological processes.[13,18] Before delving into the specifics of how fluorescence techniques can be applied to study the dynamics of DNA and RNA, it is important to first understand the basic properties of nucleic acids.

The Structure and Properties of Nucleic Acids

Over the course of evolution, five polarizable, aromatic nucleobases emerged to form the genetic code. These purines (adenine and guanine) and pyrimidines (cytosine, thymine and uracil) contain key molecular recognition information. For example, their aromatic surfaces are conducive to stacking and aromatic interactions, and their exocyclic functional groups are capable of directional H-bonding. In nucleic acids, each nitrogenous heterocyclic base is connected to D-ribose through a β-*N*-glycosidic bond, creating nucleosides.[5,19] A predominant difference between DNA and RNA nucleosides involves the pentose sugar. In RNA, the sugar is a D-ribose, while in DNA it is a 2-deoxy-D-ribose, which lacks the 2'-OH (Figure I.1). The nucleosides, the smallest repeating units of DNA and RNA, are linked through phosphodiester bonds at the 5′- and 3′-OH positions of the sugar to phosphate units, which alternate per nucleoside. A polymer of nucleoside-phosphate units forms an oligonucleotide strand. In accordance to the information stored in the individual building blocks, oligonucleotides pair with complimentary strands and fold into higher structures. The clefts, grooves and surfaces formed by folded oligonucleotides offer sites for various interactions, such as binding with small molecules, peptides and proteins. Since the higher structures of nucleic structures are crucial to biological processes, a great deal of effort goes into elucidating them.

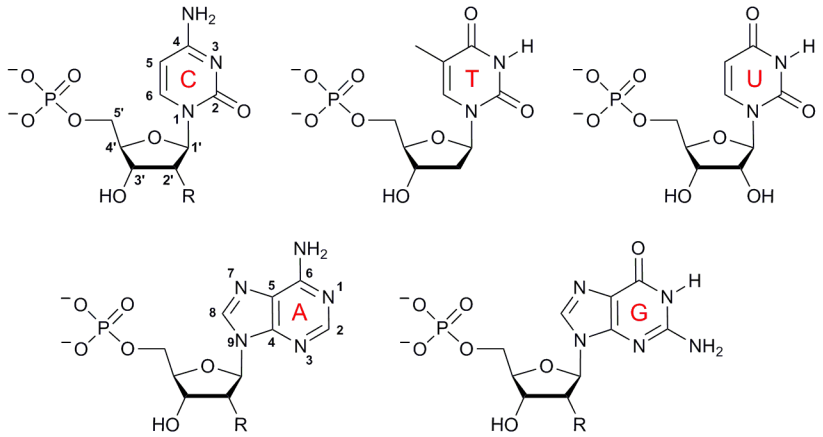

Figure I.1: Structures of common nucleotides found in nucleic acids (DNA: R=H, RNA: R=OH). *Top Left to Right* Pyrimidines: cytidine (C) monophosphate, thymidine (T) monophosphate, and uridine (U) monophosphate. *Bottom Left to Right* Purines: adenosine (A) monophosphate and guanosine (G) monophosphate.

The first major breakthrough in structural studies of nucleic acids occurred in 1953, when James Watson and Francis Crick depicted DNA's double helix, revealing specific hydrogen bonding patterns between the bases (Figure I.2).[20] Accordingly, the dominant hydrogen-bonding patterns in nucleic acids were dubbed Watson-Crick base pairs. Non-canonical base pairs also exist, and they utilize the additional hydrogen bonding sites on the nucleobases (Figure I.3).[5,19] Higher ordered structures, such as triple helical nucleic acids and quadruplexes, depend on these non-canonical base pairs. After Watson and Crick's seminal paper, many other studies followed. Fibre diffraction experiments showed that most of the secondary structures for nucleic acids exist in two different polymorphs. The formations of these conformations depend on salt concentrations and humidity. At low salt and high humidity conditions, the right-handed B-form DNA is favored, while A-form DNA is favored at low humidity and high salt concentrations.[21] The B and A forms are the predominant secondary structure conformations of DNA and RNA, respectively, but other polymorphs exist, including A′, C, C′, D, E, T, and Z.[21]

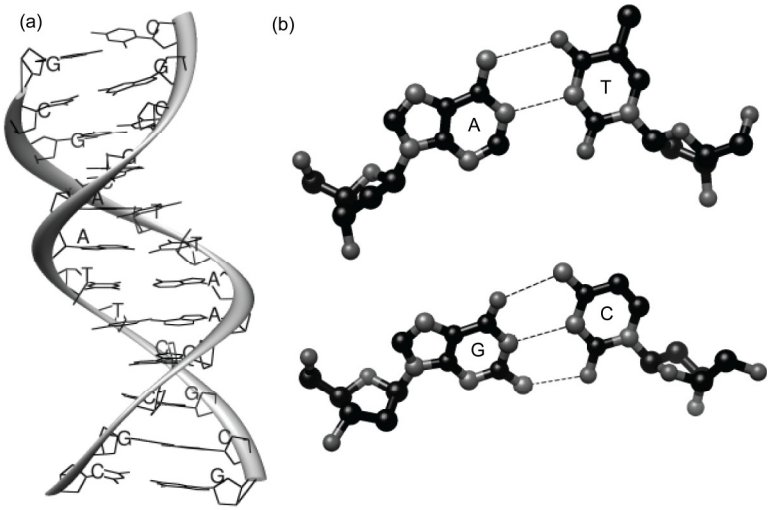

Figure I.2: X-ray crystal structure of the Dickerson-Drew B-DNA dodecamer (a) and slices of the structure that represent Watson-Crick basepairs (b). The self complementary sequence of the dodecamer is 5′–d(CGCGAATTCGCG)–3′. Hydrogen-bonding is represented by dashed lines. PDB ID: 436D.

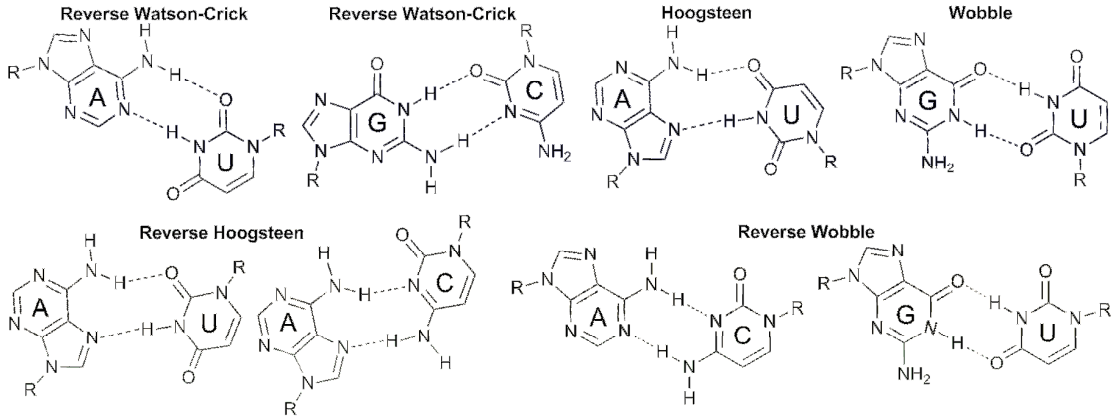

Figure I.3: Non-canonical hydrogen bonding base pairs.

The dimensions of B-form DNA and A-form RNA are quite different, which impact interactions with biomolecules. The major groove of DNA is wide and shallow compared to RNA, while DNA's minor groove is narrower and deeper than that of RNA (Figures I.4 and I.5). DNA and RNA grooves also differ in electrostatics. Since nucleic acids are negatively charged polymers, electrostatics greatly impact their interactions with ions and ligands.[5] Within the major and minor grooves, electrostatic potential is determined primarily by the orientation of individual base pairs.[22,23] In an

A•T base pair, the N3 of adenine and the O2 of thymine both point toward the minor groove, resulting in an overall negative potential. In comparison, a G•C minor groove is more neutral. Although the analogous N3 in guanine and the O2 carbonyl of cytosine add negative potential, the exocyclic N2 amino functionality neutralizes their contribution.[5,21] In the major groove, there is less of a difference in electrostatic potential between A•T and G•C bases pairs. In the A•T base pair, a negative potential contribution is made from the C4 of thymine and the N7 of adenine; however, positive electrostatic potential is provided by the exocyclic 6-amino functionality of adenine. Similarly, in G•C base pairs, positive potential from the exocyclic amine at N4 of cytosine partially diminishes the negative potential contributions from N7 and C6 of guanine. Theoretical calculations have supported the parity in groove electrostatics for DNA.[24,25]

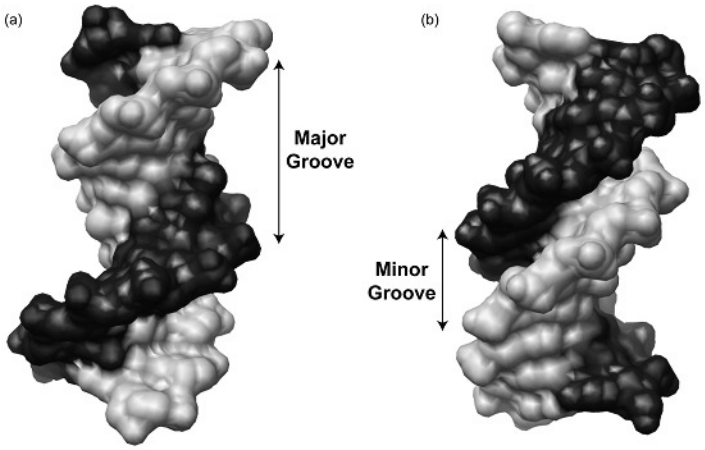

Figure I.4: X-ray crystal structure views of the (a) major and (b) minor groove of the Dickerson-Drew B-DNA Dodecamer. Each strand is shaded separately, while each view is approximately rotated 180° from one another. Major and minor groove widths are the distances between inter-strand phosphates. PDB ID: 2BNA.

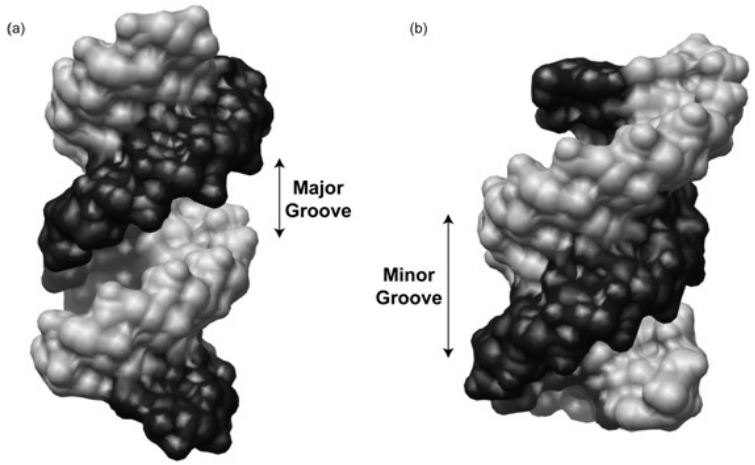

Figure I.5: Views of the (a) major groove and (b) minor groove of a representative A-form RNA duplex. The RNA duplex is an X-ray crystal structure of the self complementary 14mer sequence 5′–U(UA)$_6$A–3′. Each strand is shaded differently, while each view is approximately rotated 180° from one another. Major and minor groove widths are the distances between inter-strand phosphates. PDB ID: 1RNA.

In the minor groove of DNA, the difference in electrostatics between A•T and G•C base pairs can affect sequence selectivity for ligand–nucleic acid binding. For instance, G•C base pairs are more electron-rich, providing a preferable environment for intercalation of electron deficient aromatic ligands. Additionally, the exocyclic 2-amino functionality of guanine in the minor groove can deter binding to G·C tracts due to sterics. Instead, A·T base pair-ligand interactions would be favored. Likewise, along the major groove, the steric bulk of the thymine methyl group can direct ligands to G·C base pairs. Meanwhile, the hydrophobic property of the methyl group can facilitate van der Waals interactions with other hydrophobic residues such as the side chains of leucine, isoleucine, and alanine to promote protein binding.[5] In the A-polymorph form of RNA, the shallow and wide minor groove of RNA has a low electrostatic potential, while the deep major groove has a large electronegative potential. The major groove is, therefore, the main binding site for small molecules due to Columbic attraction and hydrogen-bonding interactions. Proteins, on the other

hand, prefer to bind in the shallow major groove because of van der Waals contacts between the groove floor and the hydrophobic amino acid side chains.

The distribution of nucleic acid electrostatics has dramatic effects on molecules in the surrounding environment. This has a specific impact on metal ions, since the negative phosphate backbone attracts cations to counter the negative potential. In the early 1970's, Manning proposed a quantitative model for describing the interactions of cations with nucleic acids.[26] Specifically, to reduce the effective negative charge of DNA, cations associate within a few angstroms of the helix; however, cations are not locked within a certain orientation. Cation association is fully dependent on axial charge density, known as the counter-ion condensation theory. Later, Record incorporated Debye-Hückel activity coefficients into Manning's model to suggest that it is necessary to consider the polarizable electron density of ions for full quantification of cation association.[27] Such an association neutralizes the negatively charged phosphate backbone, thereby diminishing repulsive forces and stabilizing the nucleic acid structure. Condensed ions energetically affect ligand binding because they occupy the same space as potential nucleic acid ligands.[28] Generally, release of condensed ions upon ligand binding provides a positive entropic contribution to the overall free energy.[26,27,279] However, counter ions stabilize DNA structures, so releasing condensed ions causes an energetic enthalpic penalty. Experimentally, a connection between salt concentration, buffer type and ligand binding exists. Ligand affinity normally increases as bulk salt ion concentration decreases due to lowering of the entropic penalty for ion displacement.

In addition to ions, water plays a pivotal role in structural stabilization of nucleic acids and ligand binding.[28] Experimentally, water molecules directly surrounding nucleic acids have different properties than the bulk solvent and are

necessary for stabilizing their secondary and tertiary structures. Water, a highly polarizable molecule, clusters around the negatively charged phosphate backbone to neutralize charge and diminish electrostatic repulsion between strands.[30] Additionally, water hydrogen bonds with the heteroatoms of base pairs, acting as both a hydrogen bond donor and acceptor. The water involved in these interactions forms the first hydration shell around DNA double helices. Studies done by infrared spectroscopy (IR) estimate that the first hydration shell consists of three water molecules per phosphate and approximately 19–20 water molecules throughout both grooves. A second, less-structured hydration shell exists, but it is short-lived and dependent on the orientation of the first.[31]

When comparing A-DNA and A-RNA duplexes, a higher degree of hydration was found surrounding the sugar-phosphate backbone of the RNA duplex. This is most likely due to the additional 2′-OH group on the ribose moiety. From observations of A-form duplexes, the phosphate backbone is more compactly spaced, allowing water molecules to form bridging interactions between intra-strand phosphates. These water bridges enthalpically stabilize the RNA helix. Due to the higher ordered hydration shell, ligand binding to RNA causes a higher entropic cost compared to DNA.[32] Experimentally, the displacement of water molecules upon ligand binding is thermodynamically difficult to quantify. Normally, the hydration shell and ions around DNA are released into the bulk solvent upon binding, causing a positive change in entropy. Recent studies have shown this hypothesis to be more complicated because osmotic stress studies have determined an uptake of water upon ligand binding.[33]

Using Fluorescence Spectroscopy to Enhance our Understanding of Nucleic Acids

An understanding of the structure and properties of nucleic acids, largely contributed to NMR and X-ray crystallography studies, have been invaluable; however, fluorescence spectroscopy has supplied crucial information, as well.[13,16,18] It provides real-time detection of biological events, such as small molecule binding,[34–36] strand cleavage,[37] and base flipping.[38,39] In particular, fluorescent nucleoside analogues have great utility in probing nucleic acid structure, dynamics, and recognition.[13,16,18] They have been used to detect single nucleotide polymorphisms (SNPs),[40] DNA lesions[41] and protein toxins,[42] and they have assisted in the discovery of new antibiotics and anti-HIV agents.[43] Such explorations can expand the understanding of vital biological processes and enhance the available tools for medicinal research.

Since native nucleobases are weakly emissive, it is essential to produce fluorescent analogs as probes.[15] In the development of fluorescent nucleoside analogs, several factors must be considered to maintain favorable photophysical properties, while avoiding significant nucleic acid structural disturbance.[17] First, it is important to design analogs that are structurally similar to native nucleobases to allow hybridization and other recognition processes to occur. Second, the analogs should have red shifted absorption spectra relative to ones belonging to native nucleosides. Minimizing the absorption overlap permits selective excitation. Third, the analogs must have sufficient quantum efficiency in order to be detectable. A long emission wavelength is also preferable, so the fluorescence can be in the visible range. Lastly, the emission of the fluorescent analogs should be sensitive to changes in its

microenvironment. While many fluorescently modified nucleosides exist, very few actually follow the ideal design criteria.

Outside of utilizing single fluorophores, it is also possible to use one or more pairs of probes for Förster Resonance Energy Transfer (FRET) experiments.[13,18] FRET is a useful tool in resolving some of the limitations of standard fluorescence assays. While utilizing one fluorescent nucleoside can monitor the binding of small molecules, peptides or proteins to nucleic acids targets, there are limits to the technique.[35] Foremost, multiple modes of binding exist between binders and targets, which can influence the ability of individual fluorescent nucleosides to accurately report binding affinity. Currently, there is no universal probe that can detect the binding in multiple systems. Existing fluorescence based assays are also unable to respond in cases of competitive binding. For instance, a furan modified ribonucleoside in the bacterial A-site will show increased fluorescence for binding of antibiotics like paromomycin or neomycin, but it cannot report the displacement of one of these aminoglycosides by the other. However, if the modified fluorescent nucleoside in a nucleic acid target is employed in a FRET pair, the onset of FRET would unambiguously report the binding, while the offset of FRET would signal displacement. As FRET is distance dependent, when binding occurs, the donor and acceptor would be brought together, leading to the increased emission of the acceptor and the quenching of the donor. If binding is disrupted, the donor and acceptor would be parted, decreasing the emission of the acceptor and simultaneously increasing the fluorescence of the donor. A FRET assay could provide both binding and competitive binding information independent to the mode of binding, which would be an invaluable asset for screening processes in drug discovery and studying protein–nucleic acid interactions. In choosing a FRET pair, it

is necessary to design an isosteric, emissive nucleoside with an emission profile that matches well with the absorbance of another fluorophore.

There are many possible motifs to choose from when designing a new family of isomorphic fluorescent nucleosides for either single fluorophore or FRET studies. Specifically, in our research, we focus on polarizable charge-transfer chromophores and nucleosides that experience excited state proton transfer. As observed in natural systems, charge-transfer analogs can have fluorescence that is environmentally sensitive. For example, in the case of luciferin, depending on the composition of the surrounding protein, different wavelengths of emission are observed in firefly's bioluminescence.[44] With excited state proton transfer, it is possible to obtain large red-shifted emissions. Upon light excitation, the acidity and basicity of Brønsted acids and Lewis bases are enhanced, respectively. Such an enhancement can be used to setup an intramolecular acid-base reaction in the excited state, which can decay to a structure that is different than the original ground state.[45] Thus, a large Stokes' shift occurs. We have synthesized polarizable charge-transfer nucleosides based on a pyrimidine core with functional groups that are *para* or *ortho* to the C4 carbonyl (Figure I.6). The properties of the nucleosides will be described in subsequent chapters, including their applications in studying biological systems.

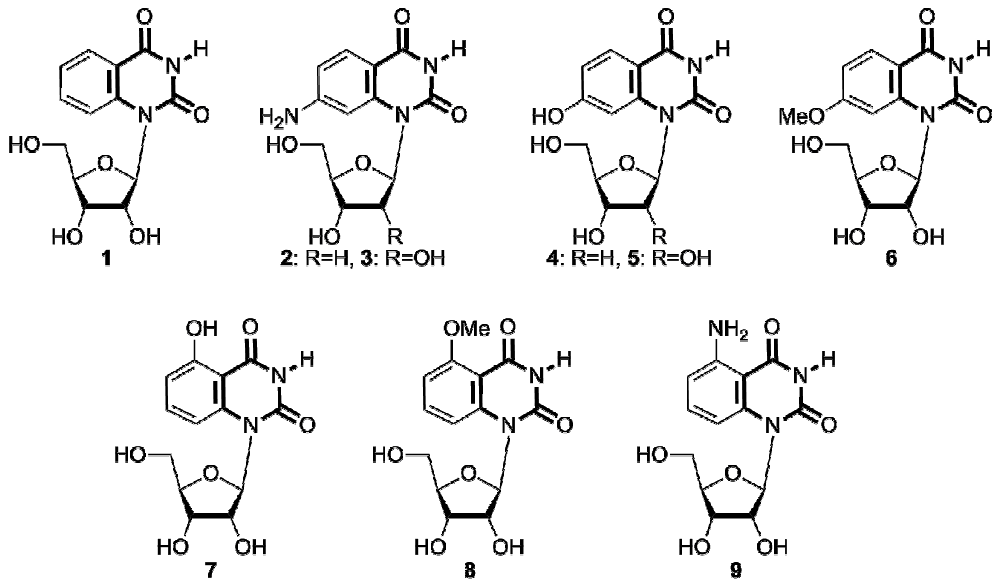

Figure I.6: Quinazoline-based fluorescent nucleoside analogues.

References

1. B. C. Stark, Kole, R., Bowman, E. J., Altman, S., *Proc. Natl. Acad. Sci. U. S. A.*, 1978, **75**, 3717–3721.

2. T. R. Cech, Zaug, A. J., Grabowski, P. J., *Cell*, 1981, **27**, 487–496.

3. K. Kruger, Grabowski, P. J., Zaug, A. J., Sands, J., Gottschling, D. E., Cech, T. R., *Cell*, 1982, **31**, 147–157.

4. M. H. F. Wilkins, Stokes, A. R., Wilson, H. R., *Nature*, 1953, **171**, 738–740.

5. W. Saenger, *Principles of nucleic acid structure*, Springer-Verlag, New York, 1984.

6. J. R. Wyatt, Tinoco, I., in *The RNA world*, ed. R. F. Gesteland, Atkins, J. F., Cold Spring Harbor Laboratory Press, Plainview, Editon edn., 1993, pp. 465–496.

7. C. S. Chow and F. M. Bogdan, *Chem. Rev.*, 1997, **97**, 1489–1514.

8. M. Gellert, M. N. Lipsett and D. R. Davies, *Proc. Natl. Acad. Sci. U. S. A.*, 1962, **48**.

9. C. M. Counter, A. A. Avilion, C. E. LeFeuvre, N. G. Stewart, C. W. Greider, C. G. Harley and S. Bacchetti, *EMBO J.*, 1992, **11**, 1921–1929.

10. N. W. Kim, M. A. Piatyszek, K. R. Prowse, C. B. Harley, M. D. West, P. L. C. Ho, G. M. Coviello, W. E. Wright, S. L. Weinrich and J. W. Shay, *Science*, 1994, **266**, 2011–2015.

11. K. Shin-ya, K. Wierzba, K. Matsuo, T. Ohtani, Y. Yamada, K. Furihata, Y. Kayakawa and H. Seto, *J. Am. Chem. Soc.*, 2001, **123**, 1262–1263.

12. A. Siddiqui-Jain, C. L. Grand, D. J. Bearss and L. H. Hurley, *Proc. Natl. Acad. Sci. U. S. A.*, 2002, **99**, 11593–11598.

13. R. W. Sinkeldam, N. J. Greco and Y. Tor, *Chem. Rev.*, 2010, **110**, 2579–2619.

14. M. Daniels and W. Hauswirth, *Science*, 1971, **171**, 675-677.

15. L. Serrano-Andrés and M. Merchán, *J. Photoch. Photobio. C*, 2009, **10**, 21-32.

16. J. N. Wilson and E. T. Kool, *Org. Biomol. Chem.*, 2006, **4**, 4265–4274.

17. Y. Tor, *Tetrahedron*, 2007, 3425-3426.

18. L. M. Wilhelmsson, *Q. Rev. Biophys.*, 2010, 1-25.

19. G. M. Blackburn, M. J. Gait, D. Loakes and D. M. Williams, *Nucleic acids in chemistry and biology*, 3rd edn., Oxford University Press, Oxford, England ; New York, 2006.

20. J. D. Watson, Crick, F. H. C., *Nature*, 1953, **171**, 737–738.

21. S. Neidle, *Nucleic acid structure and recognition*, Oxford University Press, New York, 2002.

22. R. Larvey and B. Pullman, *Theoret. Chim. Acta.*, 1979, **53**, 175–181.

23. R. Larvey and B. Pullman, *Nucl. Acids Res.*, 1982, **10**, 4383–4395.

24. D. Perahia and A. Pullman, *Theoret. Chim. Acta. (Berl.)*, 1979, **50**, 351–354.

25. K. Chin, K. A. Sharp, B. Honig and A. M. Pyle, *Nat. Struct. Biol.*, 1999, **6**, 1055–1061.

26. G. S. Manning, *Acc. Chem. Res.*, 1979, **12**, 443–449.

27. M. T. Record, C. F. Anderson and T. M. Lohman, *Quart. Rev. Biophs.*, 1978, **11**, 103–178.

28. C. J. Alden and S. H. Kim, *J. Mol. Biol.*, 1979, **132**, 411–434.

29. J. B. Chaires, *Biopolymers*, 1997, **44**, 201–215.

30. T. V. Chalikian, A. P. Sarvazyan, G. E. Plum and K. J. Breslauer, *Biochemistry*, 1994, **33**, 2394–2401.

31. M. L. Kopka, A. Fratini, H. R. Drew and R. E. Dickerson, *J. Mol. Biol.*, 1983, **163**, 129–146.

32. M. Egli, S. Portmann and N. Usman, *Biochemistry*, 1996, **35**, 8489–8494.

33. J. R. Kiser, R. W. Monk, R. L. Smalls and J. T. Petty, *Biochemistry*, 2005, **44**, 16988–16997.

34. S. G. Srivatsan and Y. Tor, *J. Am. Chem. Soc.*, 2007, **129**, 2044-2053.

35. Y. Xie, A. V. Dix and Y. Tor, *J. Am. Chem. Soc.*, 2009, **131**, 17605-17614.

36. Y. Xie, A. V. Dix and Y. Tor, *Chem. Commun.*, 2010, **46**, 5542 - 5544.

37. S. R. Kirk, N. W. Luedtke and Y. Tor, *Bioorg. Med. Chem.*, 2001, **9**, 2295.

38. M. Kaul, C. M. Barbieri and D. S. Pilch, *J. Am. Chem. Soc.*, 2004, **126**, 3447-3453.

39. S. Shandrick, Q. Zhao, Q. Han, B. K. Ayida, M. Takahashi, G. C. Winters, K. B. Simonsen, D. Vourloumis and T. Hermann, *Angew. Chem., Int. Ed.*, 2004, **43**, 3177-3182.

40. S. G. Srivatsan, H. Weizman and Y. Tor, *Org. Biomol. Chem.*, 2008, **6**, 1334-1338.

41. N. J. Greco and Y. Tor, *J. Am. Chem. Soc.*, 2005, **127**, 10784-10785.

42. S. G. Srivatsan, N. Greco, J. and Y. Tor, *Angew. Chem., Int. Ed.*, 2008, **47**, 6661-6665.

43. Y. Tor, *ChemBioChem*, 2003, **4**, 998-1007.

44. T. Nakatsu, S. Ichiyama, J. Hiratake, A. Saldanha, N. Kobashi, K. Sakata and H. Kato, *Nature*, 2006, **440**, 372–376.

45. L. G. Arnaut and S. J. Fromosinho, *J. Photochem. Photobiol. A. Chem.*, 1993, **75**, 1–20.

The introduction contains sections of text and figures that are reprinted from: Xie, Y.; Tam, V. K.; Tor, Y. In *The Chemical Biology of Nucleic Acids*; G, M., Ed.; John Wiley & Sons, Ltd: Chichester, UK, 2010. The dissertation author is the main author and researcher for this work.

CHAPTER 1: FRET Enabled Real Time Detection of RNA–Small Molecule Binding

---

Abstract. A robust analysis and discovery platform for antibiotics targeting the bacterial ribosomal RNA A-site has been developed by incorporating a new emissive U surrogate into the RNA and labeling the aminoglycosides with an appropriate fluorescence acceptor. Specifically, a 5-methoxyquinazoline-2,4(1*H*,3*H*)-dione-based emissive uracil analog was identified to be an ideal donor for 7-diethylaminecoumarin-3-carboxylic acid. This donor/acceptor pair displays a critical Förster radius (R_0) of 27 Å, a value suitable for an A-site–aminoglycoside assembly. Titrating the coumarin labeled aminoglycosides into the emissive A-site construct, labeled at position U1406, shows a decrease in donor emission (at 395 nm) and concurrent increase of the acceptor emission (at 473 nm). Titration curves, obtained by fitting the donor's emission quenching or the augmentation of the acceptor's sensitized emission, faithfully generate EC_{50} values. Titration of unlabeled ligands into the pre-formed FRET complex showed continuous increase of the donor emission, with concurrent decrease of the acceptor emission, yielding valuable data regarding competitive displacement of aminoglycosides by A-site binders. Detection of antibiotic binding is therefore not dependent on changes in the environment of a single fluorophore, but rather on the responsive interaction between two chromophores acting as a FRET pair, facilitating the determination of direct binding and competitive displacement events with FRET accuracy.

Introduction

The ribosomal decoding site, also known as the A-site, ensures high fidelity in protein synthesis by appraising codon–anticodon matching.[1–3] Numerous naturally occurring potent antibiotics, particularly the aminoglycosides family, have evolved to meddle with this precise monitoring and corrupt bacterial protein production.[4–8] Specifically, the aminoglycosides bind a small loop within the 16S rRNA and interfere with the conformational flexibility of A1492 and A1493, two key adenine residues (Figure 1.1a).[9–12] The aminoglycosides stabilize an RNA conformation similar to the one induced by the cognate acyl-tRNA–mRNA complex, causing the ribosome to lose its ability to distinguish between correct and incorrect anticodon–codon hybrids.[13–18]

The A-site, the Achilles heel of the bacterial ribosome, has remained one of the most attractive targets for the discovery and development of new antibiotics.[19–25] A number of tools have been developed to assess ligand binding to this unique RNA site.[26,27] Fluorescent A-site constructs, which contain emissive and responsive nucleoside analogs, such as 2-aminopurine at positions 1492 or 1493, have shown great promise.[28–31] Their fluorescence response is, however, antibiotic-dependent.[28,32] To overcome this drawback and devise a robust analysis and discovery platform for A-site binders, we have envisioned an approach where detection of antibiotic binding is not dependent on changes in the environment of a single fluorophore, but rather on the interaction between two chromophores acting as a Förster Resonance Energy Transfer (FRET) pair (Figure 1.1b). In this fashion, we hypothesized, one could follow direct binding of appropriately labeled antibiotics and their displacement by competing binders with “FRET accuracy” without relying on a fluorescent nucleobase as the sole sensing moiety (Figure 1.1b).

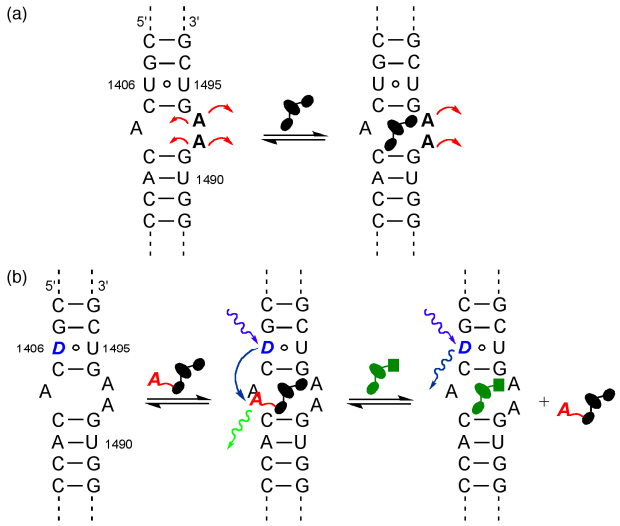

Figure 1.1: (a) The binding of aminoglycosides to the bacterial A-site impacts the placement and dynamics of the unpaired A1492 and 1493 residues. (b) By replacing one of the nucleosides in the A-site with an isosteric emissive nucleoside analog as a donor (***D***) and tagging the antibiotics with an appropriate acceptor (***A***), binding and displacement events can be accurately monitored using FRET.

To realize such a system, we have relied on two key features: (a) one of the native nucleobases in the A-site, proximal to the binding site, but not part of it, had to be replaced with an emissive isomorphic nucleobase analog acting as a FRET donor, and (b) aminoglycosides, the cognate binders of the A-site, had to be labeled with an appropriate FRET acceptor in positions that are not essential for RNA binding (Figure 1.1b).[33] By monitoring the interactions of ligands and their RNA targets based on distance and location, convoluting factors such as modes of binding can be eliminated when studying binding and displacement. Here we describe the design, assembly and utility of such a FRET-friendly and minimally perturbed RNA construct, where a new fluorescent uridine analog, serving as a fluorescent donor, is incorporated into the A-site and coumarin-labeled aminoglycosides act as FRET acceptors.

Results

Selection of the Donor and Acceptor. While diverse FRET donors and acceptors exist, small chromophores capable of serving as non-perturbing nucleobase surrogates are exceedingly rare.[34] In pursuing such unique probes, we have synthesized, examined and implemented new emissive nucleosides with absorption maxima between 290 and 350 nm and emission bands between 350 and 440 nm.[35–39] We have identified 5-methoxyquinazoline-2,4(1*H*,3*H*)-dione **1**, an emissive uracil analog, as an ideal donor for 7-diethylaminecoumarin-3-carboxylic acid **2** (Figure 1.2). The extinction coefficient of **2** at 320 nm, the absorption maximum of **1**, is minimal, while the emission of **1**, centered around 395 nm (Φ_F = 0.16), overlaps perfectly with the absorption band of **2**, which emits at 473 nm (Φ_F = 0.83), suggesting excellent FRET pairing (Figure 1.3).[40,41] Indeed, the critical Förster radius (R_0) for the **1**/**2** pair was experimentally determined to be 27 Å, a suitable value for the proposed A-site assembly.[42]

The presence and position of the methoxy group on the quinazoline-2,4(1*H*,3*H*)-dione core impact the photophysical properties and are critical for the compatibility of the FRET partners, as evident by a comparison of the parent and to two isomeric methoxy substituted heterocycles. The emission profile of quinazoline-2,4(1*H*,3*H*)-dione **3**, the parent unsubstituted heterocycle, is hypsochromically shifted compared to the emission of **1,** with a maximum at 370 nm (Figure 1.4). The emission of the isomeric 3-methoxyquinazoline-2,4(1*H*,3*H*)-dione **4** is even further shifted to the blue with emission maximum at 356 nm (Figure 1.4). Importantly, glycosylation of these heterocycles to yield the corresponding nucleosides negligibly impacts the photophysical properties.[40]

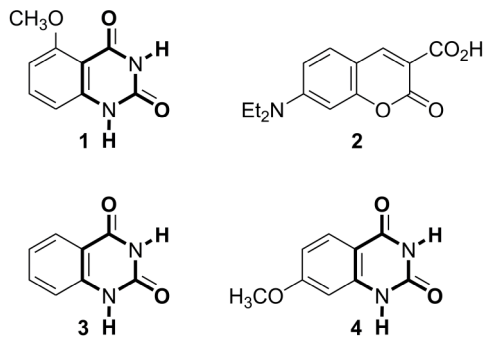

Figure 1.2: Structure of the donor **1** and acceptor **2**, as well as **3** (the parent donor heterocycle) and **4** (an isomeric methoxy substituted heterocycle).[40]

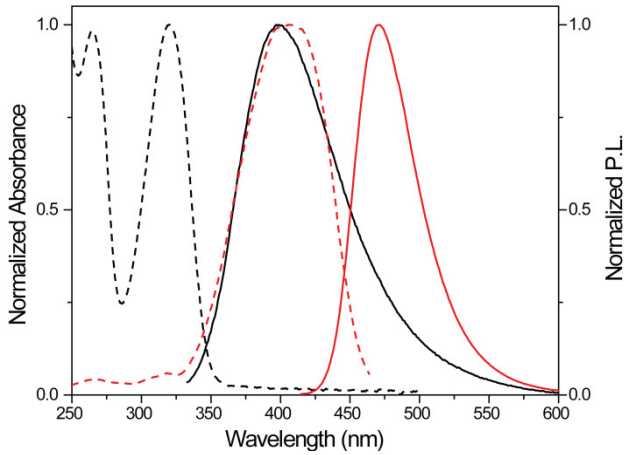

Figure 1.3: Normalized absorption (---) and emission (—) spectra of **1** (black) and **2** (red) in water.[40]

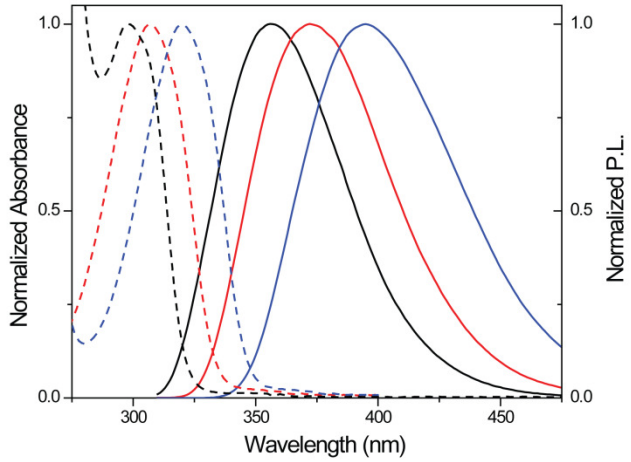

Figure 1.4: Normalized absorption (---) and emission (—) spectra of **4** (black), **3** (red), and **1** (blue) in water.

Synthesis and Photophysical Properties of Modified RNA. To modify the A-site RNA oligonucleotide, nucleoside **5** and its phosphoramidite **8** were prepared as

shown in Scheme 1.[40] The commercially available 2-methoxy-5-aminobenzoic acid was cyclized with sodium cyanate to yield the emissive heterocycle **1**, which was glycosylated to provide the modified nucleoside **5** after saponification of all esters. Protection of the 5'-hydroxyl as the 4,4'-dimethoxytrityl (DMT) derivative and the 2'-hydroxyl as the (trisisopropylsiloxy)methyl (TOM) derivative, followed by phosphitylation of the 3'-hydroxyl, provided phosphoramidite **8** (Scheme 1.1).[40]

Scheme 1.1: Synthesis of the modified nucleoside **5** and its phosphoramidite **8**.[a]

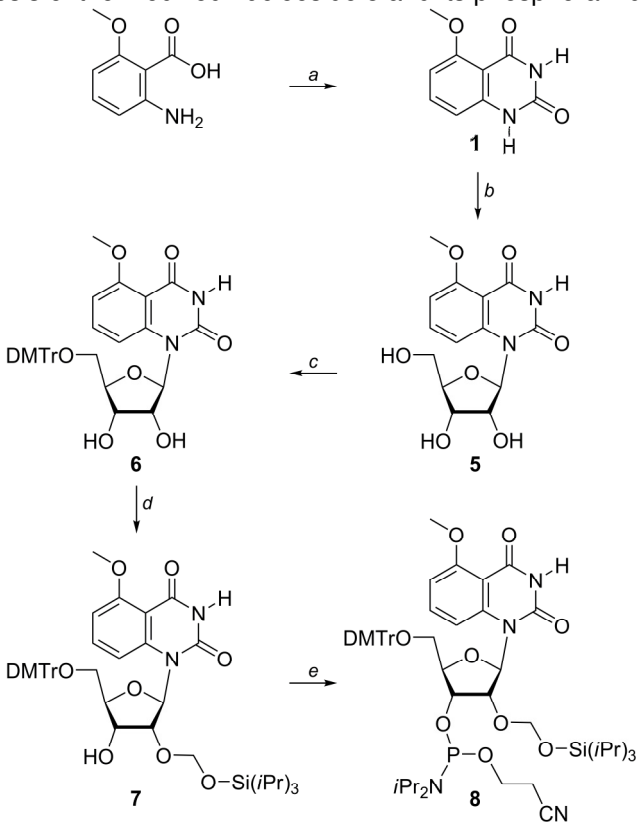

[a] Reagents: (a) NaOCN, NaOH, conc. HCl, water, 90%. (b) (i) *N,O*-bis(trimethylsilyl)acetamide, $CF_3SO_3Si(CH_3)_3$, β-D-ribofuranose 1-acetate 2,3,5-tribenzoate, CH_3CN; (ii) conc. NH_4OH, 81%. (c) DMTrCl, Et_3N, pyridine, 85%. (d) iPr_2NEt, nBu_2SnCl_2, $(iPr_3SiO)CH_2Cl$, $ClCH_2CH_2Cl$, 30%. (e) iPr_2NEt, $(iPr_2N)P(Cl)O\text{-}CH_2CH_2CN$, $ClCH_2CH_2Cl$, 60%.

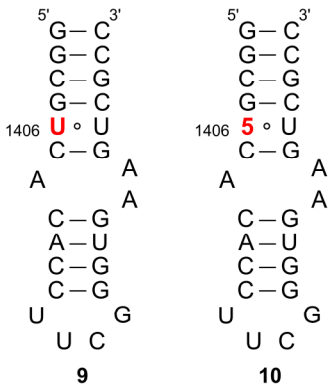

Figure 1.5: The unmodified **9** and modified **10** A-site constructs.

Standard solid-phase oligonucleotide synthesis was utilized to prepare the 27-mer bacterial A-site model construct **10**,[43] where the fluorescent U analog **5** replaces U1406 (Figure 1.5).[44] The oligonucleotide was purified by PAGE, and MALDI-TOF mass spectrometry confirmed its full length and the presence of the intact emissive nucleoside **5**.[40] Thermal denaturation studies showed that the incorporated modified nucleobase had minimal impact on the stability of the folded RNA. The emissive RNA construct **10** displayed a T_m of 71 °C, while the unmodified control A-site construct **9** had a T_m of 72 °C (cacodylate buffer pH 7.0, NaCl 1.0×10^{-1} M).[40] The emission profile of the emissive A-site construct **10**, excited at 320 nm, resembled that of the parent nucleoside in water, with a maximum emission at 395 nm, albeit with a lower emission quantum yield ($\Phi_F = 0.03$).[45]

Synthesis and Photophysical Properties of Modified Aminoglycosides. To complete the FRET pair, neomycin B and tobramycin, two distinct 2-deoxystreptamine-based aminoglycosides, were conjugated to 7-diethylaminecoumarin-3-carboxylic acid to afford **11** and **12**, respectively, by modifying their primary hydroxymethyl groups, previously shown not to be critical for RNA binding (Scheme 1.2).[7,17,40,46] Using previously reported procedures, the Boc-

protected aminoglycosides were activated at the primary hydroxymethyl group on the ribose by 2,4,6-triisopropylbenzenesulfonyl chloride (TIBS-Cl).[47] Treatment with ammonia in MeOH provided the aminomethyl substituted product (e.g., **13**, Scheme 1.2). The newly installed amine was coupled to the coumarin carboxylic acid, using standard peptide coupling conditions. The resulting Boc-protected, coumarin-labeled aminoglycosides were treated with trfluoroacetic acid to remove the Boc groups, yielding **11** and **12** as their TFA salts. The emission profile of **11** and **12** resembled that of the parent heterocycle **2**, displaying an emission maximum at 473 nm upon excitation at 400 nm, maintaining a quantum yield of 80%.

Scheme 1.2: Structure of the aminoglycosides used for binding and displacement studies (**11** and **12**) and the synthesis of coumarin-labeled neomycin **11**. [a]

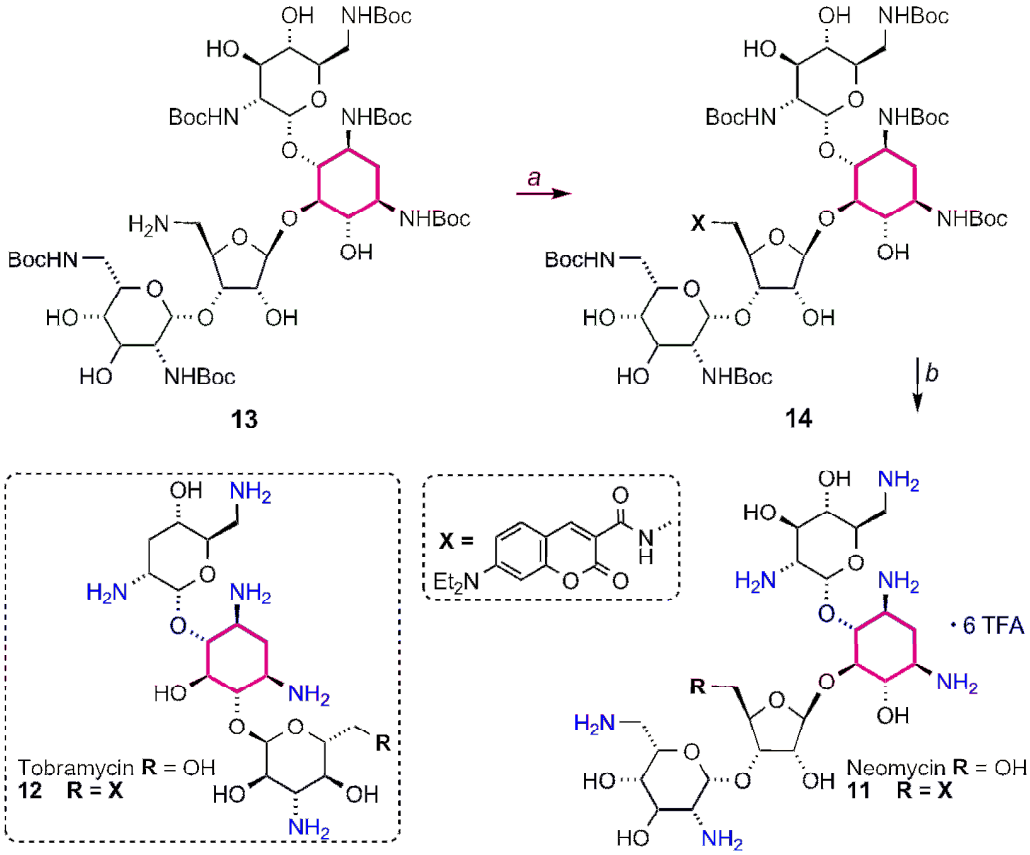

[a] Reagents: (a) 7-(Et_2N)coumarin-3-carboxylic acid, *N*-(3-dimethylaminopropyl)-*N*′-ethylcarbodiimide, 4-dimethylaminopyridine, *i*Pr_2EtN, Cl_2CH_2, 84%. (b) Trifluoroacetic acid, triisopropylsilane, CH_2Cl_2 82%.

Binding of Coumarin-Labeled Aminoglycosides to the Fluorescently Labeled A-Site. Titration of the coumarin labeled neomycin B derivative **11** into the emissive A-site construct, excited at 320 nm, showed continuous decrease of the donor emission at 395 nm, with concomitant increase of the acceptor emission at 473 nm (Figure 1.6a).[40] Similarly, titrating the coumarin labeled tobramycin derivative **12** into the emissive A-site construct, excited at 320 nm, showed decrease of the donor emission at 395 nm and concurrent increase of the acceptor emission at 473 nm. Figure 1.7 graphically illustrates the titration curves generated by plotting the fractional fluorescence saturation of the donor and acceptor. Identical EC_{50} values of 0.84 ($\pm$0.03) $\times$ 10^{-6} M are obtained from curve fitting the quenching of the donor's emission or the augmentation of the acceptor's sensitized emission (Figure 1.7a). Analogous behavior is observed for the labeled tobramycin derivative **12** (Figure 1.7b), yielding a higher EC_{50} value of 2.3 ($\pm$0.2) $\times$ 10^{-6} M.

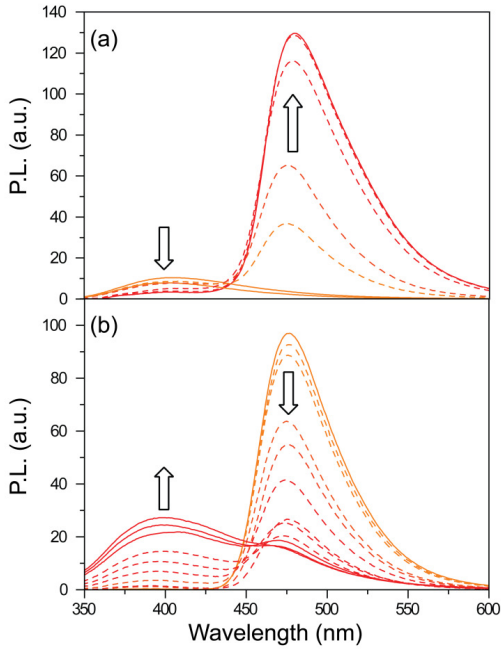

Figure 1.6: (a) Example of binding study. **11** is titrated into **10**. (b) Example of displacement study. Tobramycin is titrated into **10** saturated with **12**. Conditions: **10** (1×10^{-6} M), cacodylate buffer pH 7.0 (2.0×10^{-2} M), NaCl (1.0×10^{-1} M).

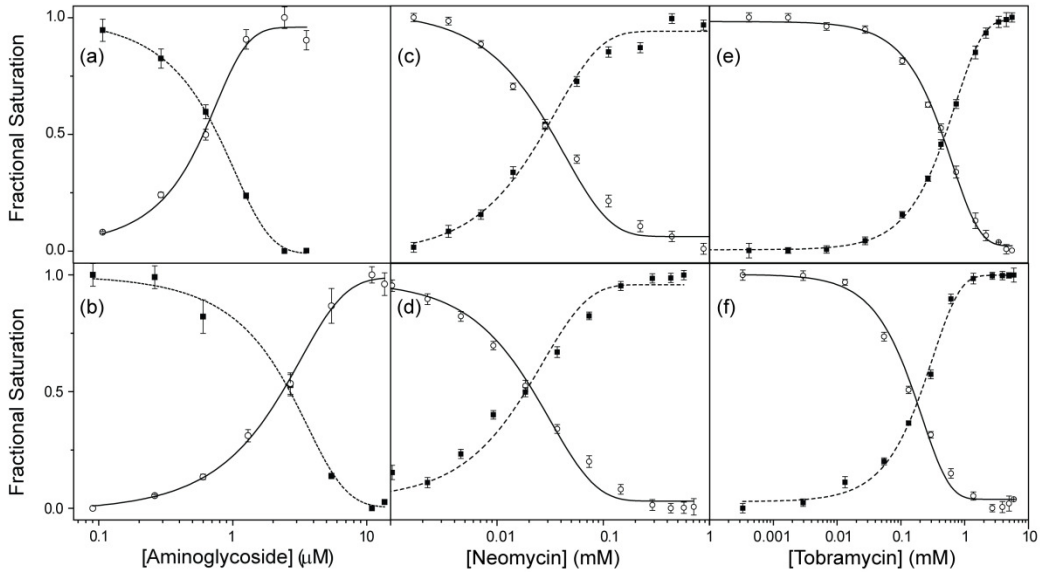

Figure 1.7: Fractional fluorescence saturation of the donor (■) in the labeled A-site and the emissive acceptor (○) in the labeled aminoglycosides in the following experiments: (a) titration of **10** with **11**; (b) titration of **10** with **12**; (c) displacement of the A-site bound **11** with neomycin; (d) displacement of the A-site bound **12** with neomycin. (e) displacement of the A-site bound **11** with tobramycin; (f) displacement of the A-site bound **12** with tobramycin. Conditions: **10** (1.0×10^{-6} M), cacodylate buffer pH 7.0 (2.0×10^{-2} M), NaCl (1.0×10^{-1} M).

Table 1.1: IC_{50} values of aminoglycosides competing off **11** and **12**.[a]

Aminoglycosides	Displacement of **11**[b]	Displacement of **12**[b]
Neomycin	0.03 ± 0.01	0.02 ± 0.01
Tobramycin	0.50 ± 0.02	0.16 ± 0.03
Paromomycin	1.14 ± 0.08	0.06 ± 0.03
Apramycin	3.00 ± 0.09	1.00 ± 0.05
Hygromycin	1.46 ± 0.06	1.00 ± 0.05
Amikacin	1.73 ± 0.07	0.56 ± 0.04
Kanamycin A	3.30 ± 0.09	1.61 ± 0.06
Amino-Kanamycin A	0.18 ± 0.03	0.05 ± 0.02
Amino Tobramycin	0.02 ± 0.01	0.01 ± 0.01

[a] Conditions: **10** (1×10^{-6} M), cacodylate buffer pH 7.0 (2.0×10^{-2} M), NaCl (1.0×10^{-1} M). [b] Aminoglycoside concentration is given in 10^{-3} M.

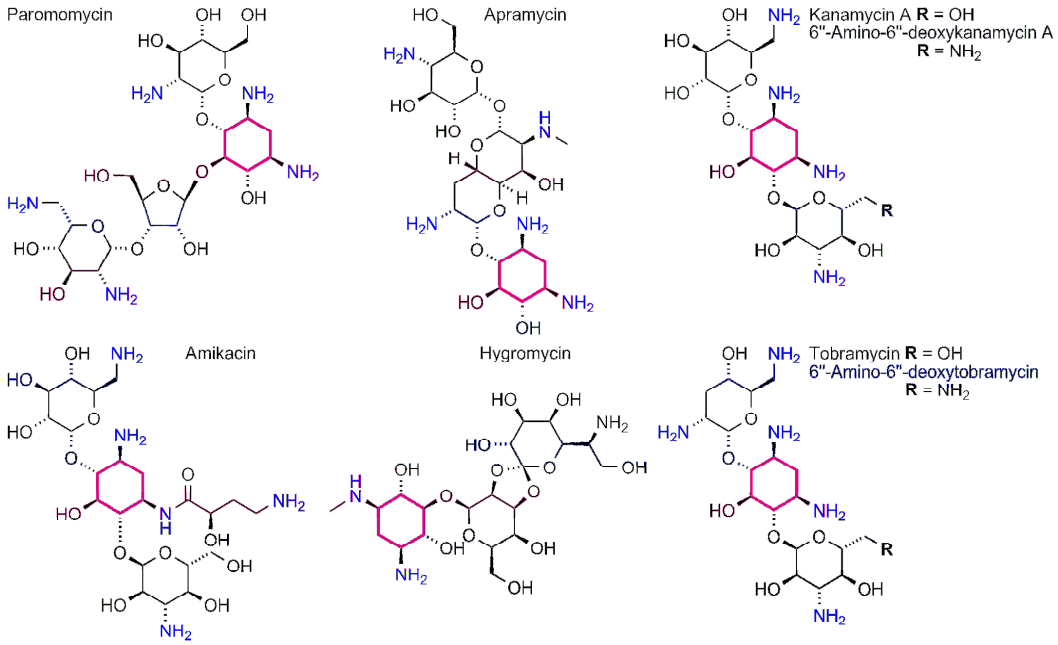

Figure 1.8: Aminoglycosides used for displacement studies.

Displacement of A-site Bound Coumarin-Labeled Aminoglycosides with Unlabeled RNA Binders. Pre-formation of the FRET complex by saturating the modified A-site construct with the labeled neomycin or tobramycin derivatives facilitates the evaluation of the relative A-site affinity of other antibiotics by competition experiments, where the resonance energy transfer is disrupted by displacing the bound coumarin labeled antibiotic.[40] Titration of the unlabeled aminoglycosides into the pre-formed FRET complex, excited at 320 nm, showed continuous increase of the donor emission at 395 nm, with concurrent decrease of the acceptor emission at 473 nm (Figure 1.6b). Titration curves were generated by plotting the fractional fluorescence saturation of the donor and acceptor against the concentration of the unlabeled aminoglycoside. Figure 1.7 (panels c–f) provides selected examples (see also Figures A1.4, A1.5). Competing off a bound neomycin, one of the strongest A-site binders, with other aminoglycosides (paromomycin, apramycin, hygromycin, kanamycin A, Figure 1.8), requires relatively high competitor

concentrations (Table 1.1). In contrast, the same competitor antibiotics more easily displace the lower affinity tobramycin. Additionally, two synthetic amino-aminoglycosides (6''-amino-6''-deoxy-kanamycin A and 6''-amino-6''-deoxy-tobramycin prepared in our lab[47a]) are found to be rather potent A-site binders (Table 1.1). Importantly, spermidine, serving as a negative control polyamine, is unable to displace any of the bound aminoglycosides (up to 5×10^{-3} M).

Discussion

Among the RNA targets explored over the past two decades, the bacterial ribosomal decoding site (or A-site) holds a unique place. It is the only validated drug target.[10,11,23,25,48-50] This conformational switch is the cognate binding site of aminoglycoside antibiotics, a diverse family of natural products evolved to interfere with the decoding process in bacteria.[2] These highly effective bactericidal agents alter the conformational flexibility of two key residues, A1492 and A1493, inducing a conformation similar to the one found in the cognate acyl-tRNA–mRNA complex (Figure 1.1).[51,52] This impairs the fidelity of ribosomal protein synthesis, ultimately leading to bacterial death.

The utility of aminoglycosides has declined over the years due to their diminished potency in resistant bacteria, their adverse side effects, and consequently, the availability of newer, potent and safer drugs.[23,25,27,53] The rapid emergence of resistant pathogens and the time-consuming and minimally productive development of new broad-spectrum antibiotics have created, however, alarming circumstances, where new antibiotics are needed to replace existing compromised drugs.[54,55] These developments have generated a renewed interest in the A-site and triggered the development of new tools to assess ligand binding to this bacterial RNA site. In

particular, fluorescent A-site constructs, which contain responsive nucleoside analogs such as 2-aminopurine, have proven useful,[56-59] although their response is antibiotic-dependent, which is most likely due to the presence of distinct binding modes, which impact the emission readout. This could affect the ability of fluorescent nucleosides to accurately respond to ligand binding. To create a robust analysis and discovery platform for A-site binders, we have developed a FRET-enabled assembly where the A-site serves as the donor and the aminoglycoside as the acceptor. The detection of antibiotic binding and competitive displacement is highly sensitive and is no longer dependent on arbitrary changes in the environment of a single fluorophore, but rather on the interaction between two matching chromophores acting as a FRET pair (Figure 1.1b).

In designing such chromophoric RNA–small molecule assemblies, two major issues need to be addressed. The first involves the position and type of modification of the RNA target with a donor and the second, which is of related significance and is partially coupled, is the selection and placement of an appropriate chromophoric partner. The identification of the donor is the most challenging, as it must fulfill strict functional criteria: it needs to be small and structurally non-perturbing, while at the same time displaying useful photophysical characteristics that can be matched to a suitable and small acceptor. Due to its imposed small molecular footprint and high similarity to the native nucleobases, such a nucleobase analog is likely to emit below or close to the visible range with a moderate emission quantum yield at best. This, in turn, impacts the selection of the acceptor to be placed on the aminoglycoside. In addition to being structurally and functionally non-perturbing (i.e., minimally impacting the recognition properties of the antibiotic), the acceptor needs to have a high degree of spectral overlap with the donor, while displaying intense emission in the visible

range. As a FRET pair, the selected donor and acceptor need to have a critical Förster radius that matches the recognition phenomenon and the anticipated distances between the RNA and the bound antibiotic.

To confer useful emissive properties upon nucleic acids, while minimally perturbing their folded structure, we have been pursuing the development of isosteric/isomorphic nucleobase analogs.[35–39] These heterocyclic surrogates can replace a native nucleobase without significantly altering the folding and recognition features of the native target, but with the added benefit of being fluorescent.[60] Specifically, we have previously demonstrated that replacing the U residue at position 1406 with emissive nucleoside analogs retains the folding and antibiotic recognition properties of the A-site.[36,61] Its proximity to the aminoglycoside binding site ensures adequate photophysical interaction with suitably labeled aminoglycoside, as shown in the modeled structure (Figure 1.9). Out of the possible motifs, we focused on a size-expanded U analogue with a methoxy group in the 5 position, which is a superior isostere to similar benzo[g]quinazoline nucleosides that have been previously utilized.[62–64]

The emission profile of the fluorescent nucleobase **1** complements the absorbance of 7-(diethylamino)coumarin (Figure 1.3), a commonly used fluorophore that can be conjugated to aminoglycosides at positions that do not significantly impact their binding to the A-site (Figure 1.9).[65] Coumarin-based fluorophores are among the smallest organic chromophores displaying emission in the visible range with high quantum yields (Φ_f > 0.5).[66,67] Specifically, 7-(diethylamino)coumarin lacks any significant molar absorptivity at 320 nm, which facilitates selective excitation of donor **1**. It is worth noting that placing the electron-donating methoxy group on the

quinazoline-2,4(1*H*,3*H*)-dione skeleton is essential for maximizing the spectral overlap between the donor and acceptor. The absence of the methoxy group, as in the unsubstituted parent heterocycle **3**, or its placement in an electronically related position, such as in the isomeric **4**, causes significant blue shift in the donors' emission, diminishes the spectral overlap and lowers FRET efficiency between the quinazoline and coumarin chromophores (Figure 1.4). We postulate that excited state stabilization (likely due to charge transfer from the methoxy to the conjugated carbonyl generating opposing dipoles in **1** only) leads to lower energy emission and optimal spectral overlap between **1** and **2**.

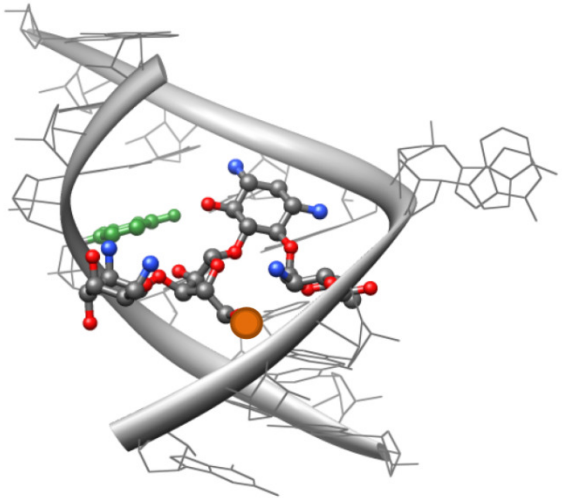

Figure 1.9: A model of neomycin bound to the A-site (PDB 2ET4). The distance from the center of U1406 (green) to the primary 5' hydroxymethyl group on the ribose (orange) is less than 10 Å.

In labeling the A-site, it was important to place **5** close to the recognition site without distorting the binding properties of the model RNA construct. Functional, isosteric nucleosides, such as a furan modified ribonucleosides, have been incorporated in place of native U1406 in the bacterial A-site for affinity assays to recognize RNA–small molecule interactions.[36,61] These modifications have been found to be minimally perturbing and effective at monitoring binding events. Thus, we

chose to replace U1406 with the fluorescent U analogue **5** for our labeled A-site model. According to thermal denaturation studies, the substitution of U1406 by **5** appeared to be insignificantly destabilizing, as the modified construct **10** and unmodified control construct **9** had essentially the same melting temperatures within error. The photophysical properties of **5** remained adequate in the A-site construct. The emission maximum of **10** was the same as that of fluorescent ribonucleoside **5** at 395 nm; however, the emission quantum yield dropped from 0.16 to 0.03. Such diminished quantum yield upon incorporation into a RNA or DNA duplexes is not uncommon among fluorescent nucleosides.[45] Nevertheless, with an almost perfect spectral overlap between **1** and **2**, the "modified" Förster radius remains suitable for this assembly (R_0 = 20 Å). As for the acceptors in our FRET pair, conjugating 7-(diethylamino)coumarin **2** to the aminoglycosides had little effect on its photophysics; **11** and **12** resembled **2** in absorption and emission profiles and maintained a high emission quantum yield.

Titrating the labeled aminoglycosides into the donor-containing A-site construct yielded the expected spectral behavior, with continuous quenching of the donor's emission and concomitant enhancement of the acceptor's sensitized emission. As stated above, the ideal spectral overlap between **1** and **2** provides efficient energy transfer even with the reduced quantum yield of the donor's emission within the RNA construct. Based on the efficiency of energy transfer at saturation, the calculated FRET distance between the bound coumarin labeled neomycin **11** and tobramycin **12** to the modified RNA construct **10** are 14 ± 1 Å and 12 ± 2 Å, respectively. This is in good agreement with the distances predicted by examining the solid-state structures of these RNA–aminoglycoside complexes.[40,42] Consequently, binding and competition experiments faithfully reproduce the expected

trends in affinity of the diverse ligands tested and suggest that this FRET assembly is indeed a useful tool for the analysis of A-site binders. Furthermore, the discovery of two high RNA affinity of amino-aminoglycoside derivatives, previously untested for A-site binding, demonstrates the potential utility of this tool for the discovery of new A-site binders.

The results of FRET-monitored binding and displacement experiments reveal distinct advantages over traditional methods that rely on singly-labeled RNA constructs. While the latter can monitor the binding of small molecules to RNA targets, multiple ligand binding modes might limit their accuracy and dependability. In fact, the popular 2-AP-modified A-site construct,[56–59] while responding well to most aminoglycoside antibiotics, does not reliably detect the binding of neomycin, the strongest naturally occurring A-site binder.[36] In addition, singly-labeled RNA constructs are unable to consistently perform in evaluating competitive binding, as displacing off a bound ligand with an equipotent one is unlikely to be "visible" to a probe only reporting the "bound" or "unbound" status of the RNA construct. Förster Resonance Energy Transfer between strategically placed donors and acceptors, on the other hand, can clearly overcome such limitations, as unequivocally demonstrated by our results. As FRET is distance dependent, when the ligand is bound, the donor and acceptor would be brought together, leading to the increased emission of the acceptor and the quenching of the donor. If another small molecule were added to the mix and competed off the original ligand, the donor and acceptor would be parted, decreasing the emission of the acceptor and simultaneously increasing the fluorescence of the donor. A FRET based system, therefore, unambiguously provides both association and competitive dissociation information that is independent of specific binding modes. Most importantly, while singly-labeled RNA

constructs might generate false positive signals due to remote binding at a non-functional state (which could alter the environment of a responsive probe), a FRET based technique, as described here, requires specific binding to the A-site pocket. A nonspecific RNA binder, for example, would not be able to displace an antibiotic from its cognate recognition site, nor would it generate an intense FRET signal in monitoring direct binding experiments.

Summary and Implications

We have constructed a useful and effective FRET pair system for the evaluation of antibiotics binding to the bacterial ribosomal decoding site. It relies on the incorporation of a new emissive uridine analog into an A-site construct, which serves as a donor for a highly emissive coumarin acceptor that is attached to aminoglycosides. The strong dependence of FRET on the donor–acceptor distance is unambiguously used to detect the onset and offset of binding more effectively than a single chromophore system (which is also incapable of monitoring displacement and competition events). As a proof of concept, we have demonstrated binding of neomycin B and tobramycin, two A-site binding antibiotics displaying distinct affinity to their native ribosomal RNA target, and their competitive displacement by a variety of aminoglycoside antibiotics. It is worth noting here that antibacterial activity does not directly correlate with affinity to the A-site, which functions as a conformational switch.[18] This further justifies the use of multiple probes that facilitate screening of potential new A-site binders with diverse affinity. We note that our design is not limited to the A-site and its binders; related FRET assemblies can be developed for other RNA–ligand recognition events. Additionally, further development of ideal FRET pairs, composed of isomorphic nucleosides and corresponding minimally

perturbing FRET acceptors, will facilitate the analysis of other RNA targets with therapeutic potential.

Experimental Section

Materials. Unless otherwise specified, materials obtained from commercial suppliers were used without further purification. 2-Methoxy-5-aminobenzoic acid and spermidine were purchased from VWR. Neomycin, tobramycin, paromomycin, amikacin, apramycin, and hygromycin were purchased as their sulfate salts from Sigma-Aldrich and were converted into the corresponding neutral form by passing through DOWEX® MONOSPHERE® 550 Å (OH) anion exchange resin. The identities of the aminoglycosides were confirmed by mass measurements, ^{1}H-NMR, and ^{13}C-NMR . 7-(Diethylamino)coumarin-3-carboxylic acid was purchased from Sigma-Aldrich. Anhydrous pyridine, dichloroethane and acetonitrile were obtained from Fluka. Anhydrous *N,N*-diisopropylethylamine and triethylamine were obtained from Acros. NMR solvents were purchased from Cambridge Isotope Laboratories (Andover, MA). The unmodified oligonucleotide was purchased from Thermo Scientific. Standard phosphoramidites and solutions necessary for solid phase RNA synthesis were purchased from Glen Research. Oligonucleotides were purified by gel electrophoresis and desalted on a Sep-Pak (Waters Corporation). Chemicals for preparing buffer solutions were purchased from Fisher Biotech (enzyme grade). Autoclaved water was used in all fluorescence titrations.

Instrumentation. NMR spectra were recorded on a Varian Mercury 400 MHz spectrometer. Mass spectra were recorded at the UCSD Chemistry and Biochemistry Mass Spectrometry Facility, utilizing either a LCQDECA (Finnigan) ESI with a quadrapole ion trap or a MAT900XL (ThermoFinnigan) FAB double focusing mass

spectrometer. UV-Vis spectra were recorded on either an Agilent 8453 Diode Array Spectrometer. MALDI-TOF spectra were collected on a PE Biosystems Voyager-DE STR MALDI-TOF spectrometer in positive-ion, delayed-extraction mode. Reversed-phase HPLC (Vydac C18 column) purification and analysis were carried out using a Hewlett-Packard 1050 Series instrument. Steady-state fluorescence experiments were carried out in a microfluorescence cell with a path length of 1.0 cm (Hellma GmH & Co KG, Mullenheim, Germany) on a Jobin Yvon Horiba FluoroMax-3 luminescence spectrometer. A background spectrum (buffer) was subtracted from each sample. Modified oligonucleotides were synthesized on a Biosearch Cyclone Plus DNA synthesizer using a 0.2 µmole scale 500 Å CPG column. All hybridization and UV melting experiments were done with a Beckman-Coulter DU® 640 spectrometer with a high performance temperature controller and micro auto six holder.

Synthesis. 5-Methoxyquinazoline-2,4(1*H*,3*H*)-dione (1). Water (36 mL) and glacial acetic acid (0.7 mL) were added to 2-methoxy-5-aminobenzoic acid (1.00 g, 5.98 mmol). The slurry was stirred at 35 ℃ for 15 min. Sodium cyanate (0.97 g, 14.92 mmol) was dissolved in water (4 mL) and added slowly to the slurry. The reaction was stirred at 35 ℃ for 30 min. Sodium hydroxide (10.68 g, 267 mmol) was added slowly to the reaction. The reaction was cooled to room temperature. The pH was adjusted to 4 with concentrated hydrochloric acid. The white precipitate was collected and washed with water (200 mL). Product: white solid (1.03 g, 5.38 mmol, 90 % yield). ^{1}H-NMR (400 MHz, DMSO-d_6): δ 10.97 (s, NH, 1H), 10.87 (s, NH, 1H), 7.47 (t, J = 2.0 Hz, 1H), 6.68 (d, J = 14 Hz, 1H), 6.67 (d, J = 7.2 Hz, 1H), 3.79 (s, OCH_3, 3H); ^{13}C-NMR (100 MHz, DMSO-d_6): δ 161.54. 161.14, 150.81, 143.79,

136.05, 107.96, 105.57, 104.81, 56.53; ESI-MS calculated for $C_9H_9N_2O_3$ $[M+H]^+$ 193.1, found 193.1.

5-Methoxyquinazoline-2,4(1*H*,3*H*)-dione ribonucleoside (5). To a suspension of **1** (0.10 g, 0.52 mmol) in anhydrous acetonitrile (5 mL), *N,O*-Bis(trimethylsilyl)acetamide (0.64 mL, 2.6 mmol) was added dropwise under argon. The reaction was stirred at 25 ℃ for 2 h. The reaction temperature was raised to 50 ℃. TMSOTf (0.14 mL, 0.77 mmol) and β-D-ribofuranose-1-acetate-2,3,5-tribenzoate (0.26 g, 0.52 mmol) were added at the same time under argon. The reaction was stirred at 50 ℃ for 24 h. The reaction was cooled to room temperature and diluted with dichloromethane (10 mL). The solution was washed with saturated sodium bicarbonate and brine. The organic layer was dried over sodium sulfate. The solvent was removed under reduced pressure, and the crude product was dissolved in dioxane (5 mL) and transferred to a 200 mL pressure tube. Ammonium hydroxide (28%, 80 mL) was added. The reaction was stirred at 80 ℃ for 24 h. The solvent was removed was removed under reduced pressure, and the product was isolated by flash chromatography (88/12 dicholromethane/methanol). Product: white solid (0.14 g, 0.42 mmol, 81 % yield over two steps). ^{1}H-NMR (400 MHz, DMSO-d_6): δ 11.25 (s, NH, 1H), 7.55 (t, *J* = 8.4 Hz, 1H), 7.26 (d, *J* = 8.4 Hz, 1H), 6.88 (d, *J* = 8.8 Hz, 1H), 6.02 (d, *J* = 5.2 Hz, 1'-H, 1H), 5.22 (d, 2'-OH, 1H), 4.99 (b, 3'-OH, 1H), 4.94 (b, 5'-OH, 1H), 4.47 (t, *J* = 5.6 Hz, H-2', 1H), 4.08 (t, *J* = 5.6 Hz, H-3', 1H), 3.82 (s, OCH_3, 3H), 3.66 (m, H-4', 1H), 3.46-3.57 (m, H-5', 2H); ^{13}C-NMR (100 MHz, DMSO-d_6): δ 161.33, 160.08, 150.81, 142.99, 135.74, 109.25, 107.27, 106.47, 91.48, 85.02, 73.97, 69.47, 61.78, 56.74; ESI-MS calculated for $C_{14}H_{17}N_2O_7$ $[M+H]^+$ 325.1, found 325.1.

5′-Dimethoxytrityl-5-methoxyquinazoline-2,4(1*H*,3*H*)-dione ribonucleoside (6). Anhydrous pyridine (3 mL), anhydrous triethylamine (51 μL, 0.37 mmol) and 4,4′-

dimethoxytrityl chloride (0.12 g, 37 mmol) were added to **3** (0.10 g, 0.31 mmol) over argon. The reaction was stirred at room temperature for 8 hours and quenched with methanol (0.5 mL). The solvent was removed under reduced pressure, and the product was isolated by flash chromatography (1% triethylamine, 2% methanol, 97 % dichloromethane). Product: white solid (0.16 g, 0.26 mmol, 85 % yield). ^{1}H-NMR (400 MHz, $CDCl_3$): δ 7.46 – 7.16 (m, 12H), 6.97 (t, *J* = 8.8 Hz, 1H), 6.75 (d, *J* = 8.8 Hz, 2H), 6.60 (d, *J* = 8.4Hz, 1H), 6.32 (d, *J* = 5.6 Hz, 1H), 4.81 (t, *J* = 6.4 Hz, 1H), 4.57 (t, *J* = 6.4 Hz, 1H), 4.05 (br, 1H), 3.88 (s, 3H), 3.73 (s, 6H), 3.47−3.55 (m, 2H); ^{13}C-NMR (100 MHz, $CDCl_3$): δ 161.48, 160.50, 158.66, 150.60, 144.99, 142.68, 136.04, 135.97, 135.81, 130.48, 128.56, 128.02, 127.01, 113.30, 109.53, 106.56, 90.79, 86.48, 83.56, 69.96, 69.39, 63.42, 63.29, 56.58, 55.45, 53.13; ESI-MS calculated for $C_{35}H_{34}N_2NaO_9$ $[M+Na]^+$ 649.2, found 649.2.

2'-(Trisisopropylsiloxy)methyl-5'-dimethoxytrityl-5-methoxyquinazoline-2,4(1*H*,3*H*)-dione ribonucleoside (7). Anydrous dichloroethane (3 mL) and *N,N*-diisopropylethylamine (0.17 mL, 1.0 mmol) were added to **4** (0.20 g, 0.32 mmol). Dibutyltin dichloride (0.10 g, 0.33 mmol) was added to the reaction under argon and stirred at room temperature for 1 h. The reaction was placed into a 80 ℃ water bath and stirred for 10 min. (Triisopropylsiloxy)methyl chloride (87 µL, 38 mmol) was added, and the reaction was stirred at 80 ℃ for 15 min. The reaction was diluted with dichloromethane (10 mL) and poured into saturated sodium bicarbonate (15 mL). The mixture was stirred vigorously for 15 min. The organic layer was extracted, and the aqueous layer was washed with dichloromethane (5 mL). The organic layers were pooled and dried over sodium sulfate. The solvent was removed under reduced pressure, and the product was isolated by flash chromatography (1% triethylamine, 35% ethyl acetate, 64 % hexanes). Product: white foam (0.078 g, 0.01 mmol, 30 %

yield). ^{1}H-NMR (400 MHz, $CDCl_3$): δ 7.43 – 7.47 (m, 3H), 7.26 –7.34 (m, 4H), 7.18 – 7.26 (m, 4H), 7.06 (t, *J* = 8.4 Hz, 1H), 6.78 (d, *J* = 8.8 Hz, 3H), 6.67 (d, *J* = 8.4 Hz, 1H), 6.35 (d, *J* = 5.2 Hz, 1H), 5.07 (d, *J* = 4.8 Hz, 1H), 4.90 – 4.95 (m, 2H), 4.61 (t, *J* = 6.4 Hz, 1H), 4.07 (dd, J_1 = 4.0 Hz, J_2 = 3.2 Hz, 1H), 3.95 (s, 3H), 3.77 (s, 6H), 3.51 (dd, *J1* = 8.0 Hz, *J2* = 2.4 Hz, 1H), 3.39 (dd, *J1* = 6.4 Hz, *J2* = 4.0 Hz, 1H), 3.28 (q, *J* = 7.2 Hz, 1H), 2.70 (q, *J* = 6.8 Hz, 1H), 1.07 − 1.00 (m, 21H); ^{13}C-NMR (100 MHz, $CDCl_3$): δ 161.71, 160.02, 158.72, 149.92, 144.96, 143.91, 136.00, 135.94, 130.45, 128.53, 128.05, 127.08, 113.33, 109.71, 106.75, 106.13, 91.08, 88.99, 86.63, 83.70, 69.70, 63.44, 59.85, 56.71, 55.45, 29.95, 17.95, 12.02; ESI-MS calculated for $C_{45}H_{56}N_2NaO_{10}Si$ $[M+Na]^+$ 835.4, found 835.4.

3′-2-Cyanoethyldiisopropylphosphoramidite-2'-(Trisisopropylsiloxy)methyl-5′-dimethoxytrityl-5-methoxyquinazoline-2,4(1*H*,3*H*)-dione ribonucleoside (8). Anhydrous dichloromethane (0.6 mL) and *N,N*-diisopropylethylamine (0.13 mL, 0.75 mmol) were added to **5** (0.05 g, 0.062 mmol). The reaction was cooled on ice, and 2-cyanoethyl *N,N*-diisopropylchlorophosphoramidite (28 µL, 0.13 mmol) was added. The reaction was stirred at room temperature for 18 h. The solvent was removed under reduced pressure, and the product was isolated by flash chromatography (1% triethylamine, 15–30% ethyl acetate in hexanes). Product: white foam (0.038 g, 0.037 mmol, 60 % yield). ^{1}H-NMR (300 MHz, $CDCl_3$): δ 7.44 –7.46 (m, 3H), 7.32 – 7.34 (m, 4H), 7.22 – 7.26 (m, 4H), 7.07 (t, *J* = 8.4 Hz, 1H), 6.78 (d, *J* = 8.1 Hz, 3H), 6.68 (d, *J* = 8.4 Hz, 1H), 6.35 (d, *J* = 5.4 Hz, 1H), 5.07 (d, *J* = 4.2 Hz, 1H), 4.91 – 4.94 (m, 2H), 4.62 (t, *J* = 6.4 Hz, 1H), 4.07 (b, 1H), 3.96 (s, 3H), 3.78 (s, 6H), 3.51 (m, 1H), 3.40 (m, 1H), 2.81 (q, *J* = 6.9 Hz, 1H), 2.01 (b, 1H), 1.20 – 1.15 (m, 8H), 1.01 (d, *J* = 6.8 Hz, 4H), 0.92−0.89 (m, 21H); ^{13}C-NMR (100 MHz, $CDCl_3$): δ 171.37, 161.62, 160.19, 158.67, 158.65, 144.88, 136.10, 136.03, 135.88, 135.50, 130.47, 130.44, 128.67,

128.56, 127.99, 127.94, 127.05, 126.99, 117.94, 117.53, 113.23, 106.61, 106.23, 86.50, 86.46, 64.56, 60.60, 59.02, 56.66, 55.40, 55.35, 43.58, 43.45, 43.31, 43.19, 30.84, 29.90, 24.82, 24.75, 24.69, 21.24, 21.21, 19.23, 17.87, 17.81, 14.40, 13.92, 12.06, 12.01, 11.98; ESI-MS calculated for $C_{54}H_{73}N_4NaO_{11}PSi[M+Na]^+$ 1035.5 and $[M+K]^+$ 1051.4, found 1035.4 and 1051.4.

Boc_6-protected coumarin-labeled-neomycin (14). Anhydrous dichloromethane (300 µL), and 7-(diethylamino)coumarin-3-carboxylic acid (6.8 mg, 0.0263 mmol) were added to **13** (26.58 mg, 0.0219 mmol). To this, *N*-(3-dimethylaminopropyl)-N′-ethylcarbodiimide hydrochloride (5.03 mg, 0.0262 mmol), *N,N*-diisopropylethylamine (8.62 µL, 0.048 mmol), and 4-(dimethylamino)pyridine (5.8 mg, 0.026 mmol) were added. The reaction was stirred for 18 h. The solvent was removed under reduced pressure and the resulting solid was dissolved in ethyl acetate and washed with water and brine. The organic layer was dried over sodium sulfate and the solvent was removed under reduced pressure. The product was isolated by flash chromatography (3% methanol in dichloromethane). Product: yellow powder (26.8 mg, 0.0184 mmol, 84% yield). ^{1}H-NMR (400 MHz, CD_3OD): δ 8.66 (s, 1H), 7.45 (d, J = 10.5 Hz, 1H), 6.81 (d, J = 9 Hz, 1H), 6.56 (s, 1H), 5.34 (s, 1H), 5.12 (s, 1H), 5.02 (s, 1H), 4.28 (s, 3H), 4.09 – 4.06 (m, 1H), 4.01 – 3.98 (m, 1H), 3.90 – 3.87 (m, 4H), 3.82 – 3.79 (m, 2H), 3.76 – 3.71 (m, 4H), 3.61 – 3.44 (m, 24H), 3.34 – 3.15 (m, 2H), 2.63 – 2.57 (m, 1H), 1.99 – 1.89 (2H), 1.46 – 1.38 (m, 54H), 1.37 (t, J = 5 Hz, 6H); ^{13}C-NMR (100 MHz, CD_3CN): δ 164.66, 163.53, 158.72, 158.21, 157.86, 157.62, 157.29, 156.55, 154.02, 149.22, 132.40, 111.34, 110.52, 109.87, 109.06, 101.22, 99.69, 97.06, 80.24, 79.90, 79, 81, 79.64, 79.56, 74.99, 73.82, 70.88, 68.43, 56.72, 53.13, 51.65, 45.70, 45.28, 42.54, 41.44, 28.69, 12.67, 12.21; ESI-MS calculated for $C_{67}H_{108}N_8O_{27}$ $[M+Na]^+$ 1479.72, found 1479.71.

Coumarin-labeled-neomycin (11). Anhydrous dichloromethane (2 mL) and triisopropylsilane (200 µL) were added to **14** (26.8 mg, 0.0184 mmol). To this, trifluoroacetic acid was added (2 mL) and the reaction was stirred at RT for 15 min. The reaction was diluted with toluene (5 mL) and the solvent was removed under reduced pressure. The resulting solid was dissolved in water and washed with dichloromethane. The aqueous layer was dried concentrated under reduced pressure and further purified by reverse phase HPLC using a gradient of 10 – 30% acetonitrile (0.1% TFA) in water (0.1% TFA) over 30 min, and eluted at 14.78 min. Product: yellow powder (21.7 mg, 0.0151 mmol, 82 % yield). ^{1}H-NMR (400 MHz, D_2O): δ 8.65 (s, 1H), 7.62 (d, J = 9.2 Hz, 1H), 6.92 (d, J = 9.2 Hz, 1H), 6.67 (s, 1H), 5.96 (s, 1H), 5.36, (s, 1H), 5.29 (s, 1H), 4.49 (t, J = 5.5 Hz, 1H), 4.39 – 4.35 (m, 2H), 4.28 (t, J = 5 Hz, 1H), 4.21 (t, J = 3.5 Hz, 1H), 3.99 – 3.95 (m, 2H), 3.89 – 3.83 (m, 2H), 3.79 (s, 2H), 3.64 (t, J = 9.5 Hz, 1H), 3.59 (s, 1H), 3.56 – 3.51 (q, J_1 = 6.5 Hz, J_2 = 7.0 Hz, 4H), 3.33 (d, J = 4 Hz, 4H), 3.18 – 3.12 (m, 1H), 2.42 – 2.33 (m, 1H), 1.83 – 1.71 (m, 1H), 1.21 (t, J = 7 Hz, 6H); ^{13}C-NMR (100 MHz, D_2O): δ 166.19, 164.44, 163.17, 162.99 (J_1 = 27.8 Hz, J_2 = 58.4 Hz), 157.78, 154.03, 149.05, 131.83, 116.25 (J = 231 Hz, J_2 = 465 Hz), 115.08, 111.53, 110.43, 108.14, 106.39, 95.97, 95.44, 94.46, 79.69, 76.50, 73.24, 69.96, 67.52, 67.27, 50.7416, 48.49, 44.99, 40.32, 39.83, 11.44; ESI-MS calculated for $C_{37}H_{60}N_8O_{15}$ $[M+2H]^{2+}$ 429.21, $[M+H]^{+}$ 857.43, and $[M+Na]^{+}$ 879.41, found 429.35, 857.43, and 879.59.

Aminoglycoside Titrations. All titrations were performed with working solutions of 1.0×10^{-6} M **9b** in 20×10^{-6} M calcodylate buffer (pH 7.0, 1.0×10^{-1} M NaCl, 5.0×10^{-4} M EDTA). The solutions were heated to 75 ºC for 5 min, cooled to room temperature over 2 h, and placed on ice for 30 min prior to titrations. For binding studies, **10** was excited at 320 nm, and changes in emission upon titration with **11** or

12 were monitored at 395 nm and 473 nm. The concentrations of **11** and **12** were determined by UV absorbance at 400 nm (ε = 20,000 $M^{-1}cm^{-1}$). For competition studies, **11** or **12** was titrated into **10** until saturation. **10** was excited at 320 nm, and changes in emission upon displacement of **11** or **12** by aminoglycosides were monitored at 395 nm and 473 nm. EC_{50} and IC_{50} values were calculated using OriginPro 8 software by fitting a dose response curve (eq 1) to the fractional fluorescence saturation (F_s) plotted against the log of aminoglycoside (AG) concentration.

$$F_s = F_0 + (F_\infty[AG]^n)/([EC_{50}]^n + [AG]^n) \qquad (1)$$

F_i is the fluorescence intensity at each titration point. F_0 and F_∞ are the fluorescence intensity in the absence of aminoglycoside or at saturation, respectively, and *n* is the Hill coefficient or degree of cooperativity associated with the binding.

Acknowledgement. We thank the National Institutes of Health for their generous support (GM 069773), Mary Noé for her assistance with MALDI experiments and the National Science Foundation (instrumentation grants CHE-9709183 and CHE-0741968).

References

1. Green, R.; Noller, H. F. *Annu. Rev. Biochem.* **1997,** *66*, 679-716.

2. Puglisi, J. D.; Blanchard, S. C.; Dahlquist, K. D.; Eason, R. G.; Fourmy, D.; Lynch, S. R.; Recht, M. I.; Yoshizawa, S. Aminoglycosides Antibiotics and Decoding. In *The Ribosome: Structure, Function, Antibiotics, and Cellular Interactions*, Garrett, R. A.; Douthwaite, S. R.; Liljas, A.; Matheson, A. T.; Moore, P. B.; Noller, H. F., Eds. ASM Press: Washington D. C., 2000; pp 419-429.

3. Rodnina, M. V.; Wintermeyer, W. *Trends Biochem. Sci.* **2001,** *26*, 124-130.

4. Gale, E. F.; Cundliffe, E.; Renolds, P. E.; Richmond, M. H.; Waring, M. J. *The Molecular Basis of Antibiotic Action*. John Wiley & Sons: London, 1981.

5. Moazed, D.; Noller, H. F. *Nature* **1987,** *327*, 389-394.

6. Brodersen, D. E.; Clemons, W. M.; Carter, A. P.; Morgan-Warren, R. J.; Wimberly, B. T.; Ramakrishnan, V. *Cell* **2000,** *103*, 1143-1154.

7. Harms, J. M.; Bartels, H.; Schlünzen, F.; Yonath, A. *J. Cell. Sci.* **2003,** *116*, 1391-1393.

8. Wirmer, J.; Westhof, E.; Minoru, F. *Method Enzymol.* **2006,** *415*, 180-202.

9. Carter, A. P.; Clemons, W. M.; Brodersen, D. E.; Morgan-Warren, R. J.; Wimberly, B. T.; Ramakrishnan, V. *Nature* **2000,** *407*, 340-348.

10. Schlunzen, F.; Zarivach, R.; Harms, J.; Bashan, A.; Tocilj, A.; Albrecht, R.; Yonath, A.; Franceschi, F. *Nature* **2001,** *413*, 814-821.

11. Vicens, Q.; Westhof, E. *ChemBioChem* **2003,** *4*, 1018-1023.

12. Francois, B.; Russell, R. J. M.; Murray, J. B.; Aboul, N.; Masquida, B.; Vicens, Q.; Westhof, E. *Nucleic Acids Res.* **2005,** *33*, 5677-5690.

13. Purohit, P.; Stern, S. *Nature* **1994,** *370*, 659-662.

14. Fourmy, D.; Recht, M. I.; Blanchard, S. C.; Puglisi, J. D. *Science* **1996,** *274*, 1367-1371.

15. Yoshizawa, S.; Fourmy, D.; Puglisi, J. D. *EMBO J.* **1998,** *17*, 6437-6448.

16. Vicens, Q.; Westhof, E. *Structure* **2001,** *9*, 647-658.

17. Vicens, Q.; Westhof, E. *Chem. Biol.* **2002,** *9*, 747-755.

18. Kaul, M.; Barbieri, C. M.; Pilch, D. S. *J. Am. Chem. Soc.* **2006,** *128*, 1261-1271.

19. Chow, C. S.; Bogdan, F. M. *Chem. Rev.* **1997,** *97*, 1489-1514.

20. Gallego, J.; Varani, G. *Acc. Chem. Res.* **2001,** *34*, 836-843.

21. Tor, Y. *ChemBioChem* **2003,** *4*, 998-1007.

22. Hermann, T.; Tor, Y. *Expert Opin. Ther. Pat.* **2005,** *15*, 49-62.

23. Sutcliffe, J. A. *Curr. Opin. Microbiol.* **2005,** *8*, 534-542.

24. Hermann, T. *Biochimie* **2006,** *88*, 1021-1026.

25. Tor, Y. *Biochimie* **2006,** *88*, 1045-1051.

26. Hofstadler, S. A.; Griffey, R. H. *Chem. Rev.* **2001,** *101*, 377-390.

27. Haddad, J.; Kotra, L. P.; Llano-Sotelo, B.; Kim, C.; Azucena, E. F.; Liu, M.; Vakulenko, S. B.; Chow, C. S.; Mobashery, S. *J. Am. Chem. Soc.* **2002,** *124*, 3229-3237.

28. Kaul, M.; Barbieri, C. M.; Pilch, D. S. *J. Am. Chem. Soc.* **2004,** *126*, 3447-3453.

29. Shandrick, S.; Zhao, Q.; Han, Q.; Ayida, B. K.; Takahashi, M.; Winters, G. C.; Simonsen, K. B.; Vourloumis, D.; Hermann, T. *Angew. Chem., Int. Ed.* **2004,** *43*, 3177-3182.

30. Barbieri, C. M.; Kaul, M.; Pilch, D. S. *Tetrahedron* **2007,** *63*, 3567-3574.

31. Parsons, J.; Hermann, T. *Tetrahedron* **2007,** *63*, 3548-3552.

32. Chao, P.-W.; Chow, C. S. *Bioorg. Med. Chem.* **2007,** *15*, 3825-3831.

33. Aminoglycosides have been fluorescently labeled before, but typically by modifying the amines that are also essential for specific RNA binding. See: a) Wang, Y.; Hamasaki, K.; Rando, R. R. *Biochemistry* **1997,** *36,* 768-779. b) Hamasaki, K.; Rando, R. R. *Biochemistry* **1997,** *36,* 12323-12328. c) Hamasaki, K.; Ueno, A. *Bioorg. Med. Chem. Lett.* **2001,** *11,* 591-594.

34. See, however: a) Martí, A. A.; Jockusch, S.; Li, Z.; Ju, J.; Turro, N. J. *Nucl. Acids Res.* **2006,** *34,* e50. b) Borjesson, K.; Preus, S.; El-Sagheer, A. H.; Brown, T.; Albinsson, B.; Wilhelmsson, L. M. *J. Am. Chem. Soc.* **2009,** *131,* 4288-4293.

35. Greco, N. J.; Tor, Y. *J. Am. Chem. Soc.* **2005,** *127*, 10784-10785.

36. Srivatsan, S. G.; Tor, Y. *J. Am. Chem. Soc.* **2007,** *129*, 2044-2053.

37. Sinkeldam, R. W.; Greco, N. J.; Tor, Y. *ChemBioChem* **2008,** *9*, 706-709.

38. Srivatsan, S. G.; Greco, N., J.; Tor, Y. *Angew. Chem., Int. Ed.* **2008,** *47*, 6661-6665.

39. Srivatsan, S. G.; Weizman, H.; Tor, Y. *Org. Biomol. Chem.* **2008,** *6*, 1334-1338.

40. See supporting information for additional details.

41. Note the red-shifted absorption of **1** compared to the native nucleobases (l_{max} 250–270 nm) and the intense blue emission of the acceptor.

42. Based on crystal structures (PDB 2ET4 and 1LC4), the estimated distance between U1406 and the fluorophore on **11** or **12** would be less than 15 Å.

43. The minimal A-site construct has been demonstrated to be an autonomous RNA domain capable of mimicking the function and antibiotics recognition features of the 16S rRNA. See ref. 13 and 24.

44. Modification of U1406 with isosteric nucleosides has been demonstrated to have minimal detrimental effect on the A-site construct's folding and antibiotic recognition properties. See ref. 36.

45. Such a decrease in the quantum yield is common among fluorescent nucleosides upon incoporation into a RNA or DNA duplex. See ref 34-39 and a) Hawkins, M. E.; Pfleiderer, W.; Balis, F. M.; Porter, D.; Knutson, J. R. *Anal. Biochem.* **1997,** *244,* 86-95. b) Hawkins, M. E. *Cell Biochem. Biophys.* **2001,** *34,* 257-281.

46. Wang, H.; Tor, Y. *J. Am. Chem. Soc.* **1997,** *119*, 8734-8735.

47. a) Wang, H.; Tor, Y. *Angew. Chem. Int. Ed.* **1998,** *37,* 109-111. b) Michael, K.; Wang, H.; Tor, Y. *Bioorg. Med. Chem.* **1999,** *7,* 1361-1371. c) Boer, J.; Blount, K. F.; Luedtke, N. W.; Elson-Schwab, L.; Tor, Y. *Angew. Chem. Int. Ed.* **2005,** *44,* 927-932.

48. Schluenzen, F.; Tocilj, A.; Zarivach, R.; Harms, J.; Gluehmann, M.; Janell, D.; Bashan, A.; Bartels, H.; Agmon, I.; Franceschi, F.; Yonath, A. *Cell* **2000,** *102*, 615-623.

49. Yoshizawa, S.; Fourmy, D.; Puglisi, J. D. *Science* **1999,** *285*, 1722-1725.

50. O'Connor, M.; Brunelli, C. A.; Firpo, M. A.; Gregory, S. T.; Lieberman, K. R.; J. Stephen Lodmell; Moine, H.; Ryk, D. I. V.; Dahlberg, A. E. *Biochem. Cell Biol.* **1995,** *73*, 859-868.

51. Vicens, Q.; Westhof, E. *Structure* **2001,** *9*, 647-658.

52. Ogle, J. M.; Brodersen, D. E.; Clemons Jr., W. M.; Tarry, M. J.; Carter, A. P.; Ramakrishnan, V. *Science* **2001,** *292*, 897-902.

53. Vakulenko, S. B.; Mobashery, S. *Clin. Microbiol. Rev.* **2003,** *16*, 430-450.

54. Smolinski, M. S.; Hamburg, M. A.; Lederberg, J. *Microbial Threats to Health: Emergence, Detection, and Response*. National Academy of Sciences: Washington DC, 2003.

55. Wax, R. G.; Lewis, K.; Salyers, A.; Taber, H. *Bacterial Resistance to Antimicrobials*. 2nd ed.; CRC Press: Boca Raton, 2007.

56. Ward, D. C.; Reich, E.; Stryer, L. *J. Biol. Chem.* **1969,** *244*, 1228-1237.

57. Kawai, M.; Lee, M. J.; Evans, K. O.; Nordlund, T. M. *J. Fluorescence* **2001,** *11*, 23-32.

58. Jean, J. M.; Hall, K. B. *Proc. Natl. Acad. Sci. U.S.A.* **2001,** *98*, 37-41.

59. Rachofsky, E. L.; Osman, R.; Ross, J. B. A. *Biochemistry* **2001,** *40*, 946-956.

60. Tor, Y. *Tetrahedron* **2007**, 3425-3426.

61. Srivatsan, S. G.; Tor, Y. *Nat. Protocols* **2007,** *2*, 1547-1555.

62. Liu, H.; Gao, J.; Kool, E. T. *J. Org. Chem.* **2005,** *70*, 639-647.

63. Lee, A. H. F.; Kool, E. T. *J. Am. Chem. Soc.* **2006,** *128*, 9219-9230.

64. Godde, F.; Toulm, J.-J.; Moreau, S. *Biochemistry* **1998,** *37*, 13765-13775.

65. According to crystal structures PDB 2ET4 and 1LC4, the positions of modification on the aminoglycosides are not involved in binding to the RNA.

66. Gold, H. Fluorescent brightening agents. In *The Chemistry of Synthetic Dyes*, Venkataraman, K., Ed. Academic Press: New York, 1971; Vol. V, pp 535-542.

67. Baindur, N.; Triggle, D. J. *Med. Res. Rev.* **1994,** *14*, 591-664.

Chapter 1 is in full a reprint from: Xie, Y.; Dix, A. V.; Tor, Y. *J. Am. Chem. Soc.* **2010**, *131*, 17605–17614. The dissertation author is the main author and researcher for this work.

CHAPTER 2: Antibiotic Selectivity for Prokaryotic vs. Eukaryotic Decoding Sites

Abstract: A FRET assembly reports antibiotic affinities to two different RNA targets. A binder was labeled with a fluorophore that acts both as an acceptor for the emissive nucleoside on the bacterial A-site and a donor fluorophore for the terminally-labeled human A-site. Unlabeled drugs were used to dissociate the labeled antibiotic.

The bacterial ribosome is targeted by the majority of diverse and clinically significant antibiotics, from both nature and synthetic origin.[1,2] The fundamental role and abundance of this translational ribonucleoprotein machinery in every cell makes it an obvious target from evolutionary and functional perspectives, but it presents a formidable challenge for the discovery and development of new antibacterials.[2,3] In particular, the similarity between functional rRNA sites in prokaryotes and eukaryotes as well as between naïve and resistant bacteria could significantly limit the therapeutic potential of new agents. While numerous factors influence the efficacy and adverse effects of any drug, its affinity to competing targets is of fundamental significance. The ability to discern the inherent target selectivity of existing and candidate antibiotics could therefore critically impact the discovery and development of new agents.

Among the most commonly targeted ribosomal sites, the decoding (or A-site) rRNA is of particular significance.[4] It acts as a conformational switch that gauges codon–anticodon recognition.[5] Altering its conformational dynamics by bound

aminoglycosides, a large family of potent naturally occurring antibiotics, lowers the fidelity of protein synthesis, leading to bacterial cell death.[5,6] Although several "mutations" distinguish the prokaryotic 16S decoding site from the corresponding eukaryotic 18S sequence (Figure 2.1), biochemical and structural studies illustrate their similarity as well as their ability to bind aminoglycosides.[7] It has also been suggested that the clinical value of aminoglycosides could potentially depend on their ability to differentiate between the two closely related targets.[8,9] We therefore sought out a straightforward approach to determine the selectivity traits of A-site binders. Here we disclose the design and implementation of a FRET-based, three-component assembly that facilitates a rapid determination of the relative affinity of any given binder to the eukaryotic and prokaryotic decoding sites in a single experiment.

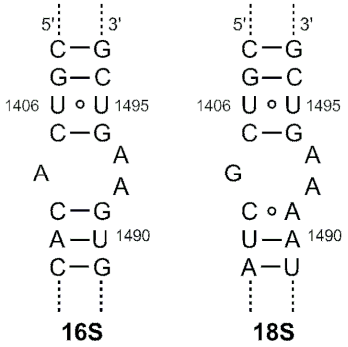

Figure 2.1: Sequences of the bacterial (16S) and human (18S) A-sites.

To accomplish this task, we have relied on the following components: 1) An aminoglycoside with modest affinity to both the prokaryotic and eukaryotic A-sites (e.g., kanamycin A), labeled with a small non-perturbing fluorophore (marked **F2**) at a position that is not essential for rRNA binding; 2) A bacterial 16S A-site RNA construct modified with an isomorphic, emissive nucleoside analog (labeled **F1**) at a position proximal to the binding site, but not part of it; and 3) A human 18S A-site rRNA construct labeled at its terminus with a third fluorophore (designated **F3**). To

generate unique spectral signatures for each binding event, the following photophysical conditions had to be met: 1) The isomorphic fluorescent probe on the bacterial A-site construct (**F1**) had to exclusively serve as a FRET donor to the fluorophore placed on the aminoglycoside antibiotic (**F2**); and 2) The latter, in turn, had to specifically serve as a FRET donor for the terminal fluorophore on the human A-site (**F3**).

The experiment is conceptually illustrated in Figure 2.2. When all three components, the tagged aminoglycoside and the two RNA constructs, are equilibrated together, the presence of the antibiotic on the 16S RNA can be visualized by selectively exciting **F1**, and monitoring the emission of **F2**. The fraction of the ligand bound to the 18S A-site can be visualized by selectively exciting **F2** and detecting the emission of the acceptor **F3**. More importantly, when an unlabeled competitor small-molecule is added to the mixture and displaces the tagged antibiotic from the 16S A-site, the acceptor emission **F2** is lost, while the fluorescence of the donor nucleoside **F1** is recovered. Accordingly, when the “placeholder” tagged antibiotic is displaced from the 18S A-site, the emission of **F2** is recovered, and the sensitized emission of **F3** is lost. Based on the relative changes in these spectral signatures, measured in one cuvette by following two different emission spectra, the affinity and selectivity of any candidate antibiotic can be determined, as it displaces the tagged ligand on the two related A-sites, according to its inherent selectivity.

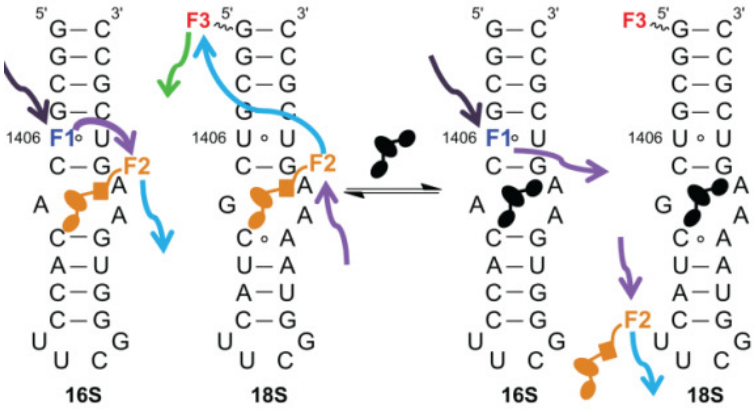

Figure 2.2: Secondary structures for the 27-base RNA models of the 16S and 18S A-sites. U1406 of the 16S A-site is replaced with an isosteric emissive nucleoside analogue as a donor (**F1**); the place-holding molecule is tagged with an appropriate fluorophore (**F2**); the 18S A-site is tagged with an acceptor (**F3**) to match the labeled "place-holder" (**F2**). The affinity and selectivity of unlabeled small-molecules for either A-sites can be accurately monitored using FRET, as the place-holder is displaced.

The selection of the two orthogonal, yet matched, FRET pairs is critical to the success of this experiment. We identified 5-methoxyquinazoline-2,4-(*1H,3H*)-dione **F1**, an emissive uracil analogue, serving as a suitable donor for 7-diethylaminocoumarin-3-carboxylic acid **F2** (Figure 2.3).[10] We also found that Dy547 **F3** is a fitting acceptor for **F2**. The absorption maximum of **F1** at 320 nm, corresponds to a wavelength with a minimal absorbance of **F2**, while the emission of **F1**, centered at 395 nm (Φ_F = 0.16), overlaps perfectly with the absorption band of **F2**, which emits at 473 nm (Φ_F = 0.83) (Figure 2.3).[10] The emission of **F2**, in turn, overlaps with the absorption band of **F3**, which exhibits absorption maxima at 516 and 549 nm and emits at 563 nm (Φ_F = 0.27). Importantly, the molar extinction coefficients of **F3** are negligible at the absorption maxima of **F1** and **F2**. The critical Förster radii for the **F1**/**F2** (R_o = 27Å) and **F2**/**F3** (R_o = 45Å) pairs are apt for the proposed experiments.[11] According to previous results[12] and control experiments,[13] the replacement of U1406 in the 16S A-site by a fluorescent nucleoside does not significantly impact the antibiotic affinity to the model construct.

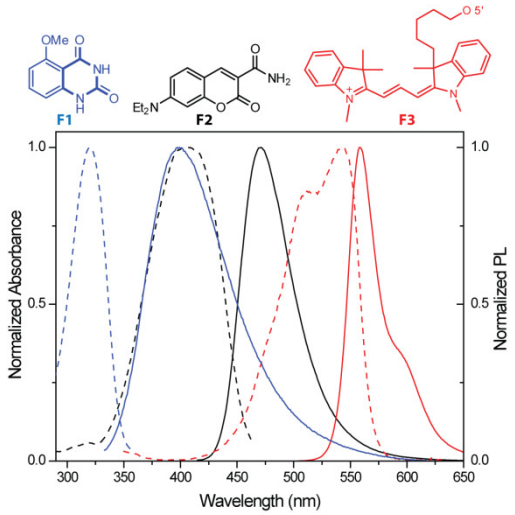

Figure 2.3: Structures of **F1** (blue), **F2** (black), and **F3** (red) along with their normalized absorption (---) and emission spectra (—) in water.

For competition studies, the two A-site constructs were pre-folded separately, mixed together and then treated with a two-mole equivalent of coumarin labeled kanamycin A (Figure 2.4).[13] Diverse antibiotics were titrated into this mixture of the kanamycin-bound A-sites. These include several aminoglycosides, semi-synthetic aminoglycosides, as well as a macrolide, a peptide and an oxazolidinone-based antibiotic (Figure 2.4). The relative emissions of all fluorophores were independently recorded. As productive competition on the 16S A-site advances, the emission intensity of the fluorescent nucleobase **F1** increased, while the emission of the coumarin **F2** was lost (Figure 2.5).[13] For the 18S A-site, the emission intensity of the Dy547 **F3** was reduced. Plotting the fractional fluorescence saturation against the concentration of the competitors yields titration curves (Figure 2.5).[13] Table 1 provides the IC_{50} values for both the 16S and 18S A-sites and the selectivity ratio.

In agreement with reported trends, aminoglycoside antibiotics, including neomycin, tobramycin and paromomycin, do not display a dramatic preference for either the bacterial or human A-sites (Table 2.1).[7c,9,13–15] Among all aminoglycosides

tested, neomycin B is the only antibiotic that displays selectivity for the prokaryotic 16S A-site. Neamine, the core aminoglycosidic pharmacophore, binds quite strongly to the eukaryotic A-site. Its affinity to the latter is comparable to that of neomycin, yet its affinity to the prokaryotic A-site is significantly lower than neomycin's and is comparable to that of tobramycin. Notably, the loss of the neobiosamine moiety from neomycin lowers the preference for the prokaryotic A-site. Two semi-synthetic amino-aminoglycoside derivatives were also tested. Amino-tobramycin and amino-kanamycin A,[16] while displaying higher affinity for both A-sites compared to the parent antibiotics, still prefer the 18S RNA, with amino-kanamycin A displaying a higher 16S/18S selectivity ratio.

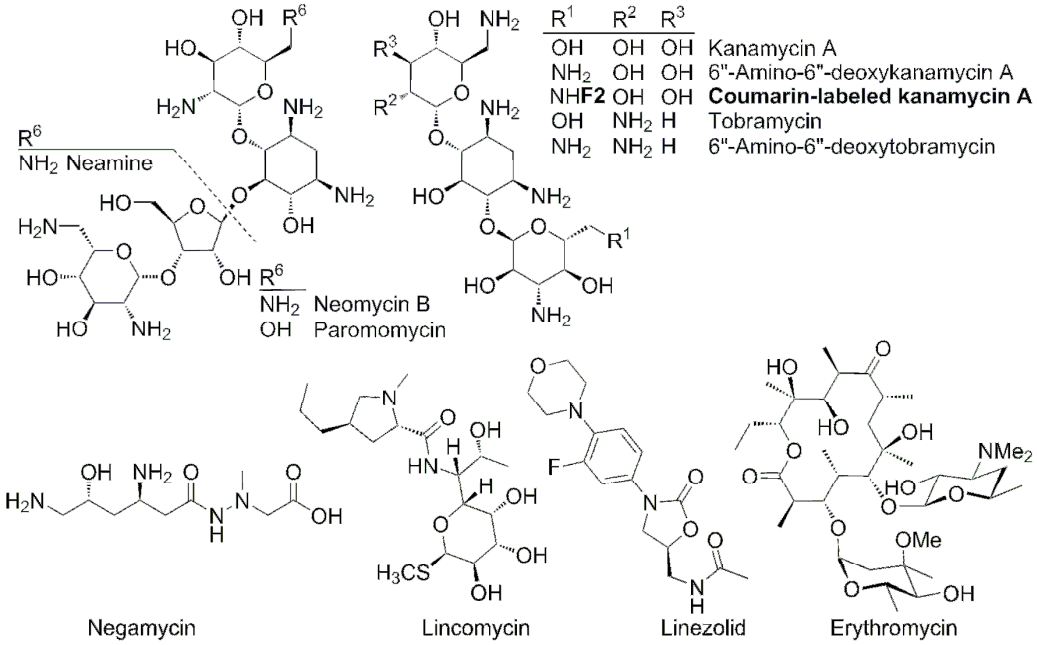

Figure 2.4: rRNA targeting antibiotics studied.

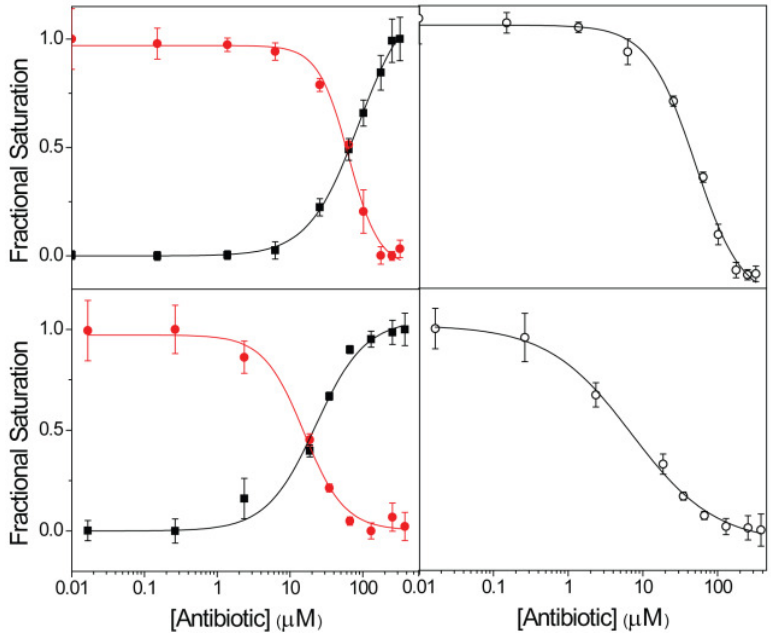

Figure 2.5: Fractional fluorescence saturation of the donor **F1** (■) in the labeled 16S A-site, the emissive fluorophore **F2** (●) tagged to kanamycin A, and the emissive acceptor **F3** (○) of the 18S A-site in studying the binding of: (top) negamycin; (bottom) neamine. Conditions: 16S RNA (5×10^{-7} M), 18S RNA (5×10^{-7} M), coumarin-labeled-kanamycin A (2.2×10^{-6} M), cacodylate buffer pH 7.0 (2.0×10^{-2} M), NaCl (1.0×10^{-1} M).[13]

Negamycin, a dipeptide antibiotic, is an active bactericidal compound discovered in the 1970s.[17] Interestingly, little is certain about its mode of action. While originally identified as a protein synthesis inhibitor with enhanced miscoding activity, suggestive of A-site binding,[18] a recent crystal structure implied that its bactericidal potency could result from its binding to the wall of the peptide exit tunnel of the large ribosomal subunit.[19] Our data show that negamycin indeed binds both A-sites with affinities similar to that of kanamycin A. Finally, a macrolide (erythromycin), a lincosamide (lincomycin) and an oxazolidinone-based antibiotic (linezolid), showed, as expected, little or no binding to both ribosomal RNA targets (Table 2.1).

While it is tempting to compare selectivity ratios and apparent antibiotic toxicities, the nature of latter complicates such correlations. In particular, the diverse organisms, conditions and antibiotics used hinder the development of firm relationships.[20] There is, however, a qualitative correlation between the trends

observed for aminoglycoside antibiotics (Table 2.1) and their nephrotoxicity as evaluated in rat models. Paromomycin, while displaying a lower affinity for the 18S A-site compared to neomycin, has a higher histopathology score than neomycin (Figure A2.1).[13, 21] This could potentially be explained by its higher preference for the human A-site. Similarly, tobramycin has a five-fold lower affinity for the 18S A-site compared to neomycin, but is more selective for the eukaryotic A-site. These opposing factors could contribute to its low histopathology score, which is similar to that of neomycin.

Table 2.1: IC_{50} Values of Antibiotics for the 16S and 18S A-sites.[a]

Antibiotics	16S A-Site (10^{-6} M)	18S A-Site (10^{-6} M)	Selectivity Ratio
Neomycin B	2.8 (± 0.3)	4.7 (± 0.2)	0.60
Tobramycin	20.2 (± 0.4)	19.5 (± 0.3)	1.0
Paromomycin	9 (± 1)	8.0 (± 0.6)	1.1
Kanamycin A	75 (± 3)	46 (± 2)	1.6
Amino-Tobramycin	4.2 (± 0.4)	3.8 (± 0.4)	1.1
Amino-Kanamycin A	11.9 (± 0.4)	4.7 (± 0.3)	2.5
Negamycin	62 (± 5)	42 (± 3)	1.5
Neamine	18 (± 2)	6 (± 1)	3
Erythromycin	1880 (± 10)	1750 (± 10)	1.1
Lincomycin	$> 8.5 \times 10^3$	$> 8.5 \times 10^3$	—
Linezolid	$> 9.6 \times 10^3$	$> 9.6 \times 10^3$	—

[a] Conditions as listed in Figure 5.

In summary, we have developed a three-component assembly that facilitates the real-time evaluation of the affinity and selectivity of small-molecules to the bacterial and human ribosomal decoding sites in a single experiment. It relies on two orthogonal FRET pairs that act in concert to generate unique spectral signatures for each binding and displacement events. The wide spectral window spanned by the absorption and emission of the selected chromophores (ca. 300–600 nm) and their sequential overlap are facilitated by the use of an isomorphic nucleoside analogue, which provides a short wavelength trigger while maintaining the bacterial RNA fold. In addition to assessing the selectivity traits of known antibiotics, we were able to

gather affinity and selectivity data for compounds that are not generally considered to be A-site binders. While we note, naturally, that a multitude of factors contribute to the apparent toxicity of any drug, where target selectivity is just one of them, having a simple tool to screen derivatives prior to advancing them into preclinical evaluation,[22] could prove highly valuable.

Acknowledgement. We thank the National Institutes of Health (GM 069773) for support and the National Science Foundation (instrumentation grants CHE-9709183 and CHE-0741968). We are grateful to Drs. Yuzuru Akamatsu and Yoshikazu Takahashi for a generous gift of negamycin and to Dr. Keiichi Ajito for helpful discussions.

References

1. E. F. Gale, E. Cundliffe, P. E. Renolds, M. H. Richmond and M. J. Waring, *The Molecular Basis of Antibiotic Action*; John Wiley & Sons: London, 1981; R. Green and H. F. Noller, *Annu. Rev. Biochem.,* 1997, **66**, 679–716; J. D. Puglisi, S. C. Blanchard, K. D. Dahlquist, R. G. Eason, D. Fourmy, S. R. Lynch, M. I. Recht and S. Yoshizawa, in *The Ribosome: Structure, Function, Antibiotics, and Cellular Interactions,* ed. R. A. Garrett, S. R. Douthwaite, A. Liljas, A. T. Matheson, P. B. Moore and H. F. Noller, ASM Press: Washington D. C., 2000, pp 419–429; M. V. Rodnina and W. Wintermeyer, *Trends Biochem. Sci.,* 2001, **26**, 124–130.

2. A. Yonath, *Annu. Rev. Biochem.,* 2005, **74**, 649–679.

3. B. T. Wimberly, *Curr. Opin. Investig. Drugs,* 2009, **10**, 750–765.

4. J. Gallego and G. Varani, *Acc. Chem. Res.,* 2001, **34**, 836–843; Y. Tor, *ChemBioChem,* 2003, **4**, 998–1007; J. A. Sutcliffe, *Curr. Opin. Microbiol.,* 2005, **8**, 534–542; T. Hermann, *Biochimie,* 2006, **88**, 1021–1026. Y. Tor, *Biochimie,* 2006, **88**, 1045–1051.

5. A. P. Carter, W. M. Clemons, D. E. Brodersen, R. J. Morgan-Warren, B. T. Wimberly and V. Ramakrishnan, *Nature,* 2000, **407**, 340–348; B. T. Wimberly, D. E. Brodersen, W. M. Clemons, R. J. Morgan-Warren, A. P. Carter, C. Vonrheins,

T. Hartschk and V. Ramakrishnan, *Nature,* 2000, **407**, 327–339; J. M. Ogle, D. E. Brodersen, W. M. Clemons Jr., M. J. Tarry, A. P. Carter and V. Ramakrishnan, *Science*, 2001, **292,** 897–902; Q. Vicens, and E. Westhof, *Structure,* 2001, **9**, 647–658.

6. F. Schlunzen, R. Zarivach, J. Harms, A. Bashan, A. Tocilj, R. Albrecht, A. Yonath and F. Franceschi, *Nature,* 2001, **413**, 814–821; Q. Vicens and E. Westhof, *ChemBioChem,* 2003, **4**, 1018–1023; B. Francois, R. J. M. Russell, J. B. Murray, N. Aboul, B. Masquida, Q. Vicens and E. Westhof, *Nucleic Acids Res.,* 2005, **33**, 5677–5690; M. Kaul, C. M. Barbieri and D. S. Pilch, *J. Am. Chem. Soc.,* 2006, **128**, 1261–1271.

7. (*a*) M. I. Recht, S. Douthwaite and J. D. Puglisi, *Embo J,* 1999, **18**, 3133–3138; (*b*) S. R. Lynch and J. D. Puglisi, *J. Mol. Biol.,* 2001, **306**, 1037–1058; (*c*) M. Kaul, C. M. Barbieri and D. S. Pilch, *J. Mol. Biol.,* 2005, **346**, 119–134; (*d*) S. N. Hobbie, S. K. Kalapala, S. Akshay, C. Bruell, S. Schmidt, S. Dabow, A. Vasella, P. Sander and E. C. Bottger, *Nucl. Acids Res.,* 2007, **35**, 6086–6093.

8. S. N. Hobbie, S. Akshay, S. K. Kalapala, C. M. Bruell, D. Shcherbakov and E. C. Böttger, *Proc. Natl. Acad. Sci. U.S.A.,* 2008, **105**, 20888–20893.

9. (*a*) D. H. Ryu and R. R. Rando, *Bioorg. Med. Chem.,* 2001, **9**, 2601–2608; (*b*) C. Wong, M. Hendrix, E. S. Priestley, and W. A. Greenberg, *Chem. Biol.,* 1998, **5**, 397–406.

10. Y. Xie, A. V. Dix and Y. Tor, *J. Am. Chem. Soc.,* 2009, **131**, 17605–17614.

11. Based on crystal structures (PDB 2ESI, 1FYO, and 1FYP), the estimated distance between **F1** and **F2** is less than 10 Å, while the distance between **F2** and **F3** is less than 20 Å.

12. S. G. Srivatsan and Y. Tor, *J. Am. Chem. Soc.,* 2007, **129**, 2044–2053.

13. See supporting information for additional details.

14. R. H. Griffey, S. A. Hofstalder, K. A. Sannes-Lowery, D. J. Ecker and S. T. Crooke, *Proc. Natl. Acad. Sci. U.S.A.,* 1999, **96**, 10129–10133.

15. Few studies have examined aminoglycoside affinity to both A-sites under identical experimental conditions.

16. H. Wang and Y. Tor, *Angew. Chem. Int. Ed.,* 1998, **37**, 109–111.

17. S. Mizuno, K. Nitta and H. Umezawa *J. Antibiot.,* 1970, **23**, 581–588; S. Kondo, S. Shibahara, S. Takahashi, K. Maeda, H. Umezawa and M. Ohno, *J. Am. Chem. Soc.,* 1971, **93**, 6305–6306.

18. M. Arakawa, M. Shiozuka, Y. Nakayama, T. Hara, M. Hamada, S. I. Kondo, D. Ikeda, Y. Takahashi, R. Sawa, Y. Nonomura, K. Sheykholeslami, K. Kondo, K. Kaga, T. Kitamura, Y. Suzuki-Miyagoe, S. I. Takeda and R. Matsuda, *J.*

Biochem., 2003, **134**, 751–758; I. Daishiro, *Treatment of muscular dystrophy by negamycin. Improving productivity of negamycin in bacteria.*, 2004.

19. S. J. Schroeder, G. Blaha and P. B. Moore, *Antimicrob. Agents Ch.,* 2007, **51**, 4462–4465.

20. J. M. Wilhelm, J. J. Jessop and S. E. Pettitt, *Biochemistry,* 1978, **17**, 1149–1153; J. M. Wilhelm, S. E. Pettitt and J. J. Jessop, *Biochemistry,* 1978, **17**, 1143–1149; E. C. Böttger, B. Springer, T. Prammananan, Y. Kidan and P. Sander, *EMBO rep.,* 2001, **2**, 318–323.

21. C. F. Kostrub, R. Diokno, J. B. Aggen, G. H. Miller, J. K. Judice and P. M. Tulkens, in *19th European Congress of Clinical Microbiology and Infectious Diseases*; Blackwell Publishing: Helsinki, Finland, 2009.

22. C. C. Gradinaru, D. O. Marushchak, M. Samim, and U. J. Krull, *Analyst*, 2010, **135**, 452–459.

Chapter 2 is in full a reprint of: Xie, Y.; Dix, A. V.; Tor, Y. *Chem. Commun*. **2010**, *64*, 5542–5544. The dissertation author is the main author and researcher for this work.

CHAPTER 3: Fluorescent Ribonucleoside as a FRET Acceptor for Tryptophan in Native Proteins

---

While tryptophan is one of the most infrequently occurring amino acids in proteins,[1] it is recurrently found at, or near, the recognition domains of RNA–binding proteins.[2,3] As such recognition phenomena are crucial for transcriptional regulation, mRNA maturation, RNA interference, translation and more, the development of biophysical tools for evaluating these fundamental processes is of key importance. Although the indole chromophore imparts useful emissive properties,[4] tryptophan's emission is highly sensitive to diverse environmental perturbations,[5] a feature that, while useful, can significantly complicate the readout and interpretation of binding events. Förster resonance energy transfer (FRET) pairs can overcome many of such difficulties, but the incorporation of large "classical FRET" chromophores into the binding partners can perturb these delicate recognition events. We have therefore sought to develop a new isomorphic ribonucleoside analog that could seamlessly be incorporated into RNA and serve as a FRET acceptor to tryptophan residues residing on RNA binding proteins. Here we report the design, synthesis, photophysical characteristics and implementation of an emissive uridine mimic that fulfills such stringent requirements and facilitates the study of RNA–protein interactions.

A fundamental challenge in developing minimally perturbing nucleoside analogs is the tendency of small aromatic chromophores to display high emission energies, which frequently overlap with the emission bands of native amino acids.[4] A molecular feature that can help alleviate such constraints and facilitate FRET pairing with Trp is the implementation of a charge-transfer character upon the chromophore,

a mechanism frequently found in naturally occurring visibly emissive fluorophores (e.g., oxyluciferin and GFP).[4] Heterocycle **1** and the corresponding ribonucleoside **2** (Scheme 3.1), containing an electron-rich ring fused into the electron-deficient pyrimidine, fulfill this requirement and display red shifted absorption and emission bands. The extinction coefficient of **2** at 280 nm, the absorption maximum of tryptophan, is minimal, while the emission of tryptophan, centered around 350 nm (Φ_F=0.12), overlaps well with the absorption band of **2**, which emits at 440 nm (Φ_F=0.42 ± 0.04), suggesting excellent FRET pairing (Figure 3.1). The critical Förster radius (R_0) was experimentally determined to be 22 Å, a suitable value for monitoring RNA–protein recognition events.

To unequivocally demonstrate the utility of this ribonucleoside and its FRET pairing with natively occurring Trp residues we have investigated the Rev peptide and the Rev Responsive Element (RRE), its cognate RNA target. Rev, a key HIV-1 regulatory protein, is involved in the transport of immature viral mRNAs from the nucleus to the cytoplasm of the host cell.[9–13] The specific and high-affinity binding between the protein and RNA have been attributed to the arginine-rich domain of Rev and Stem-loop IIB of the RRE (Figure 3.2).[11,12,14] While the Rev protein contains a single Trp residue (Trp_{45}), it is strategically embedded within the RNA binding domain.[12] Residue U66 of the RRE, neighboring the binding site, was therefore identified as the RNA modification position.[6,15,18]

To incorporate the modified nucleoside into RNA oligonucleotides, phosphoramidite **3** was prepared (Scheme 3.1). 5-Aminoquinazoline-2,4(1*H*,3*H*)-dione **1** was glycosylated to provide the modified nucleoside **2** after saponification of all esters. Protection of the 5'-hydroxyl as the 4,4'-dimethoxytrityl (DMTr) derivative and the 2'-hydroxyl as the (trisisopropylsiloxy)methyl (TOM) derivative, followed by

phosphitylation of the 3'-hydroxyl, provided phosphoramidite **3** (Scheme 3.1). Standard solid-phase oligonucleotide synthesis was utilized to prepare the 34-mer RRE model construct, where U66 is replaced by **2** (Figure 3.2). The oligonucleotide was purified by PAGE, and MALDI-TOF mass spectrometry confirmed its full length and the presence of the intact emissive nucleoside **2** (Figure A3.1). The folded RNA construct was as stable as the unmodified RRE construct (T_m = 66 and 68 ± 1 ℃, respectively, cacodylate buffer, pH 7.0), suggesting minimal perturbation by the unnatural nucleosides. The emission profile of the emissive RRE construct, excited at 350 nm, resembled that of the parent nucleoside in water, albeit with a lower quantum yield.[8]

Scheme 3.1: Heterocycle **1**, ribonucleoside **2** and the corresponding phosphoramidite **3**.[a]

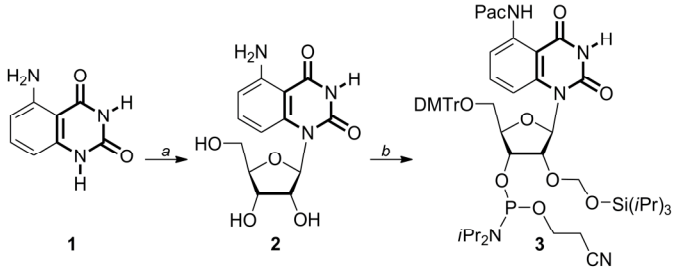

[a] *Reagents*: (a) (i) *N,O*-bis(trimethylsilyl)acetamide, $CF_3SO_3Si(CH_3)_3$, β-D-ribofuranose 1-acetate 2,3,5-tribenzoate, CH_3CN; (ii) conc. NH_4OH, 81%. (b) (i) $(CH_3)_3SiCl$, phenoxyacetic anhydride, H_2O, conc. NH_4OH, pyridine, 75%; (ii) DMTrCl, Et_3N, pyridine, 82%; (iii) *i*Pr_2NEt, *n*Bu_2SnCl_2, *i*Pr_3SiOCH_2Cl, $ClCH_2CH_2Cl$, 30%; (iv) *i*Pr_2NEt, (*i*Pr_2N)P(Cl)O-CH_2CH_2CN, $ClCH_2CH_2Cl$, 60%.[8]

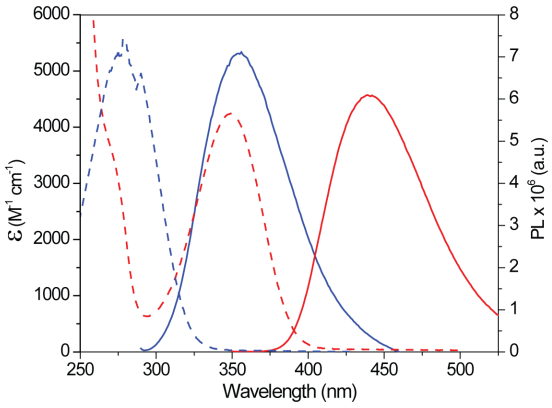

Figure 3.1: Absorption (---) and emission (—) spectra of tryptophan (blue) and **2** (red) in water.[8]

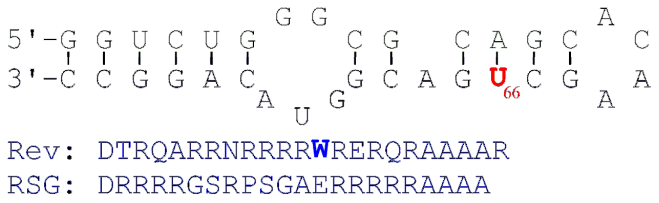

Figure 3.2: The model RRE construct and peptides used for FRET binding and competition experiments.

Titration of the Rev peptide into the emissive RRE construct, excited at 280 nm (Trp's absorption maximum), showed continuous decrease of tryptophan emission at 350 nm and increase of the acceptor emission at 440 nm (Figure 3.3). At equimolar concentrations (and saturation), the emission intensities of acceptor **2** and Trp are comparable (Figure 3.3 inset). Based on FRET efficiency, the calculated distance between nucleoside **2** and Trp is 18 (± 3) Å, which is in good agreement with our structure-based, estimated distance between U66 and Trp.[18]

Titration curves, generated by plotting the normalized sensitized emission of acceptor **2**, yield a K_D value of 7 (± 5) × 10^{-8} M, in agreement with literature values (Figure 3.4A).[12,16b,19] To ensure that the modification of U66 with **2** is non-perturbing, fluorescence anisotropy measurments[20] were used to independently determine the affinity of Rev to both the modified (K_D = 2 ± 1 × 10^{-8}) and unmodified RRE (K_D = 3 ± 2 × 10^{-8}) (Figure A3.2).[8] The placement of **2** at U66 of the RRE is therefore non-perturbing and enables a faithful monitoring of peptide–RNA binding.

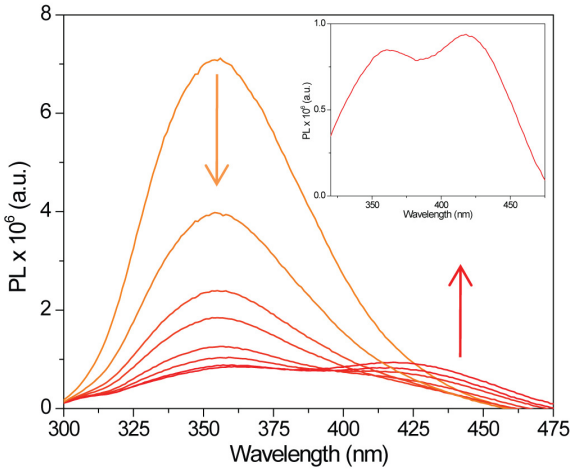

Figure 3.3: Fluorescence response as labeled RRE is titrated into Rev. Inset shows the emission spectrum at saturation. Conditions: Rev (1.0×10^{-5} M), cacodylate buffer pH 7.0 (2.0×10^{-2} M), NaCl (1.0×10^{-1} M).

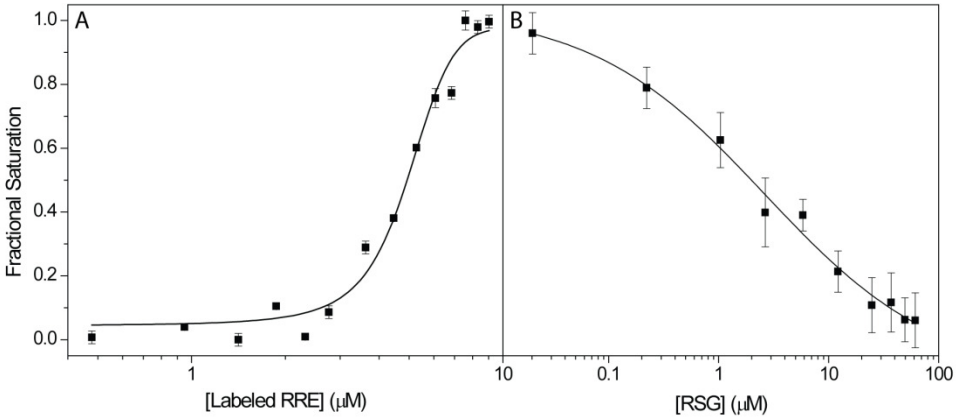

Figure 3.4: Normalized response of the fluorescent acceptor (■) in the labeled RRE in the following experiments: (A) titration of the labeled RRE into Rev; (B) displacement of Rev from the labeled RRE by RSG. Conditions same as Figure 3.

Importantly, this FRET system can also report the displacement of the Rev peptide by competing ligands that do not contain tryptophan residues. The RSG peptide (Figure 3.2) is known to have a higher affinity to the RRE compared to Rev.[11] As RSG is titrated into a solution containing the Rev bound labeled-RRE, the emission of fluorescent nucleoside **2**, acting as the acceptor, decreases (Figure 3.4B). Fitting the decreased FRET efficiency yields an IC_{50} value of 2 ($\pm$ 1) $\times 10^{-6}$ M, confirming that it is indeed a tighter binder than Rev.[8]

In conclusion, we have identified a fluorescent nucleoside analogue **2** that is suitable for monitoring protein–RNA interactions via Förster resonance energy transfer with native Trp residues. To the best of our knowledge, **2** is the first isomorphic and visibly-emitting nucleoside that can efficiently pair with tryptophan. While illustrated here for the HIV-1 Rev and RRE, the Trp–**2** FRET pair is likely to find utility in exploring other systems due to the high abundance of Trp residues within the RNA recognition domains of proteins.[21]

Acknowledgement. We thank the National Institutes of Health for their generous support (GM 069773), Mary Noé for her assistance with MALDI experiments and the National Science Foundation (instrumentation grant CHE-0741968). We also thank Prof. Akif Tezcan for the use of his fluorescence spectrometer.

References

1. Brooks, D. J.; Fresco, J. R.; Lesk, A. M.; Singh, M. *Mol. Biol. Evol.* **2002**, *19*, 1645–1655.

2. Baker, C. M.; Grant, H. G. *Biopolymers* **2007**, *85*, 456–470.

3. Trp (1.02 % average amino acid composition; Ref.1) is 1.74 times more frequently found at RNA binding sites than protein surfaces, while Phe's value is the same. Trp is also 2.56 times more frequently found at RNA binding sites than DNA binding sites (Ref. 2).

4. Sinkeldam, R. W.; Greco, N. J.; Tor, Y. *Chem. Rev.* **2010**, *110*, 2579–2619.

5. Lakowicz, J. R. In *Principles of fluorescence spectroscopy*; 3rd. ed.; Springer: New York, 2006, p 530–535.

6. Quinazoline ring substituent type and position influence the emission wavelength of the nucleoside analogue. Substituents in position 7, versus 5, cause a blue shifted emission (Ref. 7), while reduction of the electron donating property of the amino substituent also produces a hypsochromic emission shift (Ref. 8).

7. Xie, Y.; Dix, A. V.; Tor, Y. *J. Am. Chem. Soc.* **2009**, *131*, 17605–17614; Xie, Y.; Dix, A. V.; Tor, Y. *Chem. Commun.* **2010**, *64*, 5542–5544.

8. See supporting information for additional details.

9. Vaishnav, Y. N.; Wong-Staal, F. *Annu. Rev. Biochem.* **1991**, *60*, 577–630; Frankel, A. D.; Young, J. A. T. *Annu. Rev. Biochem.* **1998**, *67*, 1–25; Pollard, V. W.; Malim, M. H. *Annu. Rev. Microbiol.* **1998**, *52*, 491–532.

10. Pavlakis, G. N.; Felber, B. K. *New Biol.* **1990**, *2*, 20–31; Heguy, A. *Front Biosci.* **1997**, *1*, 283–297.; Cao, Y.; Liu, X.; Clercq, E. D. *Curr. HIV Res.* **2009**, *7*, 101–108.

11. Battiste, J. L.; Mao, H.; Rao, N. S.; Tan, R.; Muhandiram, D. R.; Kay, L. E.; Frankel, A. D.; Williamson, J. R. *Science* **1996**, *273*, 1547–1551.

12. Gosser, Y.; Hermann, T.; Majumdar, A.; Hu, W.; Frederick, R.; Jiang, F.; Xu, W.; Patel, D. J. *Nat. Struc. Biol.* **2001**, *8*, 146–150.

13. Luedtke, N. W.; Tor, Y. *Biopolymers* **2003**, *70*, 103–119.

14. Pljevaljčića, G.; Millara, D. P. *Method Enzymol.* **2008**, *450*, 233–252; Nalin, C. M.; Purcell, R. D.; Antelman, D.; Mueller, D.; Tomchak, L.; Wegrzynski, B.; McCarney, E.; Toome, V.; Kramer, R.; Hsu, M.-C. *Proc. Natl. Acad. Sci. U.S.A.* **1990**, *87*, 7593–7597.

15. Fluorescently labeled constructs and displacement assays have been previously used to explore the Rev–RRE system; nearly all have employed large fluorophores. See Refs: 13, 16, 17, and 19.

16. (a) Lacourciere, K. A.; Stivers, J. T.; Marino, J. P. *Biochemistry* **2000**, *39*, 5630–5641; (b) Zhang, J.; Umemoto, S.; Nakatani, K. *J. Am. Chem. Soc.* **2010**, *132*, 3660–3661.

17. Luedtke, N.; Tor, Y. *Angew. Chem. Int. Ed.* **2000**, *39*, 1788–1790.

18. The estimated distance between U66 in RRE and Trp on the Rev peptide is about 20Å (1ETF).

19. Zhang, C.-y.; Johnson, L. W. *J. Am. Chem. Soc.* **2006**, *128*, 5324–5325.

20. Bucci, E.; Steiner, R. F. *Biophys. Chem.* **1988**, *30*, 199–224.

21. Site-directed mutagenesis can be used to engineer Trp into the RNA binding domain of proteins lacking such residues.

Chapter 3 is in full a reprint of: Xie, Y.; Maxson, T.; Tor, Y. Fluorescent ribonucleoside as a FRET acceptor for tryptophan in native proteins. *J. Am. Chem. Soc.* **2010**, In Press. The dissertation author is the main author and researcher for this work.

CHAPTER 4: Fluorescent Nucleoside Analogue Displays Enhanced Emission upon Pairing with Guanine

---

Abstract. A fluorescent nucleobase analogue, 7-aminoquinazoline-2,4-(1H,3H)- dione, is incorporated into a DNA oligonucleotide and senses mismatched pairing by displaying G-specific fluorescence enhancement.

Single nucleotide polymorphisms (SNPs),[1] mutated base pairs, have been linked to specific diseases or susceptibility to particular therapeutics.[2] While there are several developed and commercialized approaches for detecting SNPs,[3] many recent advancements have centered around the design of base-discriminating fluorescent nucleosides.[4–7] Following incorporation into DNA hybridization probes and duplex formation with target oligonucleotides, the emissive nucleosides display characteristic photophysical signature, depending on their pairing partner.[4,8]

To develop base discriminating probes, it is important to identify heterocycles that are structurally similar to native nucleobases and capable of Watson–Crick pairing. Red shifted absorption spectra relative to native nucleosides, permiting selective excitation, are highly desirable. The emission of the fluorescent analogs should be sensitive to its hybridization microenvironment, and perhaps more importantly, fluorescence enhancement rather than quenching should be associated with positive identification of a mismatch. Detecting mismatched G residues has, therefore, presented a challenege, as guanine, being the easiest nucleobase to oxidize,[9–10] frequently quenches the emission of most

commonly used fluorophores.[11–14] Here we present a new fluorescent pyrimidine analog that, when hybridized against G, displays an enhanced emission when compared to a perfect duplex or all other mismatches.

In accordance with our design principles,[5,6,7] we have synthesized a polarizable nucleobase, 7-aminoquinazoline-2,4-(1*H*,3*H*)-dione **1** and the corresponding 2'-deoxynucleoside **2**, which contain an electron-rich ring fused into an electron-deficient pyrimidine (Scheme 4.1). We surmise that placing the electron donating amine group in a conjugated position to the pyrimidine's carbonyl would facilitate a charge transfer transition and greater sensitivity of the photophysical characteristics to environmental changes. To assess the nucleoside's sensitivity to its microenviornment, its absorption and emission spectra were recorded in solvents of distinct polarity (Figure 4.1 and Table 4.1). Solvent polarity has little effect on the lowest energy absorption maximun of nucleoside **2** (316 ± 1 nm), but the absorption band around 288 nm is sensitive to polarity changes, resulting in a greater molar absorptivity in nonpolar solvents.

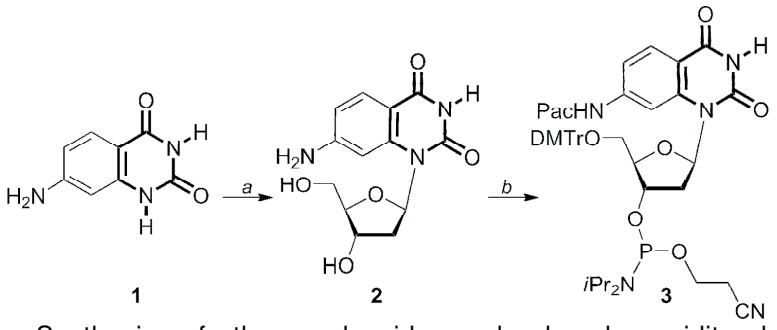

Scheme 4.1: Synthesis of the nucleoside and phosphoramidite based on 7-aminoquinazoline-2,4-(1*H*,3*H*)-dione. *Reagents*: (*a*) (*i*) $(NH_4)_2SO_4$, *N,O*-bis(trimethylsilyl)acetamide, $CF_3SO_3Si(CH_3)_3$, 2-D-3,5-di-*O*-p-toluoyl-α-L-erythro-pentofuranosyl chloride, CH_3CN; (*ii*) conc. NH_4OH, 40%. (*b*) (*i*) $(CH_3)_3SiCl$, phenoxyacetic anhydride, H_2O, conc. NH_4OH, pyridine, 75%; (*ii*) DMTrCl, Et_3N, pyridine, 85%; (*iii*) *i*Pr_2NEt, (*i*Pr_2N)P(Cl)O-CH_2CH_2CN, $ClCH_2CH_2Cl$, 65%.[15]

Table 4.1: Photophysical data of nucleoside **2**[a]

Solvent	$E_T(30)$[b]	λ_{abs}[c]/nm	λ_{em}/nm	I_{rel}[d]
Water	65.3	316	361	1.0
Methanol	55.7	316	352	3.2
Acetonitrile	45.9	316	339	3.1
Dichloromethane	40.9	316	338	2.6
Dioxane	36.4	316	336	2.9

[a] Conditions for absorption and emission spectra: 5.0 and 0.5 × 10^{-5} M, respectively. [b]Units are Kcal mol^{-1}. [c]The lowest energy maximum is given. [d]Relative emission intensity with respect to intensity in water.

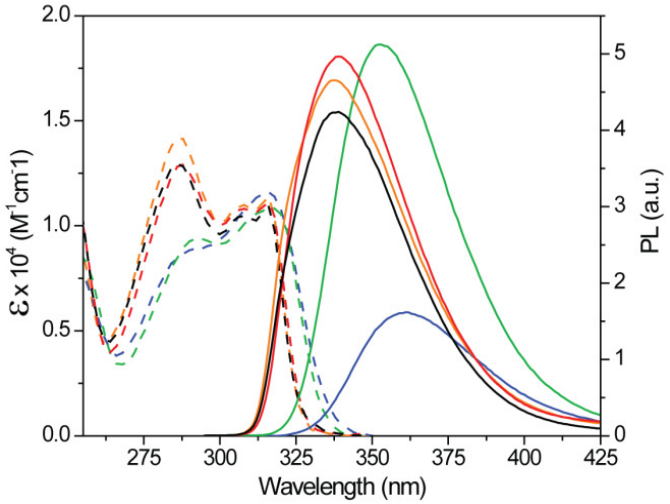

Figure 4.1: Absorption (---) and emission (—) spectra of nucleoside **2** in water (blue), methanol (green), acetonitrile (red), dioxane (orange), and dichloromethane (black).

Importantly, both emission wavelength and intensity are affected by solvent polarity. In water, the most polar solvent examined, **2** exhibits the most quenched and bathohromically shifted emission band (Figure 4.1), peaking around 361 nm (Φ_F=0.039 ± 0.006, Stoke Shift=3.9 × 10^3 cm^{-1}). In methanol, nucleoside **2** displays the most intense emission with an emission band at 352 nm (Φ_F=0.14 ± 0.01, Stoke Shift=3.2 × 10^3 cm^{-1}). In solvents of lower polarity, **2** shows more hyperchromically shifted emission with decreasing intensity (Table 4.1, Stoke Shifts=1.9–2.1 × 10^3 cm^{-1}). These observations suggest an enlarged dipole and charge transfer character of the excited state when compared to the ground state.

To incorporate the non native nucleoside into a DNA oligonucleotide, phosphoramidite **3** was prepared (Scheme 4.1). 7-Aminoquinazoline-2,4(1*H*,3*H*)-

dione **1** was glycosylated to provide the modified nucleoside **2** after saponification of all esters and isolation of the β-anomer (X-ray Structure: Figure A4.1 and Table A4.1).[15] Protection of the 5'-hydroxyl as the 4,4'-dimethoxytrityl (DMTr) derivative, followed by phosphitylation of the 3'-hydroxyl, provided phosphoramidite **3** (Scheme 4.1). Standard solid-phase oligonucleotide synthesis was utilized to prepare the 13-mer DNA construct **4**, where probe **2** was placed in the middle of the sequence (Figure 4.2). The oligonucleotide was purified by PAGE, and MALDI-TOF mass spectrometry confirmed its full length and the presence of the intact emissive nucleoside **2** (Figure A4.2).[15]

4 5'-GCG ATG **2** GTA GCG-3'
5 3'-CGC TAC **G** CAT CGC-5'
6 3'-CGC TAC **T** CAT CGC-5'
7 3'-CGC TAC **A** CAT CGC-5'
8 3'-CGC TAC **C** CAT CGC-5'

Figure 4.2: Synthesized oligonucleotide **4** and oligonucleotides used in hybridization and fluorescence experiments.

The fluorescent single strand DNA oligonucleotide **4** exhibits a similar, albeit broader, emission profile to the nucleoside in water with an emission band around 361 nm. Upon hybridization to its complement **7,** a quenched emission at 363 nm is observed (Figure 4.3 and Table 4.2). In contrast, when the fluorescently labeled DNA oligonucleotide **4** is hybridized with **5**, an oligonucleotide with a G mismatch opposite nucleoside **2**, its emission is greatly enhanced and hyperchromically shifted to 353 nm, displaying an emission more similar to nucleoside **2** in methanol (Figure 4.3 and Table 4.2). Other oligonucleotides with mismatches (**6** and **8**) failed to produce a dramatic increase in fluorescence intensity and all displayed emission bands around 362 nm, where nucleoside **2** emits in water. Importantly, thermal denaturation measurements (Table 4.2 and

Figure A4.4),[15] determined by monitoring changes in absorbance at 260 nm as a function of temperature, show that stable duplexes were formed for all oligonucleotide pairs. The T_m value for the complemented duplex **4 • 7** (T_m = 57 ± 1 ºC) was within error of the melting temperature of an unmodified control duplex (T_m =58 ± 1 ºC) (Figure A4.3–A4.4). Hybridization with DNA strands containing mismatches do show, as expected, destabilization (Table 4.2).

Table 4.2: Photophysical data of oligonucleotide **4** and its duplexes.[a]

Duplexes	**4 • 5**	**4 • 6**	**4 • 7**	**4 • 8**
λ_{em}/nm	353	362	361	365
I_{rel}[b]	2.2	1.3	1.0	0.8
TM/ºC	50±1	51±1	57±1	50±1

[a] Conditions: 5.0 × 10^{-6} M in 2.0 × 10^{-2} M Na_3PO_4, pH 7.0. [b]Relative emission intensity with respect to intensity of **4 • 7**.

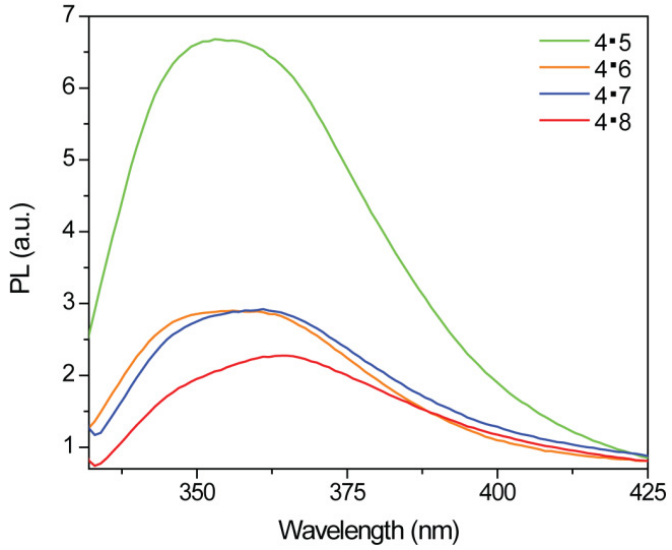

Figure 4.3: Emission spectra of **4 • 5** (green), **4 • 6** (orange), **4 •7** (blue), and **4 • 8** (red). Conditions same as listed in Table 2.

Nucleoside **2** uniquely reports the presence of a G mismatch with nearly a two-fold enhanced emission, compared to its emission intensity in a perfect duplex when found opposite A, a feature rarely seen with isosteric/isomorphic fluorescent nucleoside analogs.[11–14] While the underlying molecular factors governing this behavior are unclear at present, a disparity between the redox potential of G and

the new nucleobase, coupled to environmental factors influencing the solvation of the modified base are likely to be influencing factors. It is tempting to speculate that a formation of a wobble G•**2** pair anchors the emissive nucleoside in a partially exposed geometry, while still preserving a partially stacked and desolvated microenvironment.[16–18] Regardless of these putative structural features, the results reported here demonstrate that new emissive nucleobase analogs can display unique photophysical features and potentially find utility for mismatch detection.

Acknowledgments. We thank the National Institutes of Health for their generous support (GM 069773), the National Science Foundation (instrumentation grant CHE-0741968), and Nicholas Greco for his assistance with MALDI experiments.

References

1. (a) A. J. Brookes, *Gene*, 1999, **234**, 177; (b) A. Chakravarti, *Nat. Genet. Suppl.*, 1999, **21**, 56; (c) H. Haga, Y. Yamada, Y. Ohnishi, Y. Nakamura and T. Tanaka, *J. Hum. Genet.*, 2002, **47**, 605; (d) The International HapMap Consortium, *Nature*, 2005, vol. 437, p. 1299.

2. (a) J. J. McCarthy and R. Hilfiker, *Nat. Biotechnol.*, 2000, **18**, 505; (b) T. Pastinen and T. J. Hudson, *Science*, 2004, **306**, 647.

3. (a) P. L. Paris, J. M. Langenhan and E. T. Kool, *Nucleic Acids Res.*, 1998, **26**, 3789; (b) C. S. Carlson, T. L. Newman and D. A. Nickerson, *Curr. Opin. Chem. Biol.*, 2001, **5**, 78; (c) A. O. Crockett and C. T. Wittwer, *Anal. Biochem.*, 2001, **290**, 89; (d) P. Y. Kwok, *Annu. Rev. Genomics Hum. Genet.*, 2001, **2**, 235; (e) R. M. Twyman, *Curr. Top. Med. Chem.*, 2004, **4**, 1423; (f) K. Nakatani, *ChemBioChem*, 2004, **5**, 1623; (g) Y. Suh and C. Cantor, *Mutat. Res.*, 2005, **573**, 1; (h) B. Sobrino, M. Brion and A. Carracedo, *Forensic Sci. Int.*, 2005, **154**, 181; (i) L. Valis, N. Amann and H.-A. Wagenknecht, *Org. Biomol. Chem.*, 2005, **3**, 36; (j) U. Asseline, M. Chassignol, Y. Aubert and V. Roig, *Org. Biomol. Chem.*, 2006, **4**, 1949; (k) A. Friedrich, J. D. Hoheisel, N. Marmé and J.-P. Knemeyer, *FEBS Lett.*, 2007, **581**, 1644; (l) T. S. Kumar, J. Wengel and P. J. Hrdlicka, *ChemBioChem*, 2007, **8**, 1122; (m) E. Ergen, M. Weber, J. Jacob, A. Herrmann and K. Müllen, *Chem.–Eur. J.*, 2006, **12**, 3707.

4. A. Okamoto, Y. Saito and I. Saito, *Photochem. Photobiol. C: Photochem. Rev.*, 2005, **6**, 108.

5. R. W. Sinkeldam, N. J. Greco and Y. Tor, *Chem. Rev.*, 2010, **110**, 2579.

6. N. J. Greco and Y. Tor, *J. Am. Chem. Soc.*, 2005, **127**, 10784.

7. Y. Tor, *Tetrahedron*, 2007, **63**, 3425.

8. (a) K. Tainaka, K. Tanaka, S. Ikeda, K.-I. Nishiza, T. Unzai, Y. Fujiwara, I. Saito and A. Okamoto, *J. Am. Chem. Soc.*, 2007, **129**, 4776; (b) Y. Saito, E. Mizuno, S. S. Bag, I. Suzuka and I. Saito, *Chem. Commun.*, 2007, 4492; (c) F. Takei,H. Suda,M.Hagihara, J. Zhang, A. Kobori and K. Nakatani, *Chem.–Eur. J.*, 2007, **13**, 4452; (d) R. H. E. Hudson and A. Ghorbani-Choghamarani, *Org. Biomol. Chem.*, 2007, **5**, 1845; (e) J. H. Ryu, Y. J. Seo, T. Hwang, J. Y. Lee and B. H. Kim, *Tetrahedron*, 2007, **63**, 3538; (f) Q. Xiao, R. T. Ranasinghe, A. M. P. Tang and T. Brown, *Tetrahedron*, 2007, **63**, 3483; (g) S. G. Srivatsan, H. Weizman and Y. Tor, *Org. Biomol. Chem.*, 2008, **6**, 1334.

9. L. Kittler, G. Lober, F. A. Gollmick and H. Berg, *Bioelectroch. Bioener.*, 1980, **7**, 503.

10. H. Xie, D. Yang, A. Heller and Z. Gao, *Biophys. J.*, 2007, **92**, L70.

11. C. A. M. Seidel, A. Schulz and M. H. M. Sauer, *J. Phys. Chem.*, 1996, **100**, 5541.

12. C. Dohno and I. Saito, *ChemBioChem*, 2005, **6**, 1075.

13. M. A. Behlke, L. Huang, L. Bogh, S. Rose and E. J. Devor, *Fluorescence Quenching by Proximal G-bases*, Integrated DNA Technologies, 2005.

14. (a) W. Wang, C. Chen, M. X. Qian and X. S. Zhao, *Sensor. Actuat. B-Chem.*, 2008, **129**, 211; (b) M. Mizuta, K. Seio, A. Ohkubo and M. Sekine, *J. Phys. Chem. B.,* 2009, **113**, 9562.

15. See supporting information for additional details.

16. D. Rabinovich, T. Haran, M. Eisenstein and Z. Shakked, *J. Mol. Biol.*, 1988, **200**, 151.

17. M. W. Kalnik, M. Kouchakdjian, B. F. L. Li, P. F. Swann and D. J. Patel, *Biochemistry*, 1988, **27**, 108.

18. P. Modrich, *Annu. Rev. Biochem.*, 1987, **56**, 435.

Chapter 4 is in full a reprint of: Xie, Y.; Maxson, T.; Tor, Y. Fluorescent nucleoside analogue displays enhanced emission upon pairing with guanine. Submitted. The dissertation author is the main author and researcher for this work.

CHAPTER 5: Synthesis and Applications of Quinazoline-Based Fluorescent Nucleoside Analogues

---

Abstract: A family of quinazoline-based fluorescent nucleoside analogues is synthesized for photophysical studies and applications in probing nucleic acid structure, dynamics, and recognition. These size-expanded U analogues exhibit fluorescent emission wavelengths that span 155 nm, from 335 to 490 nm. Each nucleoside has unique characteristic response to changes in its microenvironment. These distinct features lead to a variety of functions, which have been explored. However, many applications have yet to be discovered, especially since a single nucleoside may serve multiple roles. We have recently found that the nucleoside based on 7-aminoquinazoline-2,4(1*H*,3*H*)-dione detect the presence of a bulge in RNA, which is in addition to its utility in FRET assays for examining RNA–peptide interactions.

Introduction

In the biological processes that support life, DNA and RNA undergo numerous structural changes, interact with countless molecules and regulate various biochemical reactions. Tools that monitor and detect the activities of nucleic acids have the potential to help us better understand diseases, evaluate drugs and discover therapies. A powerful technique for monitoring biological events is fluorescence spectroscopy, which can sensitively and selectively provide both local and global information,[1] such as the flipping of one nucleobase in an oligonucleotide[2,3] or the structural change as a RNA strand folds.[4,5] Native nucleobases lack sufficient

emissive properties,[6] as they have fluorescence quantum yields of 0.03 %, or less, and lifetimes on the picoseconds scale.[7] While such photophysical characteristics are advantageous for the stability of our genetic material,[6] they present a challenge for photophysical studies aimed to elucidate the dynamics, structure, and recognition events involving nucleic acids. Over the years, chemists and biologists have met this challenge by developing fluorescent nucleoside analogs that are isomorphic and isosteric to their native counterparts.[8–15] Research groups have shown that fluorescent nucleosides have great potential in detecting single nucleotide polymorphisms,[12, 16,17] DNA lesions,[18] RNA-ligand binding events,[19–21] RNA-protein interactions,[22,23] and protein toxins.[24]

While quite a few fluorescent nucleosides have been developed, the number of these small, non-perturbing probes does not match the large extensive libraries of larger chromophores that are available for studying macromolecular interactions. This difference is most apparent when comparing the number of available non-isosteric FRET pairs with the handful of FRET pairs that include fluorescent nucleoside analogues. Thus, for investigating the interactions of oligonucleotides with small molecules, or specific domains of proteins, there is a limited array of choices in tuning experiments to report across a large range of emission wavelengths. For example, out of the large pool of proteins that act upon nucleic acids, only a relatively small number of them have been studied with fluorescence. The difficulty in enhancing the emissive properties of nucleic acids with fluorescent analogs lies in the strict size and shape requirements for minimizing perturbations to the native system being studied. On top of that, probes must maintain favorable photophysical properties, such as a sufficient quantum yield, sensitivity to changes in

the microenvironment and red shifted absorption maximum to allow selective excitation.

We decided to meet this challenge by focusing our efforts in exploring size-expanded U analogues (Figure 5.1) that are simple to synthesize from commercially available compounds and have high incorporation efficiency into oligonucleotides via solid phase synthesis. The core nucleoside **1** is based on the heterocycle quinazoline-2,4(1*H*,3*H*)-dione, which is a superior isostere to similar benzo[g]quinazoline nucleobases[25,26] that have been utilized previously. We introduced different electron donating substituents to the core nucleobase in either position 5 or 7 of the quinazoline ring, producing six nucleosides **2**–**9** (Figure 5.1). Each of these analogues has unique photophysical properties, which suggests diverse applications in biological assays. A few of these applications have already been explored,[20–22] but many possibilities have yet to be explored. In this article, we will summarize the photophysical properties of each nucleoside and discuss their potential behavior in oligonucleotides that pertain to solving problems in biological chemistry.

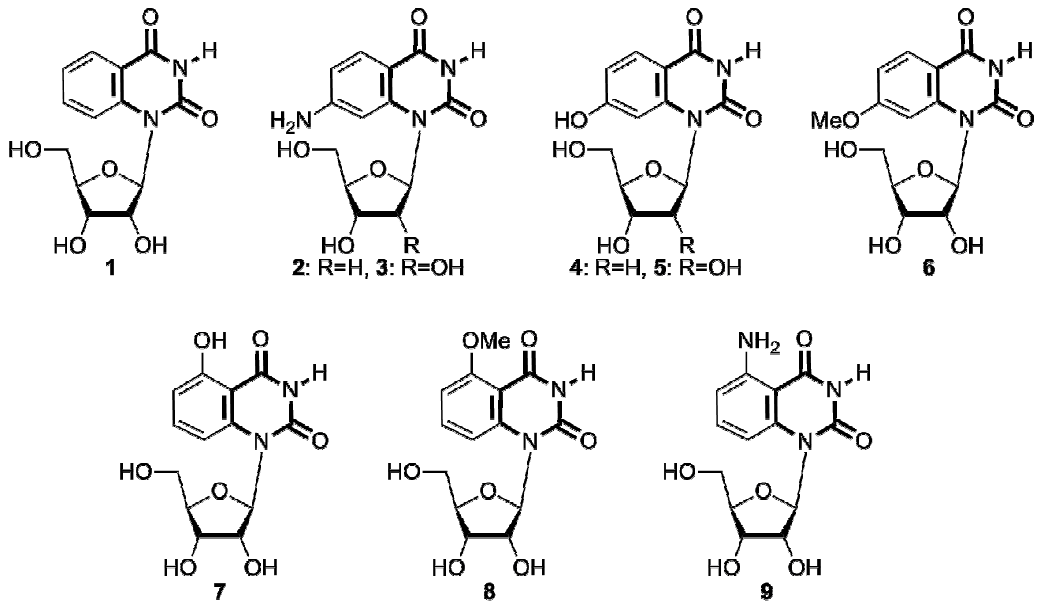

Figure 5.1: Quinazoline-based fluorescent nucleoside analogues developed for photophysical experiments.

Results

Design, Synthesis and Photophysical Properties of the Nucleosides. The design of the nucleosides involved fusing an electron-rich ring onto an electron-deficient pyrimidine (Figure 5.1), which should enhance the photophysical properties of the naturally non-emissive uracil base. Addition of the electron donating substituents are intended to enlarge the dipole of the fluorophore and thereby lead to charge transfer, or proton transfer in the case of nucleoside **8**, in the excited state. Such excited state interactions can lead to marked sensitivity to variations in the microenvironment, a phenomenon that has been observed in numerous probes.[27–29] Furthermore, our modified, size-expanded U analogues still maintain the hydrogen bonding face necessary for base pairing.

The synthesis of the nucleosides starts with the cyclization of commercially available 5-aminobenzoic acids, containing the appropriate substituent at the 2 or 4

positions, with sodium cyanate (Scheme 5.1). Ribonucleosides are synthesized from glycosylation of the formed nucleobase followed by saponification of the protection groups. Deoxyribonucleosides are similarly formed, where the nucleobases are glycosylated and deprotected. However, careful isolation of the β anomer is necessary, as glycosylation produces both α and β anomers (Figure A5.1–A5.2, Table A5.1–A5.2).[20–22, 30]

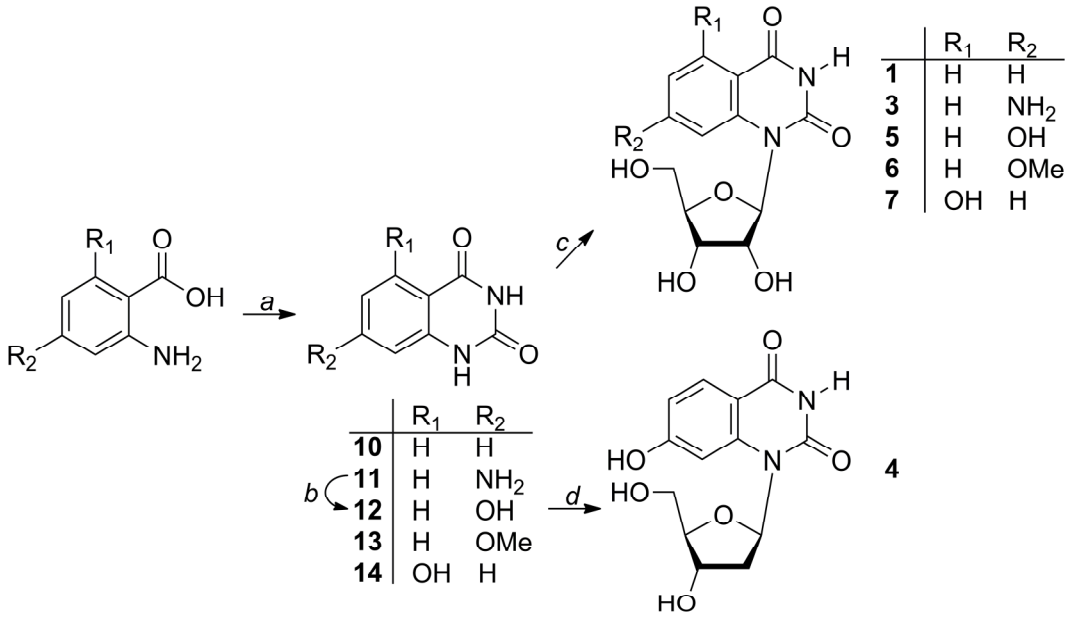

Scheme 5.1: Synthesis of the nucleosides. *Reagents*: (*a*) NaOCN, NaOH, conc. HCl, water. (*b*) $NaNO_2$, H_2SO_4, 16 hrs. (*c*) (*i*) *N,O*-bis(trimethylsilyl)acetamide, $CF_3SO_3Si(CH_3)_3$, β-D-ribofuranose 1-acetate 2,3,5-tribenzoate, CH_3CN; (*ii*) conc. NH_4OH. (*d*) (*i*) $(NH_4)_2SO_4$, *N,O*-bis(trimethylsilyl)acetamide, $CF_3SO_3Si(CH_3)_3$, 2-D-3,5-di-*O*-p-toluoyl-α-L-erythro-pentofuranosyl chloride, CH_3CN; (*ii*) conc. NH_4OH, 40%.

The photophysical properties of each nucleoside are evaluated in distinct solvents to determine how responsive they are to their microenvironment (Table 5.1, 5.2). Overall, the lowest energy absorption maxima of the nucleosides do not respond to changing solvents, but the emission wavelength does. The maximum emission wavelength of the nucleosides and their Stokes shift in each solvent are graphically represented against the corresponding $E_T(30)$ value, a mathematical term

for gauging the polarity in the microenvironment around a probe (Figure 5.2). The 7-hydroxyquinazoline-2,4(1*H*,3*H*)-dione nucleoside **7** stands out, as it has the lowest energy emission band and the largest Stokes shift. Nucleoside **7** is also relatively unresponsive to changes in polarity in terms of changes to emission and absorption wavelengths. The 7-aminoquinazoline-2,4(1*H*,3*H*)-dione nucleoside **9** is next in having the lowest energy emission band, followed by 7-methoxyquinazoline-2,4(1*H*,3*H*)-dione nucleoside **8**. The emission wavelength of nucleosides **8** and **9** bathochromically shifts with increasing solvent polarity. However, in terms of Stokes shift, nucleoside **8** and **9** behave very similarly to the nucleosides with modifications in the 5 position of the quinazoline ring, probes **2**–**6**. The core nucleoside **1** lies in the middle of emission wavelengths, while in comparison, nucleosides **2**–**6** overall have hypsochromically shifted emission wavelengths that mildly go through bathochromic shifts with increasing polarity. For Stokes shift, nucleosides **1**, **4**, **5**, **8** and **9** all have similar values. While nucleosides **1**, **8** and **9** show small degrees of increase in Stokes shift due to higher polarity; nucleosides **4** and **5** are generally nonresponsive. The 5-aminoquinazoline-2,4(1*H*,3*H*)-dione deoxyribonucleoside **2** and ribonucleoside **3** have the smallest set of Stokes shift values, followed by ribonucleoside **6**, and they display increased Stokes shifts at higher $E_T(30)$ values.

Table 5.1: Photophysical properties of the nucleosides.[a]

		1		**2**		**3**		**4**, **5**	
Solvents	$E_T(30)$[b]	λ_{abs}	λ_{em}	λ_{abs}	λ_{em}	λ_{abs}	λ_{em}	λ_{abs}	λ_{em}
Water	65.3	307	371	316	361	316	363	308	358
Methanol	55.7	307	367	316	352	316	354	306	367
Acetonitrile	45.9	305	356	316	339	316	339	306	350
Dichloromethane	40.9	306	360	316	338	316	338	306	356
Dioxane	36.4	306	354	316	336	316	336	306	352

[a]Conditions for absorption and emission spectra: 5.0 and 0.5 × 10^{-5} M, respectively. For absorption wavelength, the lowest energy maximum is given in units of nm. Units of emission wavelength are in nm. [b]Units are Kcal mol^{-1}.

Table 5.2: Photophysical properties of the nucleosides.[a]

		6		7		8		9	
Solvents	$E_T(30)^b$	λ_{abs}	λ_{em}	λ_{abs}	λ_{em}	λ_{abs}	λ_{em}	λ_{abs}	λ_{em}
Water	65.3	305	357	324	490	320	395	349	440
Methanol	55.7	305	351	324	474	319	384	352	428
Acetonitrile	45.9	306	339	324	491	316	369	350	409
Dichloromethane	40.9	306	340	325	493	318	370	350	408
Dioxane	36.4	306	335	324	488	314	362	350	403

[a]Conditions for absorption and emission spectra: 5.0 and 0.5 × 10^{-5} M, respectively. For absorption wavelength, the lowest energy maximum is given in units of nm. Units of emission wavelength are in nm. [b]Units are Kcal mol^{-1}.

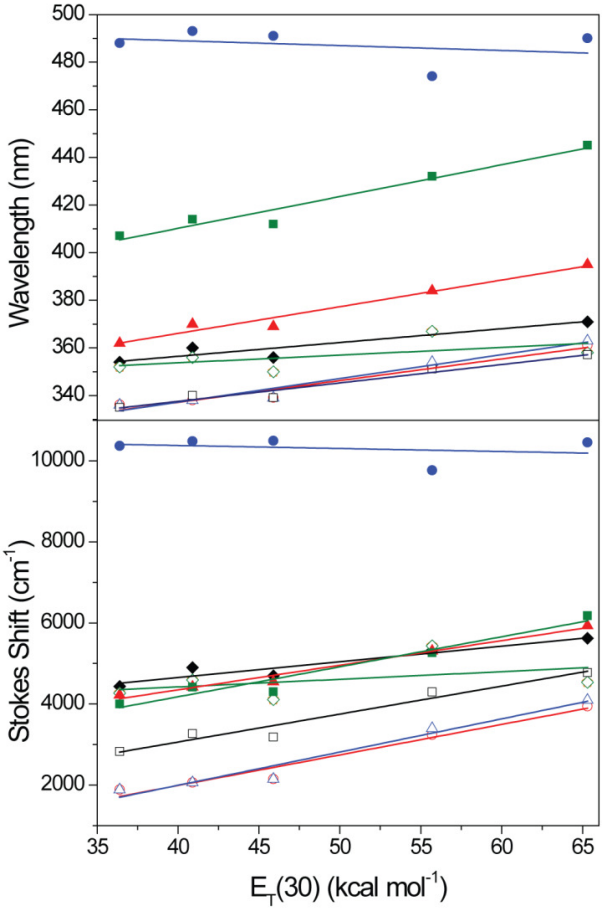

Figure 5.2: Top: $E_T(30)$ values versus the wavelength of emission of **1** (♦), **2** (○), **3** (Δ), **4** (⌂), **5** (◊), **6** (□), **7** (●), **8** (▲) and **9** (■). Bottom: $E_T(30)$ values versus the Stokes shift of **1** (♦), **2** (○), **3** (Δ), **4** (⌂), **5** (◊), **6** (□), **7** (●), **8** (▲) and **9** (■).

The fluorescent nucleoside analogues fall into two groups in their emission intensity responses to solvent polarity (Figure 5.3). Nucleosides **1** and **4**–**9** have a linear relationship with polarity, while nucleosides **2**, **3** and **7** have no discernable pattern. Nucleosides **2**, **3** and **7** all have quenched emission in water. Nucleoside **7**,

with the exception of being in methanol, show reduced emission intensity with increasing solvent polarity, but the 5-aminoquinazoline-2,4(1*H*,3*H*)-dione nucleosides **2** and **3** display relatively similar emission intensities for all other solvents. Among the other probes, the 7-methoxyquinazoline-2,4(1*H*,3*H*)-dione nucleoside **8** is the most responsive to augmentation in solvent polarity, followed by the core nucleoside **1**. The dexoy and ribonucleosides of 5-hydroxyquinazoline-2,4(1*H*,3*H*)-dione (**4** and **5**, respecitively) slightly undergo enhancement in emission intensity with increasing polarity. Finally, the 5-methoxyquinazoline-2,4(1*H*,3*H*)-dione and 7-aminoquinazoline-2,4(1*H*,3*H*)-dione nucleosides (**6** and **9**, respecitively) are nonresponsive to polarity.

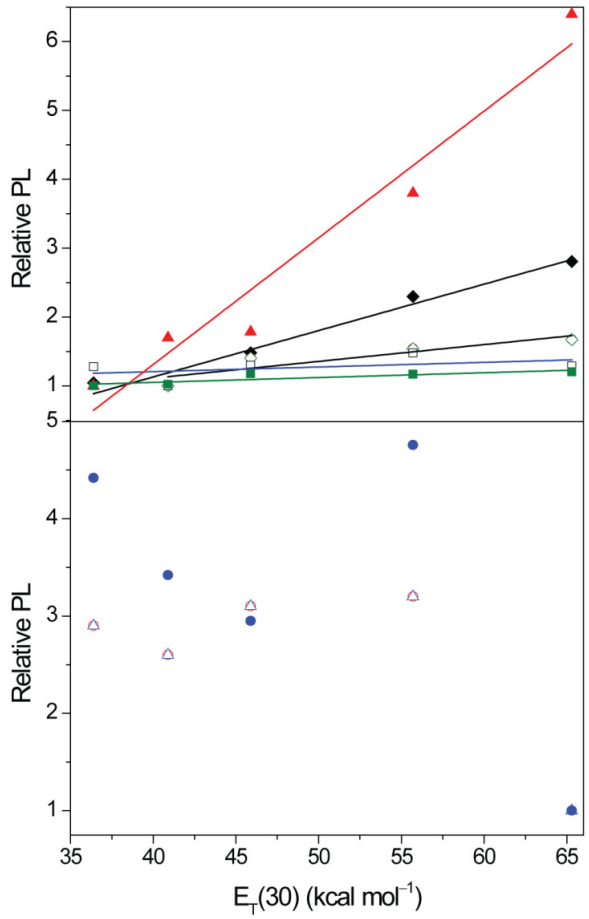

Figure 5.3: Top: $E_T(30)$ values versus the relative fluorescence intensities at the emission maxima of **1** (♦), **4** (⌂), **5** (◊), **6** (□), **8** (▲) and **9** (■). Bottom: $E_T(30)$ values versus the relative fluorescence intensities at the emission maxima of **2** (○), **3** (Δ) and **7** (●).

The relative quantum yield of each nucleoside is determined in water (Table 5.3). The range of quantum yields varies from roughly 0.01 to 0.42. Nucleoside **7** has the lowest quantum yield, while the 7-aminoquinazoline-2,4(1*H*,3*H*)-dione nucleoside **9** has the highest quantum yield, followed by the core nucleoside **1**. The 7-methoxyquinazoline-2,4(1*H*,3*H*)-dione nucleoside **8** has the third highest quantum yield, followed by the 5-methoxyquinazoline-2,4(1*H*,3*H*)-dione nucleoside **6**. Nucleosides **2**–**5** all have modest quantum yields of about 0.04.

Table 5.3: Relative quantum yield of nucleosides in water.

Nucleoside	Φ_{rel}
1	0.31 ± 0.03
2	0.039 ± 0.006
3	0.04 ± 0.01
4	0.04 ± 0.01
5	0.04 ± 0.01
6	0.08 ± 0.01
7	≤ 0.01
8	0.16 ± 0.02
9	0.42 ± 0.04

Design and Implementation of Bioassays. The unique characteristics of the probes can be applied to various studies of nucleic acids, which require incorporation of the nucleosides into DNA, or RNA. For standard solid phase synthesis of oligonucleotides, each nucleoside was synthetically transformed to its corresponding phosphoramidite.[20–22] In determining what aspect of nucleic acid function to study, the entire arsenal of photophysical properties must be considered. It is important to first decide if you wish to use a single fluorophore or multiple ones for FRET studies. In certain cases, like the detection of single nucleotide polymorphisms, a single probe could serve very well. While in other cases, such as the monitoring of RNA–ligand binding, a FRET system of two or more probes would be beneficial. If a single fluorescent nucleoside is employed,

then a responsive probe must be chosen; otherwise, it would fail to report key changes in its microenvironment. However, if a fluorescent nucleoside is to be used in a FRET pair, responsiveness is less important. Instead, it would be necessary to match the wavelengths of absorption and emission between the two components of the FRET pair to maximize FRET efficiency. If a responsive nucleoside is used in FRET experiments, it is important to perform control tests in the exact assay conditions to ensure that the observed fluorescence changes are due to a FRET interaction and not an innate feature of the probe.

Following our design principles, we have implemented our fluorescent nucleoside analogs into functional assays. We have utilized the 5-aminoquinazoline-2,4(1*H*,3*H*)-dione nucleoside **2**, a probe that is responsive to its environment, to detect mismatched DNA pairing by displaying G-specific fluorescence enhancement. We used the 7-aminoquinazoline-2,4(1*H*,3*H*)-dione nucleoside **9**, to study RNA–peptide interactions via FRET, where **9** acts as an acceptor fluorophore to tryptophan. We also examined RNA–drug binding, using 7-methoxyquinazoline-2,4(1*H*,3*H*)-dione nucleoside **8** first in a single FRET pair and then in an orthogonal FRET system. While we have sucessfully studied important aspects of nucleic acid fuction with our fluorescent nucleoside analogues, their potential have yet to be fully tapped, especially since one nucleoside can have multiple applications. Recently, we have found that nucleoside **9** can also act on its own, outside of a FRET pair, as a probe for detecting RNA bulges.

Standard solid-phase oligonucleotide synthesis was utilized to prepare the 13-mer RNA construct **15**, where probe **9** was placed in the middle of the sequence (Figure 5.3). The oligonucleotide was purified by PAGE, and MALDI-

TOF mass spectrometry confirmed its full length and the presence of the intact emissive nucleoside **9** (Figure A5.3). The fluorescently labeled single strand RNA oligonucleotide **15** exhibited an emission band around 417 nm (Table 5.3). Upon hybridization to its complement **16,** a quenched emission at 433 nm is observed (Table 5.4 and Figure 5.4). In contrast, when the fluorescently labeled RNA oligonucleotide **15** is hybridized with **22**, an oligonucleotide that is one base short, its emission is enhanced by 5-fold and hyperchromically shifted to 409 nm. Other oligonucleotides with mismatches (**17**–**21**) display emission bands of similar wavelength and intensity as that of **15•16**, the complementary duplex. Thermal denaturation measurements (Table 5.3 and Figure A5.4), determined by monitoring changes in absorbance at 260 nm as a function of temperature, show that stable duplexes were formed for all olignucleotide pairs (Table 5.3).

15 5'-GCG AUG **9** GUA GCG-3'
16 3'-CGC UAC **A** CAU CGC-5'
17 3'-CGC UAC **U** CAU CGC-5'
18 3'-CGC UAC **G** CAU CGC-5'
19 3'-CCC UAC **C** CAU CGC-5'
20 3'-CGC UAC **I** CAU CGC-5'
21 3'-CGC UAC **Y** CAU CGC-5'
22 3'-CGC UAC CAU CGC-5'

I =

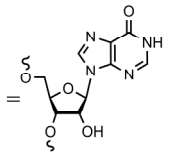

Y =

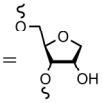

Figure 5.3: Oligonucleotides used for photophysical studies.

Table 5.4: Photophysical data of oligonucleotide **15** and its duplexes.[a]

Duplexes	**15**	**15•16**	**15•17**	**15•18**	**15•19**	**15•20**	**15•21**	**15•22**
λ_{em}/nm	417	433	430	434	433	438	432	409
I_{rel}[b]	1.4	1.0	0.87	1.0	0.98	0.96	0.76	5.1
TM/ºC	—	65±1	59±1	61±1	59±1	60±1	59±1	61±1

[a] Conditions: 5.0×10^{-6} M in 2.0×10^{-2} M Na_3PO_4, pH 7.0. [b]Relative emission intensity with respect to intensity of **15•16**.

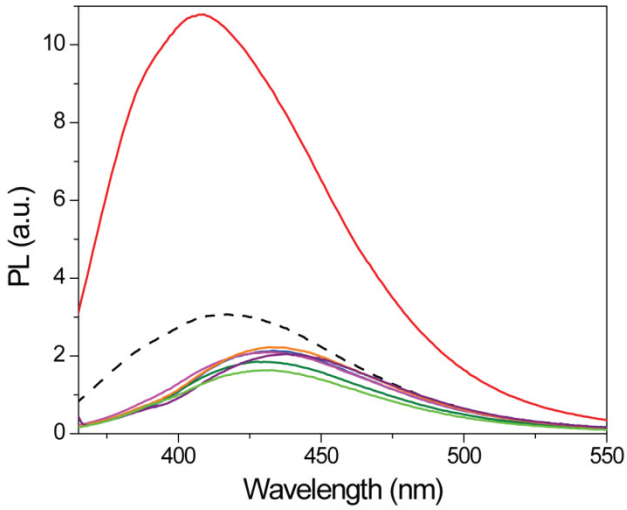

Figure 5.4: Emission profiles of **15** (**--**), **15•16** (—), **15•17** (—), **15•18** (—), **15•19** (—), **15•20** (—), **15•21** (—), and **15•22** (—).

Discussion

Design, Synthesis and Photophysical Properties of the Nucleosides. In accordance to our design proposal, fusing an electron rich ring to a uracil base and placing electron-donating substituents at either the 5 or 7 positions did augment the emissive properties. Specifically, the quantum yields showed various degrees of enhancement, and red-shifted absorption and emission bands appeared. For all of the nucleosides, the maximum wavelength of absorption varied little to changes in the microenvironment, but large shifts were observed for emission wavelengths. These observations suggest an enlarged dipole and charge, or proton, transfer character of the excited state when compared to the ground state.

The analogue that stands out in wavelength and Stokes shift is the 7-hydroxyquinazoline-2,4(1*H*,3*H*)-dione nucleoside **7**. It has the most bathochromically shifted emission wavelength and the largest Stokes shift, suggesting the greatest energy difference between the ground and excited states.

Such characteristics are indicative of excited state proton transfer, where it is possible to obtain large red-shifted emissions. Upon light excitation, the acidity and basicity of Brønsted acids and Lewis bases are enhanced, respectively. Such an enhancement can lead to an intramolecular acid-base reaction in the excited state, which can decay to a structure that is different than the original ground state. Thus, a large Stokes shift occurs, which notably persists across the range of $E_T(30)$ values for **7**. Nucleoside **7** also has the lowest quantum yield, which could be a result of the multiple pathways available to it in losing energy from the excited state, as it can go through both proton and charge transfer along with other means of nonradiative decay.

Compared with nucleoside **7**, the rest of the nucleosides (**1**–**6**, **8** and **9**) have moderate Stokes shift values, indicating that they have less energetic differences between their ground and excited states. However, unlike nucleoside **7**, the other nucleosides display positive linear realtionships relative to $E_T(30)$ values, with increasing Stokes shift from low to high polar environments. Thus, the enhanced dipole and the placement of the electron donating substituents produce an excited state charge transfer transition, which lead to greater fluorescence sensitivity to environmental changes. In looking at just the wavelength of emission, it appears that adding substituents to the 7 position of the quinazoline ring caused bathochromic emission shifts compared to the core nucleoside **1**, while modifications to the 5 position produced hypsochromic shifts. These results suggest that placing substituents ortho to the conjugated carbonyl generate opposing dipoles in the excited state, a stabilizing effect that lead to lower energy emission.

There appears to be no simple way to correlate the substituent type and position on the quinazoline ring with the corresponding nucleoside's responsiveness in emission intensity to different solvents. The 7-methoxyquinazoline-2,4(1*H*,3*H*)-dione nucleoside **8** has the strongest positive correlation with increasing polarity, followed by the core nucleoside **1** and then the nucleosides based on 5-hydroxyquinazoline-2,4(1*H*,3*H*)-dione, **4** and **5**. A hydroxyl group in the 7 position for nucleoside **7** produces a general negative relationship between emission intensity and solvent polarity; however, methanol does not fit this trend, where nucleoside **7** has the highest intensity. Both the 5-methoxy and 7-aminoquinazoline-2,4(1*H*,3*H*)-dione nucleosides (**6** and **9**, respectively) are insensitive to solvent polarity. However, an amino group in the 5 position bestows nucleosides **2** and **3** quenched emissions in water, compared to the other solvents. These observations highlight the difficulty in predicting the behavior fluorophores; a point that is reiterated when comparing the quantum yields of the nucleosides. In terms of relative quantum yield in an aqueous environment, placing electron donating substituents at the 5 position appeared to have an overall quenching effect compared the core nucleoside **1** (Table 5.3). Coupled with the observation that modifications at the 5 position also led to higher energy emission wavelengths, one can speculate that there is a destabilization in the excited state. In contrast, modifications at the 7 position had a less discernable correlation. A hydroxyl group in the 7 position, which allows for excited state proton transfer, dramatically reduced the quantum yield of the nucleoside (**7**, $\Phi_{rel} \leq 0.01$). However, an amino group in the same position enhanced the quantum yield from 0.32 ± 0.03 in nucleoside **1** to 0.42 ± 0.04 in nucleoside **9**. A methoxy group in the 7 position had a moderate quenching effect (**8**, $\Phi_{rel} = 0.16 \pm 0.02$).

Design and Implementation of Bioassays. In selecting a probe for singly-labeled oligonucleotide experiments, it's important to take responsiveness into consideration. Since you're relying on one probe, it must be able to unambiguously display varying emission signals, whether in emission wavelength, intensity, or both. Preferably, the nucleoside will exhibit variability in emission wavelength, as such a change would be more clear-cut to monitor than emission intensity. In contrast, responsiveness is not essential in nucleosides for FRET experiments. The most crucial element would be a match in the wavelengths of absorption and emission between the two components of a FRET pair to maximize FRET efficiency. If the FRET pair is used to strictly monitor distant relationships, like the onset or offset of binding between a labeled drug and RNA construct, nonresponsive probes would serve well. However, the addition of a highly responsive fluorescent nucleoside in a FRET pair could add a layer of useful complexity. For example, if a nucleoside displayed large changes in its emission wavelength with changing RNA conformation, it would affect the FRET efficiency. This change in FRET efficiency could then be useful to monitor RNA dynamics. Notably, as a fluorophore's photophysical property can vary depending on the sequence of the oligonucleotide, a responsive fluorophore could be relatively nonresponsive in certain conditions, which could further enhance its range of applications.

So far in our laboratory, we have employed fluorescent nucleosides on its own and in FRET experiments. The 5-aminoquinazoline-2,4(1*H*,3*H*)-dione nucleoside **2**, which responds to changes in its local environment in emission intensity, Stokes shift and emission wavelength, is capable of detecting the mismatched base pairing of G in DNA duplexes. Being a responsive fluorophore,

nucleoside **2** displays both a hypsochromic emission shift and significant ehancement in emission intensity when it is paired with a G. We have also utilized the 7-aminoquinazoline-2,4(1*H*,3*H*)-dione nucleoside **9** and 5-methoxyquinazoline-2,4(1*H*,3*H*)-dione nucleoside **8** in FRET experiments. Nucleoside **8**, the donor fluorophore, was matched to commercially available 7-diethylaminocoumarin, the FRET acceptor, to evaluate the binding of antibiotics to both the bacterial and human A-sites, which are reponsible for appraising the codon–anticodon matching in the ribosome. Nucleoside **9**, having ideal absorption and emission bands to act as a FRET acceptor to tryptophan, an amino acid that is frequently present in RNA–protein binding sites, was used to monitor the binding of a RNA construct, the RRE, with the Rev peptide. While nucleosides **8** and **9** are responsive nucleosides, their photophysical properties did not interfere with the emission data under the experimental conditions used in their respective FRET assays. As they were incorporated at positions near, but not directly in, the binding sites of RNA constructs, their environments were perturbed minimally enough to prevent drastic changes in their photophysical properties.

Since the sequence of oligonculeotide affects the photophysical behaviour of the incorporated fluorescent nucleoside, one probe can perform multiple functions in different constructs. We have discovered that the 7-aminoquinazoline-2,4(1*H*,3*H*)-dione nucleoside **9** has utility as a single probe, as well. Upon incorporation into a 13-mer RNA oligonucleotide **15**, the photophysical properties of nucleoside **9** exhibits a different emission profile than the nucleoside in water (445 nm) with an emission band around 417 nm, a wavelength more similar to nucleoside **9** in dichloromethane (414 nm). This suggests that there is some base stacking in the single strand oligonucleotide. Upon hybridization to its

complement **16,** a slightly quenched, bathochromically shifted emission at 433 nm is observed (Table 5.3 and Figure 5.4), displaying an emission wavelength similar to that of **9** in methanol (432 nm, Table 5.1). In contrast, when the fluorescently labeled RNA oligonucleotide **15** is hybridized to a 12-mer oligonucleotide **22**, creating a bulge in the middle of the duplex, the emission is enhanced by 5-fold and hypsochromically shifted to 409 nm, which is close to the emission wavelength of nucleoside **9** in dioxane (407 nm, Table 5.1). Other oligonucleotides with mismatches (**17**–**21**) failed to produce a dramatic increase in fluorescence intensity and all displayed emission bands similar to the **15•16** duplex (Table 5.3). Importantly, thermal denaturation measurements (Table 5.3 and Figure A5.4), determined by monitoring changes in absorbance at 260 nm as a function of temperature, show that stable duplexes were formed for all olignucleotide pairs. Nucleoside **9**'s behaviour in RNA duplexes is difficult to explain, but one can speculate that the environment of a duplex with a bulge is unique from other duplexes in that there is no base stacking. Evidently, base stacking appears to quench the fluorescence of **9** in oligonucleotides. Regardless, nucleoside **9** is able to detect a bulge formation in RNA duplexes by exhibiting distinct emission intensity and wavelength changes.

Conclusion

The quinazoline-based nucleoside synthesized and studied so far display a wide range of photophysical properties. With emissive wavelengths spanning from 335 nm to 490 nm, these fluorophores can be used to pair with a variety of fluorophores to tune FRET experiments. The nucleosides also exhibit unique responsiveness to changing microenvironments, which have resulted in successful

single-fluorophore assays. While the utility of some of these nucleosides have been explored, it is clear that many applications remain to be discovered. Each probe potentially has multiple uses, as well. In addition, other varieties of quinazoline-based nucleoside analogues can be made to enhance the range of available photophysical characteristics. Additional types of substituents can be added, and the 6 and 8 positions of the rings can be explored for modification. Finally, besides utilizing quinazoline-based nucleosides as modified U-face analogues, it is also possible to convert the U-face to a C-face, which would further expand their value in studying nucleic acids. Such explorations will advance the understanding of vital biological processes and enhance the available tools for medicinal research.

Experimental

General Procedures. NMR spectra were recorded on a Varian Mercury 400 MHz spectrometer. Mass spectra were recorded at the UCSD Chemistry and Biochemistry Mass Spectrometry Facility, utilizing either a LCQDECA (Finnigan) ESI with a quadrapole ion trap or a MAT900XL (ThermoFinnigan) FAB double focusing mass spectrometer. UV-Vis spectra were recorded on either a Hewlett Packard 8452A or 8453 Diode Array Spectrometer.

Unless otherwise specified, materials obtained from commercial suppliers were used without further purification. 2-D-3,5-di-*O*-p-toluoyl-α-L-erythro-pentofuranosyl chloride was purchased from Berry & Associates, Inc. Anhydrous pyridine, dichloroethane and acetonitrile were obtained from Fluka. Anhydrous *N,N*-diisopropylethylamine and triethylamine were obtained from Acros. The unmodified oligonucleotides were purchased from Integrated DNA Technologies. Standard phosphoramidites and solutions necessary for solid phase RNA synthesis were

purchased from Glen Research. Oligonucleotides were purified by gel electrophoresis and desalted on a Sep-Pak (Waters Corporation). Chemicals for preparing buffer solutions were purchased from Fisher Biotech (enzyme grade). Autoclaved water was used in all fluorescence titrations. NMR solvents were purchased from Cambridge Isotope Laboratories (Andover, MA).

Quinazoline-2,4(1*H*,3*H*)-dione ribonucleoside (1). To a suspension of benzoyleneyrea (1.0 g, 6.2 mmol) in anhydrous acetonitrile (90 mL), *N,O*-Bis(trimethylsilyl)acetamide (7.9 mL, 31 mmol) was added dropwise under argon. The reaction was stirred at 25 ℃ for 30 min. TMSOTf (0.36 mL, 0.30 mmol) and β-D-ribofuranose-1-acetate-2,3,5-tribenzoate (3.13 g, 6.2 mmol) were added at the same time under argon. The reaction temperature was raised to 50 ℃. The reaction was stirred at 50 ℃ for 5 h. TMSOTf (0.4 mL, 0.33 mmol) and β-D-ribofuranose-1-acetate-2,3,5-tribenzoate (3.43 g, 6.8 mmol) were added at the same time under argon again. The reaction was stirred at 50 ℃ for 24 h. The reaction was cooled to room temperature, concentrated to an oil, and diluted with dichloromethane (50 mL). The solution was washed with saturated sodium bicarbonate and brine. The organic layer was dried over sodium sulfate. The solvent was removed under reduced pressure, and the crude product was run through a silica plug (50% ethyl acetate in hexanes). The solvent was removed under reduced pressure, and the crude product was dissolved in dioxane (20 mL) and transferred to two 200 mL pressure tubes. Ammonium hydroxide (28%, 80 mL) was added to each tube. The reaction was stirred at 80 ℃ for 24 h. The solvent was removed under reduced pressure, and the product was isolated by flash chromatography (5-12% methanol in dichloromethane). Product: white solid (1.3 g, 4.3 mmol, 70 % yield over two steps). ^{1}H-NMR (400 MHz,

DMSO-d_6): δ 11.65 (s, NH, 1H), 8.00 (dd, J_1 = 6.4 Hz, J_2 = 1.6 Hz, 1H), 7.78 (d, J = 8.4 Hz, 1H), 7.65 (m, 1H), 7.28 (t, J = 7.2 Hz, 1H), 6.14 (d, J = 6.0 Hz, 1H), 5.21 (d, J = 5.6 Hz, 1H) 4.97 (m, 2H), 4.49 (q, J = 6.4 Hz, 1H). 4.12 (d, J = 6.0 Hz, 1H), 3.77 (m, 1H), 3.63 (m, 2H); ^{13}C-NMR (100 MHz, DMSO-d_6): δ 162.29, 151.02, 140.62, 135.43, 128.18, 124.00, 117.52, 117.05, 90.15, 85.30, 69.54, 69.43, 61.84; ESI-MS calculated for $C_{13}H_{14}N_2O_6$ $[M+H]^+$ 295.09, found 295.00.

7-Aminoquinazoline-2,4(1*H*,3*H*)-dione ribonucleoside (3). To a suspension of **11** (0.50 g, 2.8 mmol) in anhydrous acetonitrile (100 mL), *N,O*-Bis(trimethylsilyl)acetamide (3.6 mL, 14 mmol) was added dropwise under argon. The reaction was stirred at 25 ℃ for 30 min. TMSOTf (0.16 mL, 0.14 mmol) and β-D-ribofuranose-1-acetate-2,3,5-tribenzoate (1.41 g, 2.8 mmol) were added at the same time under argon. The reaction temperature was raised to 50 ℃. The reaction was stirred at 50 ℃ for 5 h. TMSOTf (0.16 mL, 0.14 mmol) and β-D-ribofuranose-1-acetate-2,3,5-tribenzoate (1.41 g, 2.8 mmol) were added at the same time under argon again. The reaction was stirred at 50 ℃ for 24 h. The reaction was cooled to room temperature, concentrated to an oil, and diluted with dichloromethane (70 mL). The solution was washed with saturated sodium bicarbonate and brine. The organic layer was dried over sodium sulfate. The solvent was removed under reduced pressure, and the crude product was run through a silica plug (50% ethyl acetate in hexanes). The solvent was removed under reduced pressure, and the crude product was dissolved in dioxane (20 mL) and transferred to a 200 mL pressure tube. Ammonium hydroxide (28%, 80 mL) was added to the tube. The reaction was stirred at 70 ℃ for 24 h. The solvent was removed under reduced pressure, and the product was isolated by flash chromatography (5-12% methanol in dichloromethane).

Product: white solid (0.56 g, 1.8 mmol, 65 % yield over two steps). ^{1}H-NMR (400 MHz, DMSO-d_6): δ 11.07 (s, NH, 1H), 7.62 (d, J_1 = 7.2 Hz, J_2 = 1.6 Hz, 1H), 7.23 (b, 2H), 6.59 (s, 1H), 6.43 (d, J = 8.8 Hz, 1H), 6.22 (s, 1H), 5.88 (s, 1H), 5.24 (d, J = 4.8 Hz, 1H), 4.94 (d, J = 6.4 Hz, 1H), 4.84 (t, J = 4.8 Hz, 1H), 4.53 (d, J = 5.6 Hz, 1H), 4.10 (m, 1H), 3.71–3.64 (m, 1H), 3.57–3.53 (m, 1H); ^{13}C-NMR (100 MHz, DMSO-d_6): δ 161.85, 155.59, 151.23, 142.99, 129.85, 110.70, 104.95, 98.22, 91.09, 84.91, 70.00, 62.61; ESI-MS calculated for $C_{13}H_{15}N_3O_6$ $[M+H]^+$ 310.10, found 309.96.

7-Hydroxyquinazoline-2,4(1*H*,3*H*)-dione (12). To 7-aminoquinazoline-2,4(1*H*,3*H*)-dione[20] (1.0 g, 5.6 mmol), H_2SO_4 (1M, 100 mL) was added. The solution was cooled on ice, and $NaNO_2$ (0.58 g, 8.4 mmol) was added slowly. The reaction was stirred at 4 ℃ for 16h. The reaction was refluxed for 4 h, until a red suspension forms. The solid was collected on a frit and washed with water (500 mL). Product: red solid (0.80 g, 4.5 mmol, 80 % yield over two steps). ^{1}H-NMR (400 MHz, DMSO-d_6): δ 10.97 (s, 1H), 10.92 (s, 1H), 10.52 (s, 1H), 7.68 (d, J = 8.8 Hz, 1H), 6.56 (dd, J_1 = 6.8 Hz, J_2 = 2.0 Hz, 2H), 6.507 (d, J = 2.0 Hz, 1H); ^{13}C-NMR (100 MHz, DMSO-d_6): δ 163.91, 163.08, 151.33, 143.51, 129.69, 112.29, 107.14, 100.63; ESI-MS calculated for $C_8H_6N_2O_3$ $[M–H]^-$ 177.03, found 177.23.

7-Hydroxyquinazoline-2,4(1*H*,3*H*)-dione deoxyribonucleoside (4). To a suspension of **12** (0.50 g, 2.8 mmol) and ammonium sulfate (0.19 g, 1.4 mmol) in anhydrous acetonitrile (30 mL), *N,O*-bis(trimethylsilyl)acetamide (3.5 mL, 14 mmol) was added dropwise under argon. The reaction was stirred at 25 ℃ for 30 min. 2-D-3,5-di-*O*-p-toluoyl-α-L-erythro-petofuranosyl chloride (1.1 g, 2.8 mmol) was added to the reaction over ice and under argon. TMSOTf (0.37 mL, 2.0 mmol) was dissolved in 1mL of anhydrous acetonitrile and added dropwise over ice. The reaction

temperature was raised to room temperature and stirred for 12 h. The reaction was concentrated to an oil, and diluted with dichloromethane (50 mL). The solution was washed with saturated sodium bicarbonate and brine. The organic layer was dried over sodium sulfate. The solvent was removed under reduced pressure, and the crude product was isolated by flash chromatography (0.4-0.8% methanol in dichloromethane). Dioxane (20 mL) was added the crude product and transferred to a pressure tube. Ammonium hydroxide (30%, 80 mL) was added to the tube. The reaction was stirred at 70 °C for 24 h. The solvent was removed under reduced pressure, and the product was isolated by flash chromatography (10% methanol in ethyl acetate). Product: white solid (0.330 g, 1.12 mmol, 40 % yield over two steps). ^{1}H-NMR (400 MHz, CD_3OD): δ 7.95 (d, *J* = 7.2 Hz, 1H), 7.08 (d, *J* = 2.4 Hz, 1H), 6.73 (d, *J* = 8.8 Hz, 1H), 6.59 (t, *J* = 7.6 Hz, 1H), 4.45 (m, 1H), 4.27 (m, 1H), 3.78–3.64 (m, 2H), 2.67 (m, 2H); ^{13}C-NMR (100 MHz, DMSO-d_6): δ 164.07, 151.12, 142.49, 129.97, 128.74, 112.02, 108.58, 101.92, 86.54, 85.67, 71.39, 62.03, 36.62; ESI-MS calculated for $C_{13}H_{14}N_2O_6$ $[M+H]^+$ 295.09 and $[M+Na]^+$ 317.07, found 295.02 and 317.19, respectively.

7-Hydroxyquinazoline-2,4(1*H*,3*H*)-dione ribonucleoside (5). To a suspension of **12** (0.20 g, 1.1 mmol) in anhydrous acetonitrile (11 mL), *N,O*-Bis(trimethylsilyl)acetamide (1.4 mL, 5.5 mmol) was added dropwise under argon. The reaction was stirred at 25 °C for 30 min. TMSOTf (0.13 mL, 0.11 mmol) and β-D-ribofuranose-1-acetate-2,3,5-tribenzoate (0.55 g, 1.1 mmol) were added at the same time under argon. The reaction temperature was raised to 50 °C. The reaction was stirred at 50 °C for 5 h. TMSOTf (0.13 mL, 0.11 mmol) and β-D-ribofuranose-1-acetate-2,3,5-tribenzoate (0.55 g, 1.1 mmol) were added at the same time under

argon again. The reaction was stirred at 50 °C for 24 h. The reaction was cooled to room temperature, concentrated to an oil and diluted with dichloromethane (25 mL). The solution was washed with saturated sodium bicarbonate and brine. The organic layer was dried over sodium sulfate. The solvent was removed under reduced pressure, and the crude product was run through a silica plug (50% ethyl acetate in hexanes). The solvent was removed under reduced pressure, and the crude product was dissolved in dioxane (15 mL) and transferred to a 100 mL pressure tube. Ammonium hydroxide (30%, 55 mL) was added to the tube. The reaction was stirred at 70 °C for 24 h. The solvent was removed under reduced pressure, and the product was isolated by flash chromatography (5-12% methanol in dichloromethane). Product: white solid (0.24 g, 0.77 mmol, 70 % yield over two steps). ^{1}H-NMR (400 MHz, CD_3OD): δ 7.92 (d, J = 8.4 Hz, 1H), 6.92 (d, J = 2.0 Hz, 1H), 6.71 (dd, J_1 = 6.8 Hz, J_2 = 2.0 Hz, 1H), 6.03 (d, J = 4.8 Hz, 1H), 4.70 (dd, J_1 = 4.4 Hz, J_2 = 2.0 Hz, 1H), 4.35 (t, J_1 = 6.8 Hz, 1H), 3.91 (m, 1H), 3.86–3.73 (m, 2H); ^{13}C-NMR (100 MHz, CD_3OD): δ 165.44, 162.73, 151,02, 143,48, 129.90, 112.57, 107.85, 101.45, 91.69, 84.57, 70.78, 69.74, 62.18; ESI-MS calculated for $C_{13}H_{14}N_2O_7$ $[M+H]^+$ 311.09 and $[M+Na]^+$ 333.07, found 310.92 and 332.99, respectively.

7-Methoxyquinazoline-2,4(1*H*,3*H*)-dione ribonucleoside (6). To a suspension of **13**[20] (0.20 g, 1.0 mmol) in anhydrous acetonitrile (15 mL), *N,O*-Bis(trimethylsilyl)acetamide (1.3 mL, 5.0 mmol) was added dropwise under argon. The reaction was stirred at 25 °C for 30 min. TMSOTf (0.12 mL, 0.10 mmol) and β-D-ribofuranose-1-acetate-2,3,5-tribenzoate (0.50 g, 1.0 mmol) were added at the same time under argon. The reaction temperature was raised to 50 °C. The reaction was stirred at 50 °C for 5 h. TMSOTf (0.12 mL, 0.10 mmol) and β-D-ribofuranose-1-

acetate-2,3,5-tribenzoate (0.50 g, 1.0 mmol) were added at the same time under argon again. The reaction was stirred at 50 ℃ for 28 h. The reaction was cooled to room temperature, concentrated to an oil, and diluted with dichloromethane (20 mL). The solution was washed with saturated sodium bicarbonate and brine. The organic layer was dried over sodium sulfate. The solvent was removed under reduced pressure, and the crude product was run through a silica plug (50% ethyl acetate in hexanes). The solvent was removed under reduced pressure, and the crude product was dissolved in dioxane (15 mL) and transferred to a 200 mL pressure tube. Ammonium hydroxide (28%, 55 mL) was added to the tube. The reaction was stirred at 70 ℃ for 24 h. The solvent was removed under reduced pressure, and the product was isolated by flash chromatography (5-12% methanol in dichloromethane). Product: white solid (0.23 g, 0.70 mmol, 70 % yield over two steps). ^{1}H-NMR (400 MHz, DMSO-d_6): δ 11.52 (s, NH, 1H), 7.91 (d, J = 8.8 Hz, 1H), 7.07 (s, 1H), 6.87 (dd, J_1 = 8.0 Hz, J_2 = 0.8 Hz, 1H), 6.17 (d, J = 6.4 Hz, 1H), 5.25 (d, J = 4.4 Hz, 1H), 5.03 (d, J = 4.8 Hz, 1H), 4.99 (t, J = 4.8 Hz, 1H), 4.46 (d, J = 3.6 Hz, 1H), 4.14 (s, 1H), 3.84 (s, 3H), 3.70 (dd, J_1 = 5.6 Hz, J_2 = 4.4 Hz, 1H), 3.59 (m, 1H); ^{13}C-NMR (100 MHz, DMSO-d_6): δ 164.93, 161.79, 151.44, 142.30, 130.06, 111.84, 110.24, 101.38, 90.24, 84.75, 69.10, 68.84, 61.10, 56.68; ESI-MS calculated for $C_{14}H_{16}N_2O_7$ $[M+H]^+$ 324.10 and $[M+Na]^+$ 347.09, found 324.87 and 347.03, respectively.

5-Hydroxyquinazoline-2,4(1*H*,3*H*)-dione (14). 5-methoxyquinazoline-2,4(1*H*,3*H*)-dione[20] (0.39 g, 2.0 mmol) was dried overnight in a 50 mL round bottom flask with a stir bar. Anhydrous dichloromethane (5 mL) was added, and the reaction was cooled on ice. BBr_3 (5.1 mL, 1M in dichloromethane) was added drop-wise. The reaction was stirred at room temperature for 24 h. The reaction was concentrated via reduced

pressure, and the product was isolated by column chromatography (50–100% ethyl acetate in hexanes). Product: white solid (0.21 g, 1.2 mmol, 60 % yield over two steps). ^{1}H-NMR (400 MHz, DMSO-d_6): δ 11.60 (b, 2H), 11.26 (b, 1H), 7.45 (t, J = 8.4 Hz, 1H), 6.56 (d, J = 8.0 Hz, 1H), 6.52 (d, J = 8.0 Hz, 1H); ^{13}C-NMR (100 MHz, DMSO-d_6): δ 168.75, 160.94, 150.28, 142.17, 137.39, 109.32, 105.75, 101.05; ESI-MS calculated for $C_8H_6N_2O_3$ $[M-H]^-$ 177.03, found 177.15.

5-Hydroxyquinazoline-2,4(1*H*,3*H*)-dione ribonucleoside (7). To a suspension of **14** (0.20 g, 1.1 mmol) in anhydrous acetonitrile (11 mL), *N,O*-Bis(trimethylsilyl)acetamide (1.4 mL, 5.5 mmol) was added dropwise under argon. The reaction was stirred at 25 °C for 30 min. TMSOTf (0.13 mL, 0.11 mmol) and β-D-ribofuranose-1-acetate-2,3,5-tribenzoate (0.55 g, 1.1 mmol) were added at the same time under argon. The reaction temperature was raised to 50 °C. The reaction was stirred at 50 °C for 5 h. TMSOTf (0.13 mL, 0.11 mmol) and β-D-ribofuranose-1-acetate-2,3,5-tribenzoate (0.55 g, 1.1 mmol) were added at the same time under argon again. The reaction was stirred at 50 °C for 24 h. The reaction was cooled to room temperature, concentrated to an oil and diluted with dichloromethane (25 mL). The solution was washed with saturated sodium bicarbonate and brine. The organic layer was dried over sodium sulfate. The solvent was removed under reduced pressure, and the crude product was run through a silica plug (50% ethyl acetate in hexanes). The solvent was removed under reduced pressure, and the crude product was dissolved in dioxane (15 mL) and transferred to a 100 mL pressure tube. Ammonium hydroxide (30%, 55 mL) was added to the tube. The reaction was stirred at 70 °C for 24 h. The solvent was removed under reduced pressure, and the product was isolated by flash chromatography (5-12% methanol in dichloromethane).

Product: white solid (0.26 g, 0.83 mmol, 75 % yield over two steps). ^{1}H-NMR (400 MHz, DMSO-d_6): δ 12.06 (b, 2H), 7.50 (t, J = 8.4 Hz, 1H), 7.15 (d, J = 8.8 Hz, 1H), 6.67 (d, J = 8.4 Hz, 1H), 6.06 (d, J = 6.0 Hz, 1H), 5.22 (b, 1H), 5.00 (b, 1H), 4.94 (b, 1H), 4.49 (t, J = 6.0 Hz, 2H), 4.10 (s, 1H), 3.75 (dd, J_1 = 2.8 Hz, J_2 = 4.8 Hz, 1H), 3.67–3.55 (m, 2H); ^{13}C-NMR (100 MHz, DMSO-d_6): δ 167.89, 161.57, 150.43, 141.34, 137.14, 111.05, 107.29, 102.39, 90.74, 85.27, 69.57, 63.46, 61.86; ESI-MS calculated for $C_{13}H_{14}N_2O_7$ $[M+H]^+$ 311.09, found 310.96.

Photophysical Studies of Oligonucleotides. Steady state fluorescence experiments were carried out at 21 ºC in a 150 µL quartz fluorescence cell with a path length of 1.0 cm (Hellma GmbH & Co KG, Müllheim, Germany) on a Jobin Yvon Horiba FluoroMax-3 luminescence spectrometer with excitation and emission slit-widths of 8 nm. RNA samples were hybridized by heating to 75 ºC for 5 min and subsequently allowed to cool to room temperature over 2 h prior to measurements. RNA samples were measured at 5 × 10^{-6} M concentration in 20 mM sodium phosphate buffer (pH 7.0, 500 mM NaCl).

Thermal Denaturation Measurements. All hybridizations and UV melting experiments were carried out at 5 × 10^{-6} M concentration in 20 mM sodium phosphate buffer (pH 7.0, 500 mM NaCl), using a Beckman-Coulter DU® 640 spectrometer with a high performance temperature controller and micro auto six holder. Samples were heated to 90 ºC for 5 min, cooled to room temperature over 2 h, and placed on ice for 30 min prior to measurements. Samples were placed in a stoppered 1.0-cm path length cell (Beckman-Coulter) and a background spectrum (buffer) was subtracted from each sample. Denaturation runs were performed between 25 and 90 ºC at a scan rate of 1.0 ºC min^{-1} with optical monitoring every ºC

at 260 nm. Beckman-Coulter software (provided with T_m Analysis Accessory for DU® Series 600 Spectrometers) determined the melting temperatures utilizing the first derivative from the melting profile.

References

1. J. R. Lakowicz, in *Principles of fluorescence spectroscopy*, Springer, New York, Editon edn., 2006, pp. 530-535.
2. S. Shandrick, Q. Zhao, Q. Han, B. K. Ayida, M. Takahashi, G. C. Winters, K. B. Simonsen, D. Vourloumis and T. Hermann, *Angew. Chem., Int. Ed.*, 2004, **43**, 3177-3182.
3. M. Kaul, C. M. Barbieri and D. S. Pilch, *J. Am. Chem. Soc.*, 2004, **126**, 3447-3453.
4. S. Chauhan, R. Behrouzi, P. Rangan and S. A. Woodson, *J. Mol. Biol.*, 2009, **386**, 1167–1178.
5. R. Zhao and D. Rueda, *Methods*, 2009, **49**, 112-117.
6. L. Serrano-Andrés and M. Merchán, *J. Photoch. Photobio. C*, 2009, **10**, 21-32.
7. M. Daniels and W. Hauswirth, *Science*, 1971, **171**, 675-677.
8. N. J. Greco and Y. Tor, *Tetrahedron*, 2007, **63**, 3515-3527.
9. J. N. Wilson and E. T. Kool, *Org. Biomol. Chem.*, 2006, **4**, 4265–4274.
10. R. W. Sinkeldam, N. J. Greco and Y. Tor, *Chem. Rev.*, 2010, **110**, 2579–2619.
11. Y. Tor, *Tetrahedron*, 2007, 3425-3426.
12. A. Okamoto, Y. Saito and I. Saito, *Photochem. Photobiol. C: Photochem. Rev.*, 2005, **6**, 108.
13. Q. Xiao, R. T. Ranasinghe, A. M. P. Tang and T. Brown, *Tetrahedron*, 2007, **63**, 3483-3490.
14. J. H. Ryu, Y. J. Seo, T. Hwang, J. Y. Lee and B. H. Kim, *Tetrahedron*, 2007, **63**, 3538-3547.
15. R. W. Sinkeldam, N. J. Greco and Y. Tor, *ChemBioChem*, 2008, **9**, 706-709.

16. S. G. Srivatsan, H. Weizman and Y. Tor, *Org. Biomol. Chem.*, 2008, **6**, 1334-1338.

17. N. J. Greco, R. W. Sinkeldam and Y. Tor, *Org. Lett.*, 2009, **11**, 1115-1118.

18. N. J. Greco and Y. Tor, *J. Am. Chem. Soc.*, 2005, **127**, 10784-10785.

19. S. G. Srivatsan and Y. Tor, *J. Am. Chem. Soc.*, 2007, **129**, 2044-2053.

20. Y. Xie, A. V. Dix and Y. Tor, *J. Am. Chem. Soc.*, 2009, **131**, 17605-17614.

21. Y. Xie, A. V. Dix and Y. Tor, *Chem. Commun.*, 2010, **46**, 5542 - 5544.

22. Y. Xie, T. Maxson and Y. Tor, *J. Am. Chem. Soc.*, 2010, In Press.

23. C. Hariharan and L. J. Reha-Krantz, *Biochemistry*, 2005, **44**, 15674-15684.

24. S. G. Srivatsan, N. Greco, J. and Y. Tor, *Angew. Chem., Int. Ed.*, 2008, **47**, 6661-6665.

25. A. H. F. Lee and E. T. Kool, *J. Am. Chem. Soc.*, 2006, **128**, 9219-9230.

26. H. Liu, J. Gao and E. T. Kool, *J. Org. Chem.*, 2005, **70**, 639-647.

27. L. G. Arnaut and S. J. Fromosinho, *J. Photochem. Photobiol. A. Chem.*, 1993, **75**, 1–20.

28. T. Nakatsu, S. Ichiyama, J. Hiratake, A. Saldanha, N. Kobashi, K. Sakata and H. Kato, *Nature*, 2006, **440**, 372–376.

29. H. Gold, in *The Chemistry of Synthetic Dyes*, ed. K. Venkataraman, Academic Press, New York, Editon edn., 1971, vol. V, pp. 535-542.

30. See supporting information for additional details.

Chapter 5 contains sections from: Xie, Y.; Tor, Y. Synthesis and Applications of Quinazoline-Based Fluorescent Nucleoside Analogues. In Preparation. The dissertation author is the main author and researcher for this work.

Appendix 1: Supporting Information for Chapter 1

Supporting Information

A1.1 – Synthesis

General Procedures

NMR spectra were recorded on a Varian Mercury 400 MHz spectrometer. Mass spectra were recorded at the UCSD Chemistry and Biochemistry Mass Spectrometry Facility, utilizing either a LCQDECA (Finnigan) ESI with a quadrapole ion trap or a MAT900XL (ThermoFinnigan) FAB double focusing mass spectrometer. UV-Vis spectra were recorded on either a Hewlett Packard 8452A or 8453 Diode Array Spectrometer. Unless otherwise specified, materials obtained from commercial suppliers were used without further purification. NMR solvents were purchased from Cambridge Isotope Laboratories (Andover, MA).

Synthetic Schemes

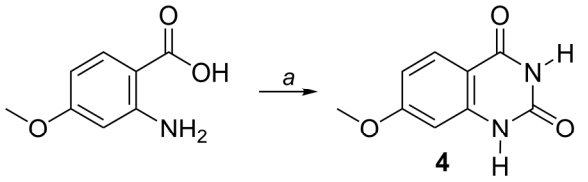

Scheme A1.1: Synthesis of **4**. (a) NaOCN (2.5 eq.), NaOH (45 eq.), conc. HCl, water, 90%.

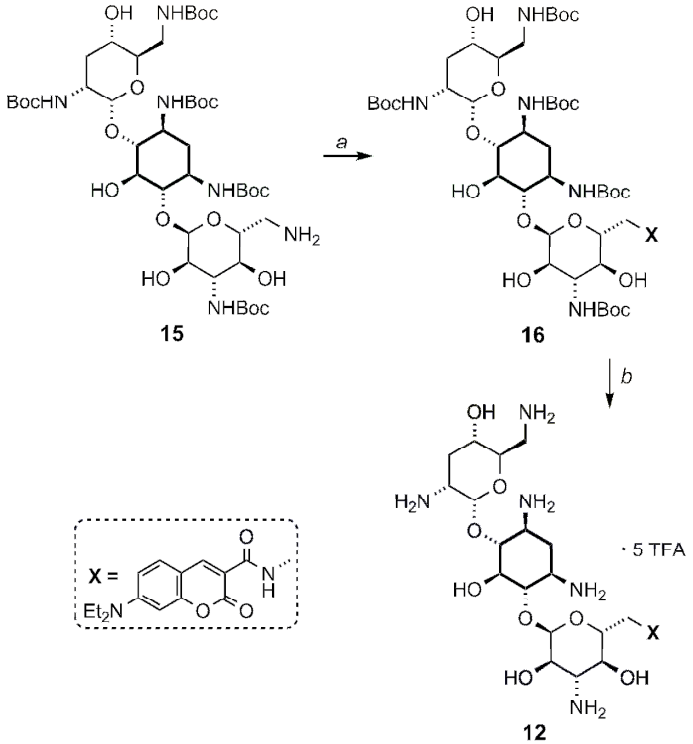

Scheme A1.2: Synthesis of tobramycin-coumarin conjugate **12**. (a) 7-(Et_2N)coumarin-3-carboxylic acid (1.2 eq.), EDC (1.2 eq.), DMAP (1.2 eq.), *i*Pr_2EtN (2.2 eq.), dichloromethane, 78%. (b) TFA, triisopropylsilane, CH_2Cl_2, 86%.

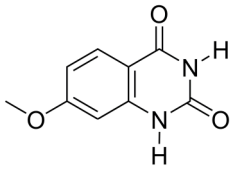

4

3-Methoxyquinazoline-2,4(1*H*,3*H*)-dione (**4**). Water (36 mL) and glacial acetic acid (0.7 mL) were added to 4-methoxy-2-aminobenzoic acid (1.00 g, 5.98 mmol). The slurry was stirred at 35 °C for 15 min. Sodium cyanate (0.97 g, 14.92 mmol) was dissolved in water (4 mL) and added slowly to the slurry. The reaction was stirred at 35 °C for 30 min. Sodium hydroxide (10.68 g, 267 mmol) was added slowly to the reaction. The reaction was cooled to room temperature. The pH was adjusted to 4 with conc. hydrochloric acid. The white precipitate was collected and washed with water (200 mL). Product: white solid (1.00 g, 5.37 mmol, 90 % yield). ^{1}H-NMR (400 MHz, DMSO-d_6): δ 11.09 (s, NH, 1H), 11.01 (s, NH, 1H), 7.78 (d, J = 8.8 Hz, 1H), 6.74 (dd, J_1 = 6.0 Hz, J_2 = 2.8 Hz, 1H), 6.60 (d, J = 2.4 Hz, 1H), 3.80 (s, OCH_3, 3H); ^{13}C-NMR (100 MHz, DMSO-d_6): δ 165.03, 163.03, 151.23, 143.49, 129.53, 111.20, 108.35, 103.88, 56.29; ESI-MS calculated for $C_9H_9N_2O_3$ $[M+H]^+$ 193.1, found 193.1.

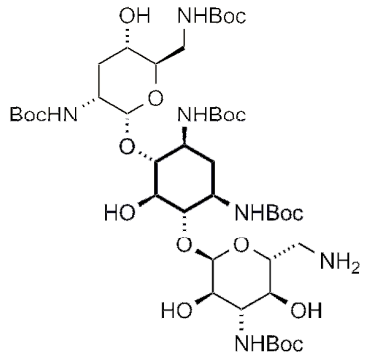

15

6''-Amino-6''-deoxy-(Boc)$_5$tobramycin (15). Synthesis and characterization of precursors previously reported.[S1]

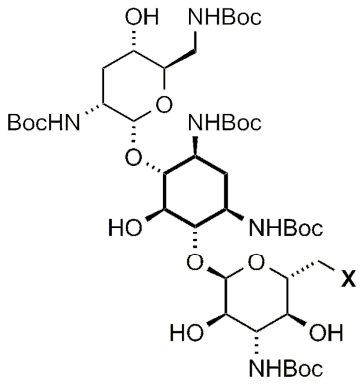

16

Boc$_5$-protected coumarin-labeled-tobramycin (16). Anhydrous dichloromethane (300 µL), and 7-(diethylamino)coumarin-3-carboxylic acid (12.4 mg, 0.0473 mmol) were added to **15** (38.1 mg, 0.0394 mmol). To this, *N*-(3-dimethylaminopropyl)-*N'*-ethylcarbodiimide hydrochloride (11.3 mg, 0.0473 mmol), *N,N*-diisopropylethylamine (15 µL, 0.087 mmol), and 4-(dimethylamino)pyridine (6 mg, 0.04728 mmol) were added. The reaction was stirred for 18 h. The solvent was removed under redusced pressure and the resulting solid was dissolved in ethyl acetate and washed with water and brine. The organic layer was dried over sodium sulfate and the solvent was removed under reduced pressure. The product was isolated by flash chromatography (3% methanol in dichloromethane). Product: yellow powder. (37.2 mg, 0.0307 mmol, 78% yield).). ^{1}H-NMR (400 MHz, D_2O): δ 8.63 (s, 1H), 7.56 (d, J = 9 Hz, 1H), 6.83 (dd, J_1 = 9 Hz, J_2 = 2.5 Hz, 1H), 6.57 (s, 1H), 5.16 (s, 1H), 5.03 (s, 1H), 4.59 (s, 1H), 4.23 – 4.19 (m, 1H), 3.75 – 3.69 (m, 2H), 3.61 – 3.58 (m, 2H), 3.53 (q, J_1 = 7 Hz, J_2 = 5 Hz, 4H), 3.44 – 3.36 (m, 6H), 3.20 (t, J = 10.5 Hz, 1H), 1.45 – 1.38 (m, 45H), 1.24 (t, J = 7.5 Hz, 4H); ^{13}C-NMR (125 MHz, DMSO): 162.65, 161.47, 157.41, 155.01, 152.37, 132.10, 131.70, 129.75, 110.35, 108.85, 107.71, 104.56, 97.87, 95.68, 77.89, 77.19, 69.76, 44.29, 35.16, 29.07, 28.73, 28.19, 26.53, 21.95, 13.77, 12.32; ESI-MS calculated for $C_{57}H_{91}N_7O_{21}$ $[M+H]^+$ 1210.63 and $[M+Na]^+$ 1232.62, found 1210.43 and 1232.65.

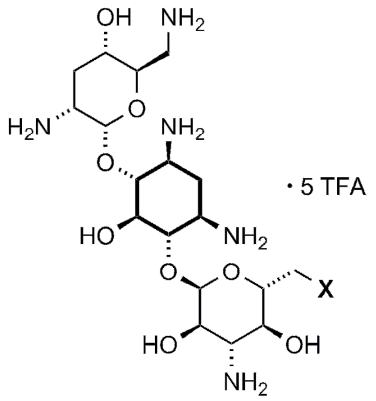

12

Coumarin-labeled-tobramycin (12). Anhydrous dichloromethane (2 mL) and triisopropylsilane (200 µL) were added to **16** (37.2 mg, 0.0307 mmol). To this, trifluoroacetic acid was added (2 mL) and the reaction was stirred for 15 min. The reaction was diluted with toluene (5 mL) and the solvent was removed under reduced pressure. The resulting solid was dissolved in water and washed with dichloromethane. The aqueous layer was dried concentrated under reduced pressure and further purified by reverse phase HPLC (10 – 25% acetonitrile, 0.1% TFA) in water (0.1% TFA) over 22 min) and eluted at 20.6 min. Product: yellow powder (31.5 mg, 0.0264 mmol, 86% yield). ^{1}H-NMR (400 MHz, D_2O): δ 8.65 (s, 1H), 7.63 (d, *J* = 9.2 Hz, 1H), 6.93 (d, *J* = 9.2 Hz, 1H), 6.71 (s, 1H), 5.60 (d, *J* = 3.2 Hz, 1H), 5.03 (d, *J* = 3.2 Hz, 1H), 4.06 (t, *J* = 9.2 Hz, 1H), 3.97 (dd, *J* = 3.6 Hz, 6.4, 1H), 3.88 – 3.79 (m, 3H), 3.71 – 3.43 (m, 10H), 3.33(d, *J* = 12.4 Hz, 1H), 3.24 – 3.20 (m, 1H), 3.16 – 3.13 (m, 1H), 2.71 (dd, *J* = 8.8 Hz, 13.2, 1H), 2.50 – 2.47 (m, 1H), 2.16 – 2.12 (m, 1H), 1.89 – 1.84 (m, 2H), 1.20 (t, *J* = 6.8 Hz, 6H); ^{13}C-NMR (100 MHz, D_2O): δ 166.25, 164.23, 163.31 (J_1 = 2.9 Hz, J_2 = 5.5 Hz), 157.78, 153.91, 149.31, 132.19, 116.63 (J_1 = 230 Hz, J_2 = 469 Hz), 111.56, 108.43, 107.15, 101.44, 96.10, 84.50, 71.59, 68.17, 65.19, 54.81, 49.87, 48.88, 45.32, 29.58, 27.83, 11.81; ESI-MS calculated for $C_{33}H_{53}N_7O_{10}$ $[M+H]^+$ 710.37 and $[M+Na]^+$ 732.35, found 710.38 and 732.56.

A1.2 – Photophysical Studies of Nucleoside 5.

UV-Vis spectra were recorded on a Hewlett Packard 8453 Diode Array Spectrometer in a 0.5 mL quartz fluorescence cell with a path length of 1.0 cm (Hellma GmbH & Co KG, Müllheim, Germany) at ambient temperature (21°C). Steady state fluorescence experiments were carried out at ambient temperature (21°C) in a 0.5 mL quartz fluorescence cell with a path length of 1.0 cm (Hellma GmbH & Co KG, Müllheim, Germany) on a Jobin Yvon Horiba FluoroMax-3 luminescence spectrometer with excitation and emission slit-widths of 5 nm. The $E_T(30)$ values of

solvents were determined experimentally by taking the long wavelength absorption maximum of the dissolved Reichardt's dye.

All emission maxima in cm^{-1} were determined after correction of the intensity according:

$$\text{Intensity } [\upsilon] = \lambda^2 \times \text{Intensity } [\lambda].$$

Curve fits were generated using OriginPro 8. All reported standard deviations were calculated using STDEVP in Microsoft Excel.

Quantum yield for nucleoside **5** ($\Phi_F = 0.16$) on its own and in **10** ($\Phi_F = 0.03$) relative to the 2-aminopurine standard was determined using the following equation.[S2]

$$\Phi F(x) = (As/Ax)(Fx/Fs)(nx/ns)^2 \, \Phi F(s)$$

Where s is the standard, x is the nucleoside, A is the absorbance at excitation wavelength, F is the area under the emission curve, *n* is the refractive index of the solvent and ΦF is the quantum yield.[S3]

Table A1.1: Photophysical properties of nucleoside **5**.

Solvent	$E_T(30)$	λ_{em} (nm)	λ_{abs} (nm)	Stokes Shift (cm^{-1})
Water	63.1	395	320	5930
Methanol	55.4	384	319	5310
Acetonitrile	45.5	369	316	4550
Dichloromethane	40.6	370	318	4420
Dioxane	36.1	362	314	4220

A1.3 – Absorption and Emission Spectra of 1 and 2

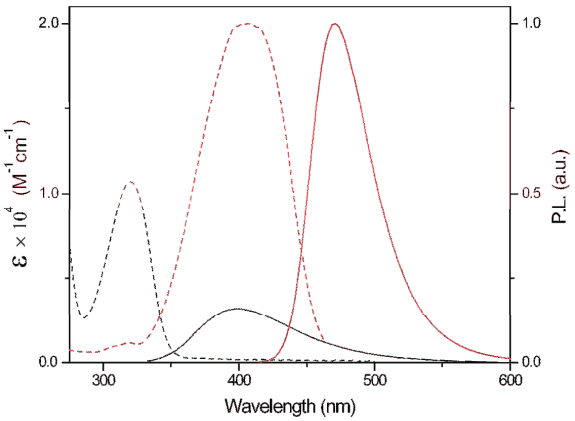

Figure A1.1: Absorption (---) and emission (—) spectra of **1** (black) and **2** (red) in water. Conditions: **1** (1.0×10^{-5} M) and **2** (1×10^{-5} M).

A1.4 – Oligonucleotide Synthesis and Purification

The unmodified oligonucleotide was purchased from Thermo Scientific. The modified oligonucleotide was synthesized on a Biosearch Cyclone Plus DNA synthesizer using a 0.2 µmole scale 500 Å CPG column. Phosphoramidite **8** was site specifically incorporated into the oligonucleotide by trityl-off synthesis of the base oligonucleotide, followed by manual coupling of phosphoramidite **8**. Typically, the modified phosphoramidite was dissolved in 100 µL of anhydrous acetonitrile to give a final concentration of 0.1M. The phosphoramidite solution was pushed into the CPG column via syringe and then 200 µL of 0.45M 1*H*-tetrazole was pushed into the other end of the column via syringe. Coupling reactions, performed twice, were allowed to proceed for 5 minutes (97% coupling efficiency) and were subsequently followed by standard oxidation and capping steps. The rest of the oligonucleotide was synthesized via the standard trityl-off procedure. Upon completion of the oligonucleotide synthesis, the CPG column was dried completely. The beads from the column were transferred into a 2.5 mL conical glass vial. 1mL of $MeNH_2$ in water and 1mL of $MeNH_2$ in ethanol were added. The vial was capped tightly and allowed to react for 15 h at room temperature. The supernatant from the reaction vial was transferred into Eppendorf tubes. The remaining beads were washed with 3x500 µL of 33% ethanol in water. The supernatant was evaporated in speed vac. The solid residue was dissolved in 1 mL of 1M TBAF in THF and warmed to 50 ℃ for 5min. The deprotection took place overnight at 25 ℃. The reaction was quenched by adding 1 mL of Tris buffer (1M, pH 7.4). The volume was reduced to half by speed vac. The residue was desalted on a G10 sephadex column. The residue was loaded onto the column in 1 mL of water and eluted with 10 mL of water. The fractions were

collected and analyzed by UV (260 nm). Fractions containing RNA were evaporated and desalted again on a G10 sephadex column. The desalted RNA was pooled together and evaporated in speed vac. The RNA was purified by 20% polyacrylamide gel electrophoresis. The oligonucleotide was visualized by UV shadowing; bands were excised from the gel and extracted with 0.3M sodium acetate buffer overnight. The resulting solution was filtered (Bio Rad poly-prep chromatography column) and desalted using a Sep-Pak cartridge (Waters Corporation, MA). The following 260 nm extinction coefficients were used to determine the concentration of oligonucleotides: rG = 11,700, rC = 7,300, rA = 15,400, rU = 10,100, and **5** = 10,700.

A1.5 – Oligonucleotide Sequencing Using MALDI-TOF MS

The MW and sequencing of the modified oligonucleotide was determined via MALDI-TOF MS. 1 µL of a ~200 µM stock solution of the synthesized RNA was combined with 1 µL of 100 mM ammonium citrate buffer (PE Biosystems), 1 µL of a 75 µM DNA standard (17-mer) and 4 µL of saturated 3-hydroxypicolinic acid. The samples were desalted with an ionexchange resin (PE Biosystems) and spotted onto a gold-coated plate where they were air dried. The resulting spectra were calibrated relative to the +1 and +2 ions of the internal DNA standard (5225.8 and 2613.4, respectively), thus the observed oligonucleotides should have a resolution of ±2 mass units. MALDI-TOF MS calc. for the +1 and +2 oligonucleotide ions: 8720.5 and 4360.8, respectively; found 8718.5 and 4358.3.

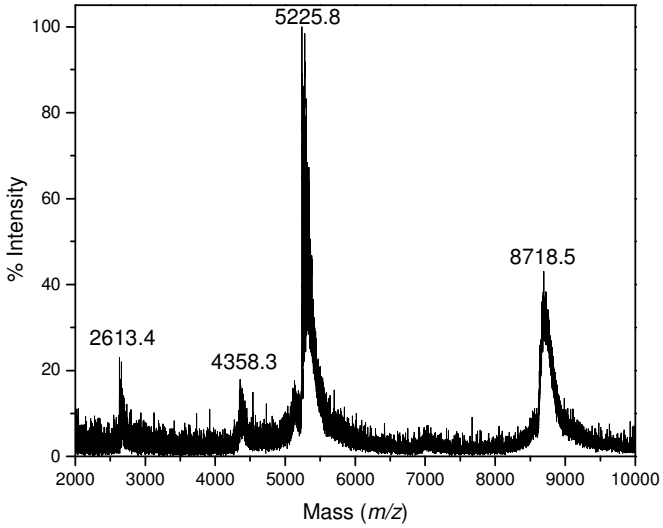

Figure A1.2: MALDI-TOF MS spectrum of the modified RNA calibrated relative to the +1 and +2 ions of an internal 17-mer DNA standard (m/z: 5225.8 and 2613.4). Calculated mass = 8720.5; observed mass = 8718.5.

A1.6 – Photophysical Studies of Oligonucleotides

Steady state fluorescence experiments were carried out at 21 ºC in a 150 µL quartz fluorescence cell with a path length of 1.0 cm (Hellma GmbH & Co KG, Müllheim, Germany) on a Jobin Yvon Horiba FluoroMax-3 luminescence spectrometer with excitation and emission slit-widths of 8 nm. RNA samples were hybridized by heating to 75 ºC for 5 min and subsequently allowed to cool to room temperature over 2 h prior to measurements. RNA samples were measured at 1 × 10^{-6} M concentration in 20 mM cacodylate buffer (pH 7.0, 100 mM NaCl, 0.5 mM EDTA).

A1.7 – Thermal Denaturation Measurements

All hybridizations and UV melting experiments were carried out at 1 × 10^{-6} M concentration in 20 mM cacodylate buffer (pH 7.0, 100 mM NaCl, 0.5 mM EDTA), using a Beckman-Coulter DU® 640 spectrometer with a high performance temperature controller and micro auto six holder. Samples were heated to 75 ºC for 5 min, cooled to room temperature over 2 h, and placed on ice for 30 min prior to measurements. Samples were placed in a stoppered 1.0-cm path length cell (Beckman-Coulter) and a background spectrum (buffer) was subtracted from each sample. Denaturation runs were performed between 25 and 90 ºC at a scan rate of 1.0 ºC min^{-1} with optical monitoring every ºC at 260 nm. Beckman-Coulter software (provided with T_m Analysis Accessory for DU® Series 600 Spectrometers) determined the melting temperatures utilizing the first derivative from the melting profile.

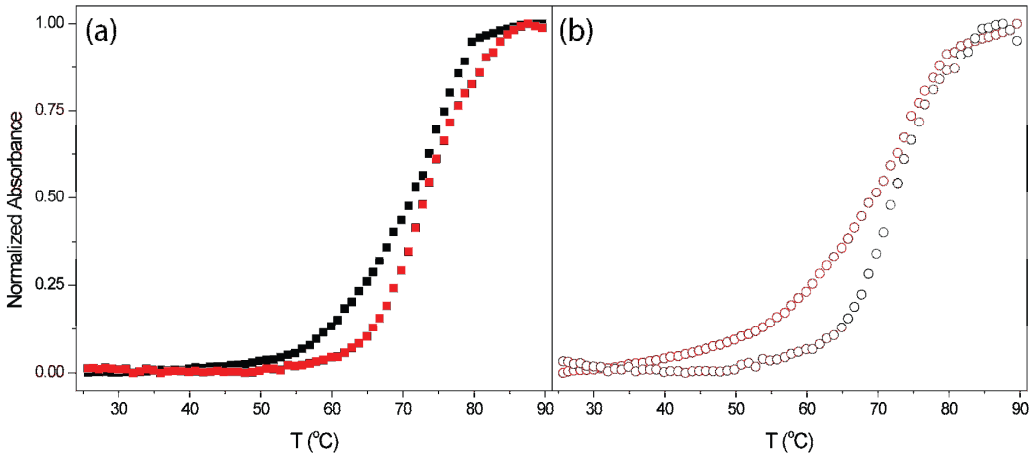

Figure A1.3: (a) Thermal denaturation curve (■) and reverse thermal denaturation curve (■) for control RNA construct **9**. (b) Thermal denaturation curve (o) and reverse thermal denaturation curve (o) for modified RNA **10**. T_m of control RNA = 72 ºC. T_m of modified RNA = 71 ºC.

A1.8 – Aminoglycoside Titrations

All titrations were performed with working solutions of 1μM **10** in 20μM calcodylate buffer (pH 7.0, 100 mM NaCl, 0.5 mM EDTA). The solutions were heated to 75 ºC for 5 min, cooled to room temperature over 2 h, and placed on ice for 30 min prior to titrations. The solutions were placed in a 0.5 mL quartz fluorescence cell with a path length of 1.0 cm (Hellma GmbH & Co KG, Müllheim, Germany). Steady state fluorescence experiments were carried out at ambient temperature (21℃) on a Jobin Yvon Horiba FluoroMax-3 luminescence spectrometer with excitation and emission slit-widths of 8 nm. A background spectrum (buffer) was subtracted from each sample. For binding studies, **10** was excited at 320 nm, and changes in emission upon titration with **11** or **12** were monitored at 395 nm and 470 nm. The concentrations of **11** or **12** was determined by UV absorbance at 400 nm (ε = 20,000 $M^{-1}cm^{-1}$). For competition studies, **11** or **12** was titrated into **10** until saturation. **10** was excited at 320 nm, and changes in emission upon displacement of **11** or **12** by aminoglycosides were monitored at 395 nm and 470 nm. Errors were generated from three sets of measurements.

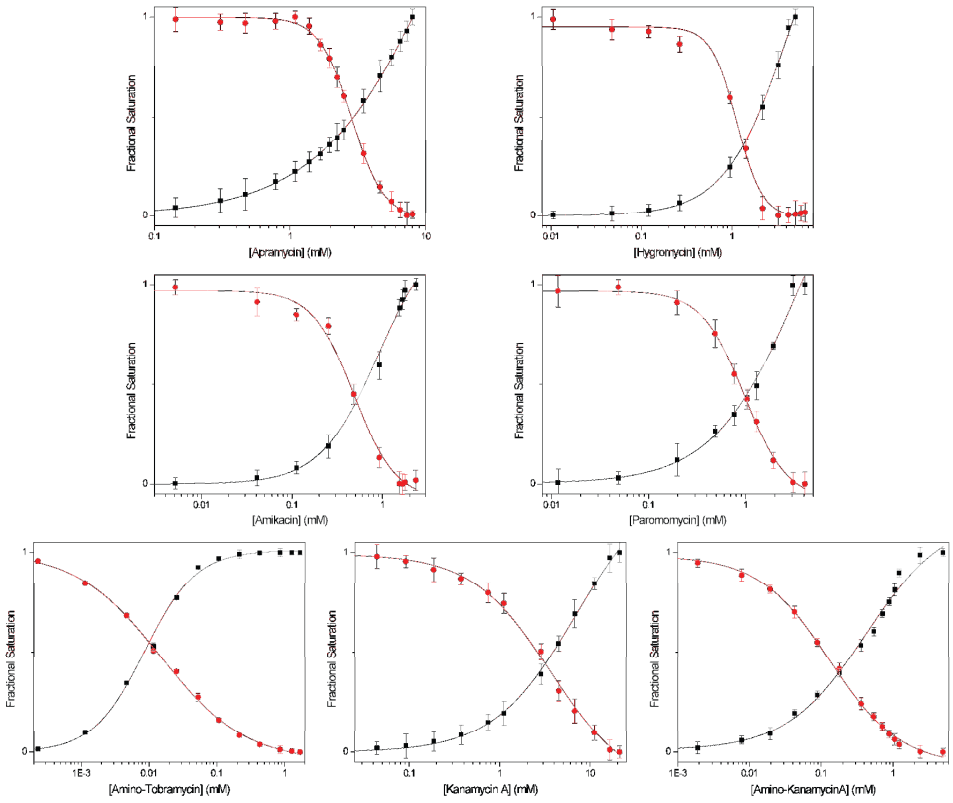

Figure A1.4: Response of the fluorescent donor (■) in the labeled A-site and the emissive acceptor (●) in the labeled aminoglycoside **11** in the displacement of the A-site bound **11** with

aminoglycosides. Conditions: **10** (1×10^{-6} M), cacodylate buffer pH 7.0 (2.0×10^{-2} M), NaCl (1.0×10^{-1} M).

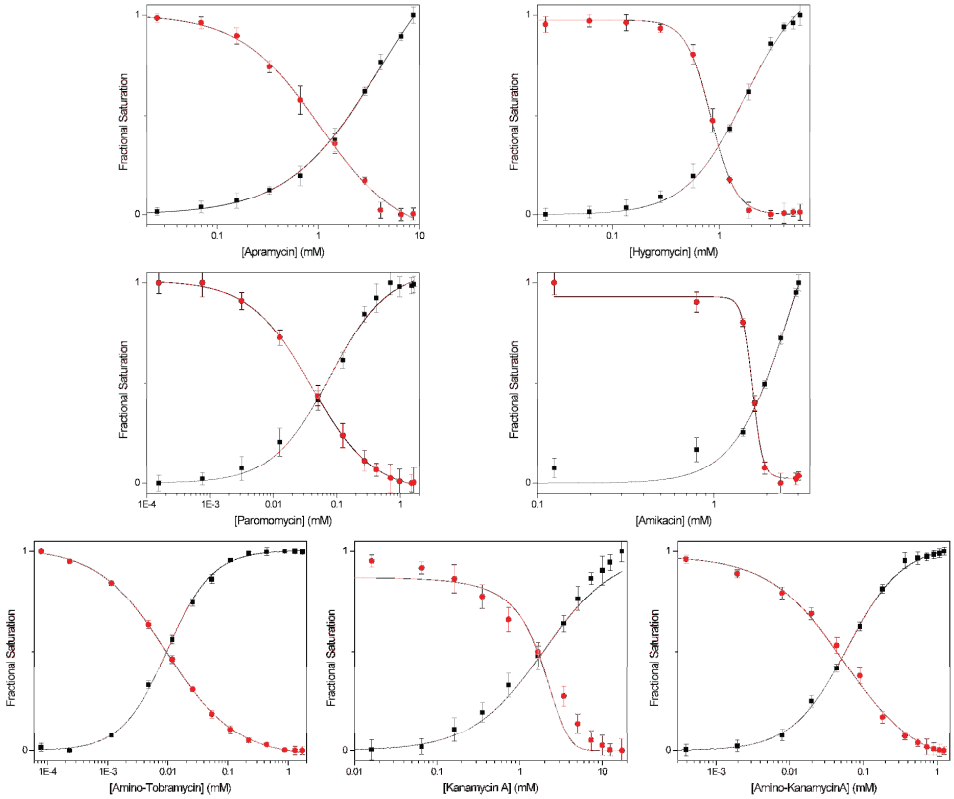

Figure A1.5: Response of the fluorescent donor (■) in the labeled A-site and the emissive acceptor (●) in the labeled aminoglycoside **12** in the displacement of the A-site bound **12** with aminoglycosides. Conditions: **10** (1×10^{-6} M), cacodylate buffer pH 7.0 (2.0×10^{-2} M), NaCl (1.0×10^{-1} M).

A1.9 – References

(A1) a) Wang, H.; Tor, Y. *Angew. Chem. Int. Ed.* **1998,** 37, 109–111. b) Michael, K.; Wang, H.; Tor, Y. *Bioorg. Med. Chem.* **1999,** 7, 1361–1371. c) Boer, J.; Blount, K. F.; Luedtke, N. W.; Elson-Schwab, L.; Tor, Y. *Angew. Chem. Int. Ed.* **2005,** 44, 927–932.

(A2) Du, H.; Fuh, R. A.; Li, J.; Corkan, A.; Lindsey, J. S. *Photochem. and Photobiol.,* **1998**, *68*, 141–142.

(A3) Lavabre, D.; Fery-Forgues, S. *J. Chem. Educ.*, **1999**, *76*, 1260–1264.

Appendix 2: Supporting Information for Chapter 2

Supporting Information

A2.1 – Selectivity Ratio and Average Histopathology Score

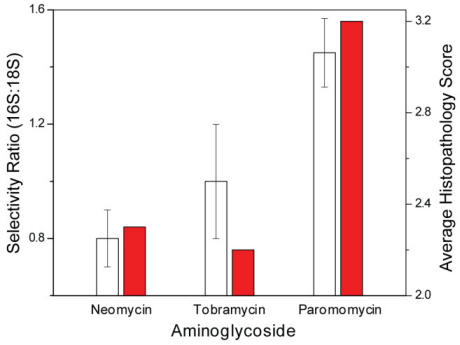

Figure A2.1: The selectivity ratio and average histopathology score[S1] for neomycin, tobramycin, and paromomycin.

A2.2 – Synthesis

General Procedures

NMR spectra were recorded on a Varian Mercury 400 or 500 MHz spectrometer. Mass spectra were recorded at the UCSD Chemistry and Biochemistry Mass Spectrometry Facility, utilizing either a LCQDECA (Finnigan) ESI with a quadrapole ion trap or a MAT900XL (ThermoFinnigan) FAB double focusing mass spectrometer. UV-Vis spectra were recorded on either a Hewlett Packard 8453 Diode Array Spectrometer or Shimadzu UV-2450. Unless otherwise specified, materials obtained from commercial suppliers were used without further purification. NMR solvents were purchased from Cambridge Isotope Laboratories (Andover, MA).

Synthetic Schemes

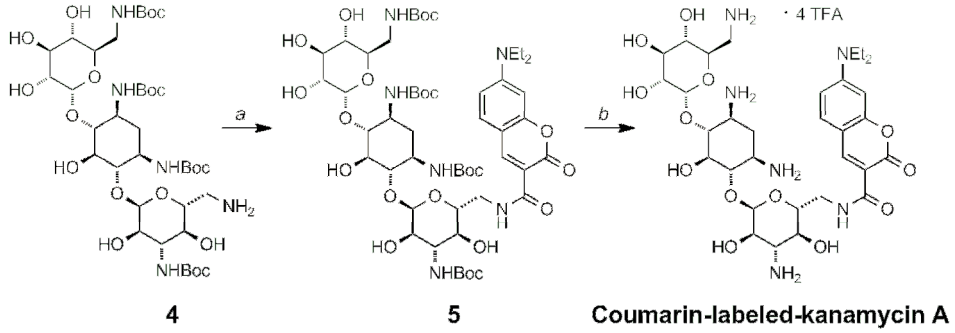

Scheme A2.1: Synthesis of coumarin-labeled-kanamycin A. (a) 7-(Et_2N)coumarin-3-carboxylic acid (1.2 eq.), EDC (1.2 eq.), DMAP (1.2 eq.), iPr$_2$EtN (2.2 eq.), dichloromethane, 87%. (b) TFA, triisopropylsilane, CH_2Cl_2, 72%.

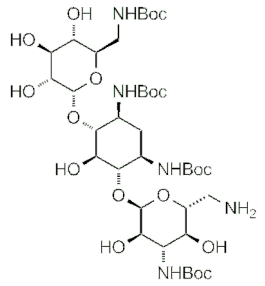

4

6''-Amino-6''-deoxy-(Boc)$_4$kanamycin A (4). Synthesis and characterization of precursors previously reported.[S2]

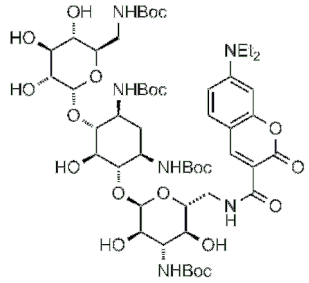

5

Boc$_4$-protected coumarin-labeled-kanamycin A (5). Anhydrous *N,N*-dimethylformamide (300 µL), and 7-(diethylamino)coumarin-3-carboxylic acid (20 mg, 76.6 µMol) were added to **4** (45.2 mg, 51.1 µMol). To this, EDC (11.8 mg, 61.3 µMol), *N,N*-diisopropylethylamine (22 µL, 127.7 µMol), and 4-(dimethylamino)pyridine (1.9 mg, 15.3 µMol) were added. The reaction was stirred at RT for 18 h. The solvent was removed under reduced pressure and the resulting solid was dissolved in ethyl acetate and washed with water and brine. The organic layer was dried over sodium sulfate and the solvent was removed under reduced pressure. After flash chromatography (5-10% methanol in dichloromethane), a green product (50.1 mg, 44.5 µMol, 87% yield) was isolated. ^{1}H-NMR (400 MHz, CD_3OD): δ 8.61 (s, 1H), 7.54 (d, *J*=12, 1H), 7.31–7.24 (m, 1H), 6.82 (dd, *J*=4, 10, 1H), 6.56 (d, *J*=4, 1H), 5.14 (s, 1H), 4.96 (s, 1H), 4.72 (s, 1H), 4.51–4.43 (m, 1H), 3.85–3.81 (m, 1H), 3.63–3.30 (m, 19H), 3.19–3.14 (m, 4H), 3.08 (t, *J*=10, 1H), 2.06–1.97 (m, 2H), 1.44 (s, 36H), 1.23–1.17 (m, 10H); ^{13}C-NMR (125 MHz, DMSO-d_6): δ 174.25, 162.64, 161.80, 161.75, 157.25, 156.17, 154.89, 152.49, 147.79, 131.67, 129.64, 110.20, 107.64, 95.79, 77.85, 77, 71, 77.27, 44.30, 35.13, 31.29, 29.09, 29.03, 28.99, 28.83, 28.69, 28.58, 28.22, 28.16, 27.33, 26.56, 25.09, 22.08, 13.89, 12.30; ESI-MS calculated for $C_{52}H_{82}N_6O_{21}$ $[M+Na]^+$ 1149.33, found 1149.54.

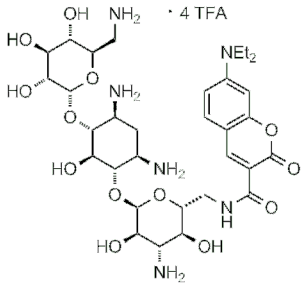

Coumarin-labeled-kanamycin A. Anhydrous dichloromethane (2 mL) and triisopropylsilane (200 µL) were added to **5** (8.64 mg, 7.67 µmol). To this solution, trifluoroacetic acid (2 mL) was added and the reaction was stirred at RT for 15 min. The reaction was diluted with toluene (5 mL) and the solvent was removed under reduced pressure. The resulting solid was dissolved in water and washed with dichloromethane. The aqueous layer was dried concentrated under reduced pressure and further purified by reverse phase HPLC, 15 – 26% acetonitrile (0.1% TFA) in water (0.1% TFA) over 16 min, and eluted at 13.2 min. Product: yellow powder (7.1 mg, 6.0 µmol, 72% yield).^{1}H-NMR (500 MHz, D_2O): δ 8.67 (s, 1H), 7.65 (d, *J* = 9.3, 1H), 6.95 (dd, *J* = 2.4, 9.3, 1H), 6.72 (d, *J* = 2.0, 1H), 5.37 (d, *J* = 3.9, 1H), 5.10 (d, *J* = 3.5, 1H), 4.13–4.08 (m, 1H), 4.01 (dd, *J* = 3.9, 9.2, 1H), 3.91 (dd, *J* = 3, 14.4, 1H), 3.85 (t, *J* = 8.75, 1H), 3.79–3.48 (m, 22H), 3.36 (dd, *J* = 2.5, 13.2, 1H), 3.21 (dd, *J* = 7.3, 14.9, 2H), 3.10 (dd, *J* = 6.6, 11.1, 1H), 2.94 (t, *J* = 9.8, 1H), 2.79 (dd, *J* = 9.3, 13.5, 1H), 2.50–2.45 (m, 1H), 1.88–1.80 (m, 1H), 1.29 (t, *J* = 7.3, 4H), 1.25 (t, *J* = 7.1, 6H); ^{13}C-NMR (125 MHz, D_2O): δ 166.22, 164.36, 163.68 (q, J_1 = 42 Hz, J_2 = 85.5)158.09, 153.21, 149.42, 132.70, 117.04 (q, J_1 = 343.5 Hz, J_2 = 694.5),112.85, 109.91, 101.49, 98.09, 96.55, 84.71, 77.20, 73.83, 72.24, 69.36, 68.72, 68.24, 55.39, 50.44, 49.04, 47.35, 46.62, 41.30, 40.82, 28.27, 12.27, 8.91; ESI-MS calculated for $C_{32}H_{50}N_6O_{13}$ $[M+2H]^{2+}$ 364.18, $[M+H]^+$ 727.35, and $[M+Na]^+$ 749.33, found 364.22, 727.14, and 749.29, respectively.

A2.3 – Absorption and Emission Spectra of F1, F2, and F3.

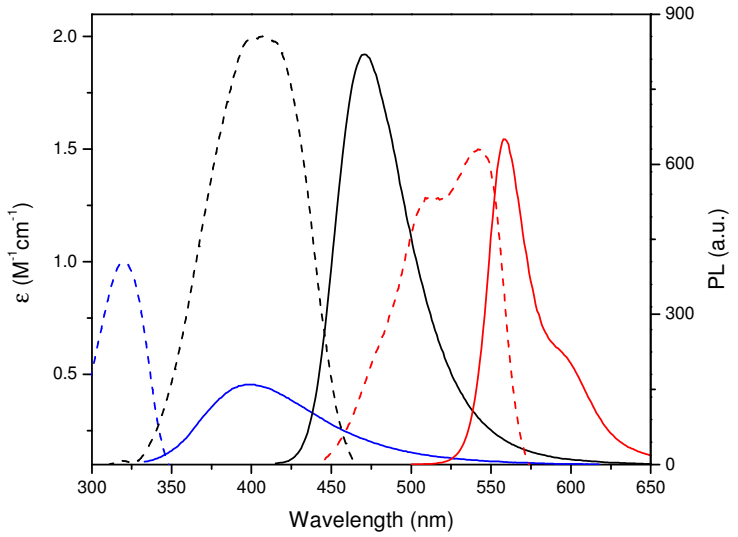

Figure A2.2: Absorption (---) and emission (—) spectra of **F1** (blue), **F2** (black), and **F3** (red) in water. Conditions: **F1** (1.0×10^{-5} M), **F2** (1.0×10^{-5} M), and **F3** (1×10^{-5} M).

A2.4 – Oligonucleotide Purification

The Dy547 18S A-site RNA construct was purchased from Thermo Scientific. The modified 16S oligonucleotide was synthesized and characterized according to previously reported procedures.[S3]

A2.5 – Antibiotic Titrations

All titrations were performed with working solutions of 0.5 μM **16S** and **18S** A-site RNAs in 20mM calcodylate buffer (pH 7.0, 100 mM NaCl, 0.5 mM EDTA). Separate solutions of each RNA were heated to 75 ºC for 5 min, cooled to room temperature over 2 h, and placed on ice for 30 min prior to titrations. Then an equimolar amount of the two annealed RNA constructs were combined with a two mole equivalent of coumarin-labeled-kanamycin A to give a final concentration of 0.5 μM for each of the RNA components and 2 μM for coumarin-labeled-kanamycin. The solutions were placed in a 0.125 mL quartz fluorescence cell with a path length of 1.0 cm (Hellma GmbH & Co KG, Müllheim, Germany). Steady state fluorescence experiments were carried out at ambient temperature (21 ºC) on a Jobin Yvon Horiba FluoroMax-3 luminescence spectrometer with excitation and emission slit-widths of 8 nm. A background spectrum was subtracted from each sample. For binding studies, the **16S** A-site was excited at 320 nm and changes in emission upon titration with antibiotics were monitored at 395 nm and 473 nm. For the **18S** A-site, antibiotics

were titrated and the system was excited at 400 nm. Changes in emission were monitored at 561 nm. Errors were generated from three sets of measurements.

IC_{50} values were calculated using OriginPro 8 software by fitting a dose response curve (eq 1) to the fractional fluorescence saturation (F_s) plotted against the log of antibiotic (A) concentration.

$$F_s = F_0 + (F_\infty[A]^n)/([EC_{50}]^n + [A]^n) \qquad (1)$$

F_i is the fluorescence intensity at each titration point. F_0 and F_∞ are the fluorescence intensity in the absence of aminoglycoside or at saturation, respectively, and *n* is the Hill coefficient or degree of cooperativity associated with the binding.

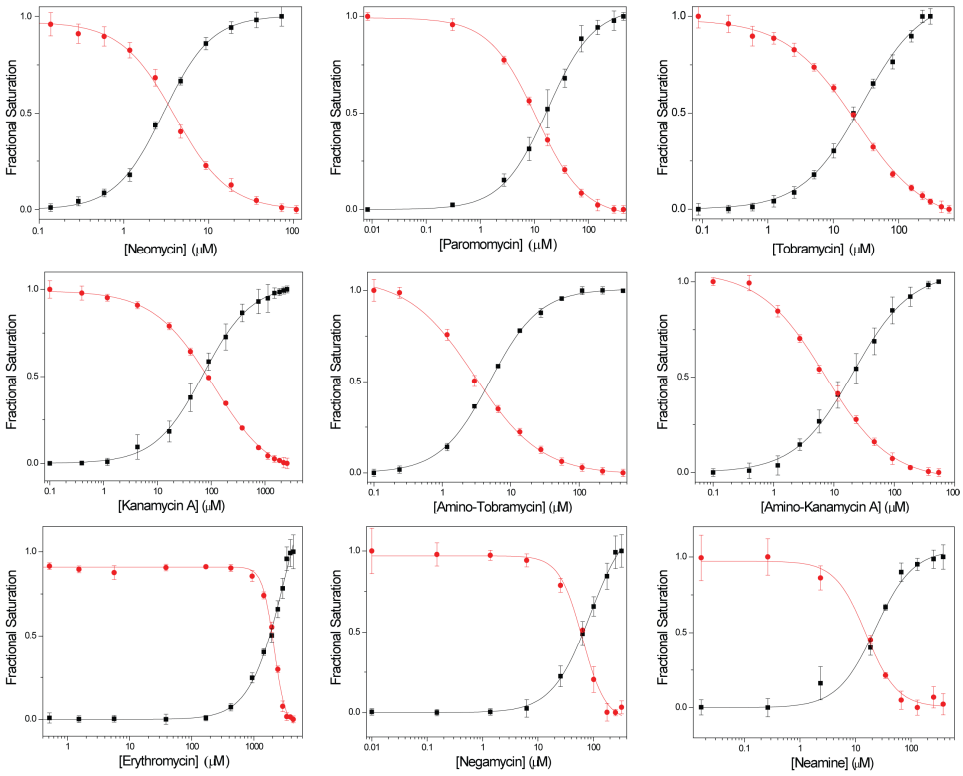

Figure A2.3: Fractional fluorescence saturation of the donor F1 (■) in the labeled 16S A-site and the emissive fluorophore F2 (●) tagged to kanamycin A in studying the binding of different antibiotics. Conditions: 16S RNA (5×10^{-7} M), 18S RNA (5×10^{-7} M), coumarin-labeled-kanamycin A (2.2×10^{-6} M), cacodylate buffer pH 7.0 (2.0×10^{-2} M), NaCl (1.0×10^{-1} M).

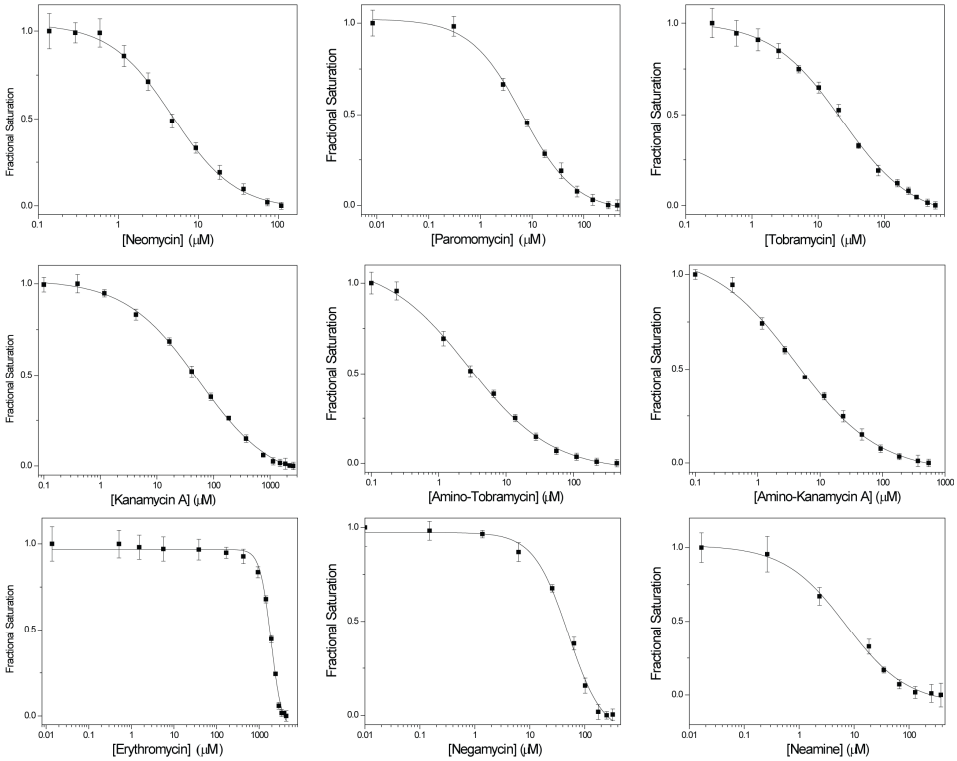

Figure A2.4: Fractional fluorescence saturation of the emissive acceptor F3 (■) of the 18S A-site in studying the binding of different antibiotics. Conditions: 16S RNA (5×10^{-7} M), 18S RNA (5×10^{-7} M), coumarin-labeled-kanamycin A (2.2×10^{-6} M), cacodylate buffer pH 7.0 (2.0×10^{-2} M), NaCl (1.0×10^{-1} M).

A2.6 – Independent Titration Data

To determine if the placement of an internal fluorescent nucleoside in the A-site construct would inherently produce a difference in affinity as compared to end labeling the RNA, an independent experiment was conducted. A 16S A-site construct was labeled at the 5' end with Dy547 (Figure A5), which is how the 18S construct was labeled for the double FRET experiments. IC_{50} values (Table A1) were determined for unlabeled antibiotics by monitoring the displacement of coumarin-labeled-kanamycin A from the 16S-Dy547 A-site RNA. The IC_{50} values obtained were in good agreement and within experimental error for the values obtained in the 16S A-site that was labeled with an isosteric fluorescent nucleoside analogue at position 1406.

In addition, to determine if the system would be sensitive to a possible 16S RNA/18S RNA interaction, the 5' end Dy547 labeled 18S A-site construct was used alone to monitor the displacement of coumarin-labeled-kanamycin A by unlabeled neomycin (IC_{50} = 5.0 ± 0.4) and tobramycin (IC_{50} = 21 ± 2). The data is within error to the values obtained from the orthogonal FRET system, indicating that a 16S RNA/18S RNA interaction is unlikely to occur.

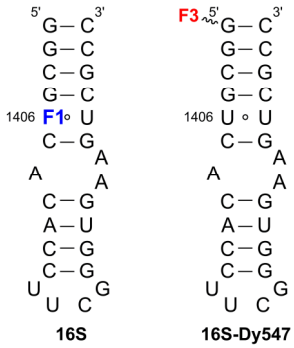

Figure A2.5: Secondary structures for the 27-base RNA models of the internally- and end-labeled 16S A-sites.

Table A2.1: IC_{50} Values of Antibiotics for the 16S and 16S-Dy547 A-sites.[a]

Antibiotics	16S A-Site (10^{-6} M)	16S-Dy547 A-Site (10^{-6} M)
Neomycin B	2.8 (± 0.3)	2.6 (± 0.4)
Tobramycin	20.2 (± 0.4)	18.5 (± 0.5)
Paromomycin	9 (± 1)	10 (± 1)
Kanamycin A	75 (± 3)	80 (± 4)
Amino-Tobramycin	4.2 (± 0.4)	3.5 (± 0.6)
Amino-Kanamycin A	11.9 (± 0.4)	11 (± 1)
Negamycin	62 (± 5)	60 (± 4)
Neamine	18 (± 2)	19 (± 1)
Erythromycin	1880 (± 10)	—
Lincomycin	$> 8.5 \times 10^3$	—
Linezolid	$> 9.6 \times 10^3$	—

[a] Conditions: 16S RNA (5×10^{-7} M), 16S-Dy547 RNA (5×10^{-7} M), coumarin-labeled-kanamycin A (2.2×10^{-6} M), cacodylate buffer pH 7.0 (2.0×10^{-2} M), NaCl (1.0×10^{-1} M).

A2.7 – References

(A1) C. F. Kostrub, R. Diokno, J. B. Aggen, G. H. Miller, J. K. Judice and P. M. Tulkens, in *19th European Congress of Clinical Microbiology and Infectious Diseases*; Blackwell Publishing: Helsinki, Finland, 2009.

(A2) H. Wang and Y. Tor, *Angew. Chem. Int. Ed.,* 1998, **37**, 109–111.

(A3) Y. Xie, A. V. Dix and Y. Tor, *J. Am. Chem. Soc.,* 2009, **131**, 17605–17614.

Appendix 3: Supporting Information for Chapter 3

Supporting Information

A3.1 – Synthesis

General Procedures

NMR spectra were recorded on a Varian Mercury 400 MHz spectrometer. Mass spectra were recorded at the UCSD Chemistry and Biochemistry Mass Spectrometry Facility, utilizing either a LCQDECA (Finnigan) ESI with a quadrapole ion trap or a MAT900XL (ThermoFinnigan) FAB double focusing mass spectrometer. UV-Vis spectra were recorded on either a Hewlett Packard 8452A or 8453 Diode Array Spectrometer.

Unless otherwise specified, materials obtained from commercial suppliers were used without further purification. 2-amino-6-nitrobenzoic acid was purchased from Accela ChemBio Inc. Anhydrous pyridine, dichloroethane and acetonitrile were obtained from Fluka. Anhydrous *N,N*-diisopropylethylamine and triethylamine were obtained from Acros. The unmodified oligonucleotides were purchased from Integrated DNA Technologies. Standard phosphoramidites and solutions necessary for solid phase RNA synthesis were purchased from Glen Research. Oligonucleotides were purified by gel electrophoresis and desalted on a Sep-Pak (Waters Corporation). Chemicals for preparing buffer solutions were purchased from Fisher Biotech (enzyme grade). Autoclaved water was used in all fluorescence titrations. NMR solvents were purchased from Cambridge Isotope Laboratories (Andover, MA).

Synthetic Schemes

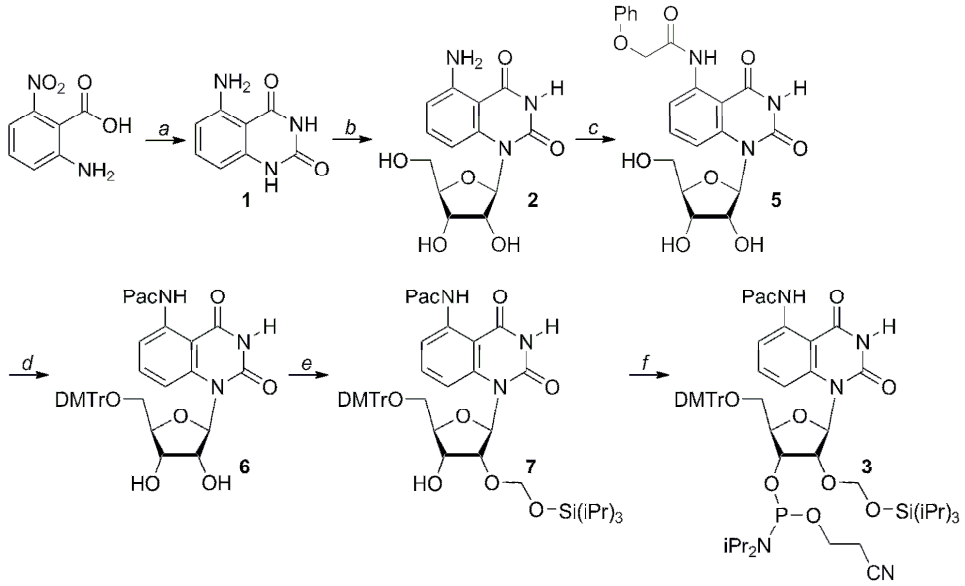

Scheme A3.1: Synthesis of **3**. (a) (i) Urea; (ii) $SnCl_2$, conc. HCl, 20%. (b) (i) *N,O*-bis(trimethylsilyl)acetamide, $CF_3SO_3Si(CH_3)_3$, β-D-ribofuranose 1-acetate 2,3,5-tribenzoate, CH_3CN; (ii) conc. NH_4OH, 80%. (c) $(CH_3)_3SiCl$, phenoxyacetic anhydride, H_2O, conc. NH_4OH, pyridine, 75%. (d) DMTrCl, Et_3N, pyridine, 82%. (e) *i*Pr_2NEt, *n*Bu_2SnCl_2, (*i*$Pr_3SiO)CH_2Cl$, $ClCH_2CH_2Cl$, 30%. (f) *i*Pr_2NEt, (*i*$Pr_2N)P(Cl)O$-CH_2CH_2CN, $ClCH_2CH_2Cl$, 60%.

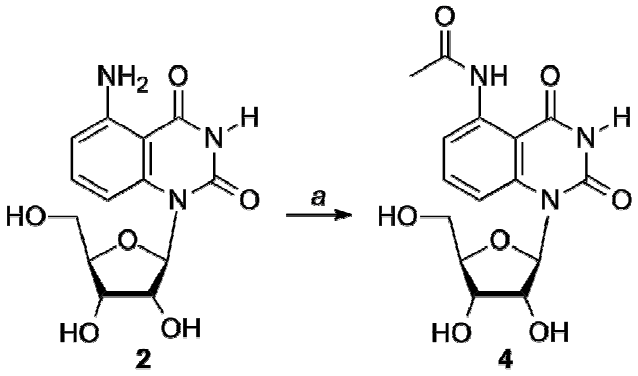

Scheme A3.2: Synthesis of **4**. (a) $(CH_3)_3SiCl$, acetic anhydride, H_2O, conc. NH_4OH, pyridine, 75%.

5-Aminoquinazoline-2,4(1*H*,3*H*)-dione (1). Urea (4.99 g, 83.2 mmol) was mixed with to 2-amino-6-nitrobenzoic acid (4.96 g, 27.3 mmol). The powder was heated to 200 °C for 4 h. The reaction was cooled to room temperature. Using a coarse frit, the solid was washed with water (125 mL), 5% sodium bicarbonate (100 mL), 10% sodium carbonate (200 mL), dilute sulfuric acid (140 mL), and boiling methanol (125 mL). The solid was stirred in boiling 50% acetic acid (400 mL) for 1 h. The remaining solid was filtered off and the solution was brought back to boiling. The solution was allowed to cool to room temperature and crystals were collected by filtration. The crystals were redissolved in boiling 50% acetic acid. Activated carbon was added to the solution and boiled for 10 min. The solution was filtered hot and allowed to crystallize. The clear yellow crystals, 5-nitroquinazoline-2,4(1*H*,3*H*)-dione, were used without further purification. A suspension of tin chloride (4.1 g, 21.6 mmol) in concentrated HCl (50 mL) was brought to boiling. 5-Nitroquinazoline-2,4(1*H*,3*H*)-dione (1.11 g, 5.4 mmol) was added, and the suspension was refluxed for 5 h. The boiling suspension was filtered with a coarse frit, and the solid was washed with water (200 mL). Product: white solid (0.95 g, 5.35 mmol, 20 % yield over two steps). ^{1}H-NMR (400 MHz, DMSO-d_6): δ 10.86 (s, NH, 1H), 10.73 (s, NH, 1H), 7.14 (t, J = 8.0 Hz, 1H), 7.06 (s, NH_2, 2H), 6.27 (d, J = 8.0 Hz, 1H), 6.13 (d, J = 7.6 Hz, 1H); ^{13}C-NMR (100 MHz, DMSO-d_6): δ 166.36, 151.98, 150.76, 142.77, 135.61, 108.50, 100.76, 98.34; ESI-MS calculated for $C_8H_7N_3O_2$ $[M+H]^+$ 178.06, found 178.29.

5-Aminoquinazoline-2,4(1*H*,3*H*)-dione ribonucleoside (2). To a suspension of **1** (1.2 g, 6.8 mmol) in anhydrous acetonitrile (100 mL), *N,O*-Bis(trimethylsilyl)acetamide (8.7 mL, 34 mmol) was added dropwise under argon. The reaction was stirred at 25 °C for 30 min. TMSOTf (0.4 mL, 0.33 mmol) and β-D-ribofuranose-1-acetate-2,3,5-tribenzoate (3.43 g, 6.8 mmol) were added at the same time under argon. The reaction temperature was raised to 50 °C. The reaction was stirred at 50 °C for 5 h. TMSOTf (0.4 mL, 0.33 mmol) and β-D-ribofuranose-1-acetate-2,3,5-tribenzoate (3.43 g, 6.8 mmol) were added at the same time under argon again. The reaction was stirred at 50 °C for 26 h. The reaction was cooled to room temperature,

concentrated to an oil, and diluted with dichloromethane (70 mL). The solution was washed with saturated sodium bicarbonate and brine. The organic layer was dried over sodium sulfate. The solvent was removed under reduced pressure, and the crude product was dissolved in dioxane (30 mL) and transferred to two 200 mL pressure tubes. Ammonium hydroxide (28%, 80 mL) was added to each tube. The reaction was stirred at 70 °C for 24 h. The solvent was removed under reduced pressure, and the product was isolated by flash chromatography (5-12% methanol in dichloromethane). Product: white solid (0.14 g, 0.42 mmol, 81 % yield over two steps). ^{1}H-NMR (400 MHz, DMSO-d_6): δ 11.22 (s, NH, 1H), 7.22 (s, NH_2, 2H), 7.20 (t, J = 8.4 Hz, 1H), 6.61 (d, J = 8.4 Hz, 1H), 6.44 (d, J = 8.4 Hz, 1H), 5.94 (d, J = 5.2 Hz, 1'-H, 1H), 5.16 (d, J = 5.6 Hz, 1H), 4.92 (d, J = 6.0 Hz, 1H), 4.84 (t, J = 5.2 Hz, 1H), 4.49 (q, J = 6.0 Hz, 1H), 4.05 (q, J = 6.0 Hz, 1H), 3.69 (m, 1H), 3.63 (m, 1H), 3.52 (quintet, J = 6.0 Hz, 1H); ^{13}C-NMR (100 MHz, DMSO-d_6): δ 165.16, 152.54, 150.79, 142.16, 135.33, 110.44, 102.24, 99.44, 91.22, 84.92, 69.63, 62.02; ESI-MS calculated for $C_{13}H_{15}N_3O_6$ $[M+H]^+$ 310.10, found 310.15.

5*N*-phenoxyacetylaminoquinazoline-2,4(1*H*,3*H*)-dione ribonucleoside (5). To a suspension of **2** (0.37 g, 1.19 mmol) in anhydrous pyridine (10.2 mL), chloro trimethylsilane (0.50 mL, 3.94 mmol) was added dropwise under argon. The reaction was stirred at 25 °C for 1.5 h. Phenoxyacetic anhydride (0.35 g, 1.31 mmol) was added under argon. The reaction was stirred at 25 °C for 21 h. The reaction was cooled on ice, and cold water (3.1 mL) was added. The reaction was stirred at 0 °C for 15 min. Cold aqueous ammonium hydroxide (4.1 mL) was added, and the reaction was stirred at 0 °C for 15 min. The solvent was removed under reduced pressure, and the product was isolated by flash chromatography (2-5.5% methanol in dichloromethane). Product: white solid (0.40 g, 0.90 mmol, 75 %). ^{1}H-NMR (400 MHz, CD_3OD): δ 8.60 (d, J = 8.4 Hz, 1H), 7.65 (t, J = 8.4 Hz, 1H), 7.45 (d, J = 8.4 Hz, 1H), 7.31 (t, J = 7.2 Hz, 2H), 7.12 (d, J = 8.4 Hz, 2H), 7.00 (t, J = 7.6, 1H), 6.11 (d, J = 4.8, 1H), 5.47 (s, 2'-OH, 1H), 4.78 (t, J = 4.4 Hz, 1H), 4.68 (s, 2H), 4.48 (s, 3'-OH, 1H), 4.36 (t, J = 6.0, 1H), 3.94 (s, 1H), 3.89 (s, 1H), 3.86 (t, 1H), 3.76 (d, J = 6.0 Hz, 1H), 3.73 (d, J = 6.0 Hz, 1H), 3.59 (s, 1H); ^{13}C-NMR (100 MHz, CD_3OD): δ 168.91, 164.97, 158.11, 135.49, 129.43, 121.81, 110.90, 92.02, 88.27, 84.78, 70.67, 69.62, 67.57, 61.93; ESI-MS calculated for $C_{21}H_{21}N_3O_8$ $[M-H]^-$ 442.13, found 442.39.

5′-Dimethoxytrityl-5*N*-phenoxyacetylaminoquinazoline-2,4(1*H*,3*H*)-dione ribonucleoside (6). Anhydrous pyridine (2.5 mL), anhydrous triethylamine (36 µL, 0.26 mmol) and 4,4′-dimethoxytrityl chloride (0.088 g, 0.26 mmol) were added to **5** (0.10 g, 0.23 mmol) over argon. The reaction was stirred at room temperature for 6 hours and quenched with methanol (0.5 mL). The solvent was removed under reduced pressure, and the product was isolated by flash chromatography (1% triethylamine, 40% ethylacetate, 59 % hexanes). Product: off-white solid (0.14 g, 0.18 mmol, 82 % yield). ^{1}H-NMR (400 MHz, $CDCl_3$): δ 8.45 (d, J = 8.4 Hz, 1H), 7.55 (d, J = 8.4 Hz, 1H), 7.41 (d, J = 7.2 Hz, 1H), 7.24–7.16 (m, 12H), 7.15–6.95 (m, 7H),

6.39 (d, *J* = 5.6 Hz, 1H), 5.36 (s, 1H), 4.84 (t, *J* = 5.4 Hz, 1H), 4.59 (s, 2H), 4.07 (br, 1H), 3.73 (s, 6H), 3.50−3.41 (m, 2H); ^{13}C-NMR (100 MHz, $CDCl_3$): δ 168.13, 165.50, 158.69, 157.59, 150.80, 144.97, 141.45, 141.14, 136.04, 135.98, 135.92, 130.48, 129.88, 128.54, 128.05, 127.06, 122.23, 115.14, 114.64, 113.33, 112.02, 103.94, 94.61, 90.66, 86.55, 83.64, 69.79, 69.38, 67.98, 63.37, 63.18, 55.44, 53.08, 46.14; HR-MS calculated for $C_{42}H_{39}N_3NaO_{10}$ $[M+Na]^+$ 768.25, found 768.25.

2'-(Trisisopropylsiloxy)methyl-5′-dimethoxytrityl-5*N*-phenoxyacetylaminoquinazoline-2,4(1*H*,3*H*)-dione ribonucleoside (7). Anydrous dichloroethane (2 mL) and *N,N*-diisopropylethylamine (0.11 mL, 63 mmol) were added to **6** (0.13 g, 0.17 mmol). Dibutyltin dichloride (0.052 g, 0.17 mmol) was added to the reaction under argon and stirred at room temperature for 1 h. The reaction was placed into a 80 ℃ water bath and stirred for 10 min. (Triisopropylsiloxy)methyl chloride (52 µL, 20 mmol) was added, and the reaction was stirred at 80 ℃ for 15 min. The reaction was diluted with dichloromethane (10 mL) and poured into saturated sodium bicarbonate (15 mL). The mixture was stirred vigorously for 15 min. The organic layer was extracted, and the aqueous layer was washed with dichloromethane (5 mL). The organic layers were pooled and dried over sodium sulfate. The solvent was removed under reduced pressure, and the product was isolated by flash chromatography (1% triethylamine, 35% ethyl acetate, 64% hexanes). Product: off-white foam (0.05 g, 0.05 mmol, 30 % yield). ^{1}H-NMR (400 MHz, CD_3OD): δ 8.60 (s, 1H), 7.46 (d, *J* = 6.8 Hz, 1H), 7.32 (m, 6H), 7.11–7.18 (m, 6H), 6.99 (m, 2H), 6.67–6.77 (m, 5H), 5.86 (d, *J* = 5.6 Hz, 1H), 4.67 (s, 1H), 4.48 (s, 1H), 4.16 (s, 2H), 4.11 (m, 2H), 3.90 (m, 1H), 3.75 (s, 6H), 3.16–3.20 (m, 2H), 2.08 (s, 1H), 2.01 (m, 3H), 1.39−1.19 (m, 18H); ^{13}C-NMR (100 MHz, $CDCl_3$): δ 168.33, 165.81, 158.79, 157.61, 150.87, 145.02, 141.51, 141.28, 136.66, 136.58, 136.48, 130.44, 130.41, 129.88, 128.49, 128.08, 128.02, 127.16, 122.35, 115.04, 113.37, 112.09, 103.85, 94.62, 90.69, 86.54, 81.48, 69.81, 69.66, 67.97, 67.94, 55.44, 55.41, 54.11, 29.93, 18.01, 17.93, 12.03; HR-MS calculated for $C_{52}H_{61}N_3NaO_{11}Si$ $[M+Na]^+$ 954.40, found 954.40.

3′-2-Cyanoethyldiisopropylphosphoramidite-2'-(Trisisopropylsiloxy)methyl-5′-dimethoxytrityl-5*N*-phenoxyacetylaminoquinazoline-2,4(1*H*,3*H*)-dione ribonucleoside (3). Anhydrous dichloroethane (1 mL) and *N,N*-diisopropylethylamine (0.11 mL, 0.64 mmol) were added to **7** (0.05 g, 0.05 mmol). The reaction was cooled on ice, and 2-cyanoethyl *N,N*-diisopropylchlorophosphoramidite (24 µL, 0.1 mmol) was added. The reaction was stirred at room temperature for 18 h. The solvent was removed under reduced pressure, and the product was isolated by flash chromatography (1% triethylamine, 15–30% ethyl acetate in hexanes). Product: white foam (0.036 g, 0.032 mmol, 60 % yield). ^{1}H-NMR (300 MHz, $CDCl_3$): δ 8.58 (m, 1H), 7.41 (m, 1H), 7.35 (d, 1H), 7.31–7.29 (m, 5H), 7.23–7.00 (m, 11H), 6.80–6.71 (m, 3H), 6.46 (m, 1H), 5.07 (d, *J* = 4.2 Hz, 1H), 4.91 – 4.94 (m, 2H), 4.62 (t, *J* = 6.4 Hz, 1H), 4.07 (b, 1H), 3.96 (s, 3H), 3.78 (s, 6H), 3.51 (m, 1H), 3.40 (m, 1H), 2.81 (q, *J* =

6.9 Hz, 1H), 2.01 (b, 1H), 1.20 – 1.15 (m, 12H), 1.01 (d, *J* = 6.8 Hz, 4H), 0.92–0.89 (m, 18H); ^{31}P-NMR (121 MHz, $CDCl_3$): δ 148.37, 147.94; HR-MS calculated for $C_{61}H_{78}N_5KO_{12}PSi$ $[M+K]^+$ 1170.48, found 1170.50.

5*N*-acetylaminoquinazoline-2,4(1*H*,3*H*)-dione ribonucleoside (4). To a suspension of **2** (0.049 g, 0.16 mmol) in anhydrous pyridine (1.4 mL), chloro trimethylsilane (0.1 mL, 0.83 mmol) was added dropwise under argon. The reaction was stirred at 25 ℃ for 1.5 h. Acetic anhydride (26 µL, 0.28 mmol) was added under argon. The reaction was stirred at 25 ℃ for 18 h. The reaction was cooled on ice, and cold water (0.4 mL) was added. The reaction was stirred at 0 ℃ for 15 min. Cold aqueous ammonium hydroxide (0.5 mL) was added and the reaction was stirred at 0 ℃ for 15 min. The solvent was removed under reduced pressure, and the product was isolated by flash chromatography (2% aq. ammonium hydroxide in acetonitrile). Product: white solid (0.017 g, 0.048 mmol, 30% yield). ^{1}H-NMR (400 MHz, CD_3OD): δ 8.40 (d, *J* = 8.0 Hz, 1H), 7.60 (t, *J* = 8.4 Hz, 1H), 7.35 (d, *J* = 8.4 Hz, 1H), 6.08 (d, *J* = 4.0 Hz, 1'-H, 1H), 4.77 (t, *J* = 5.2 Hz, 1H), 4.36 (t, *J* = 6.0 Hz, 1H), 3.93 (m, 1H), 3.87 (m, 1H), 3.76 (m, 1H), 3.73 (m, 1H), 2.21 (s, 3H); ^{13}C-NMR (100 MHz, CD_3OD): δ 170.45, 142.44, 141.74, 135.52, 114.06, 110.26, 92.01, 84.75, 70.69, 69.61, 61.93, 29.59, 24.07, 20.87, 13.80; ESI-MS calculated for $C_{15}H_{17}N_3O_7$ $[M+H]^+$ 352.11, found 352.15.

A3.2 – Photophysical Studies of Nucleoside 2.

UV-Vis spectra were recorded on a Hewlett Packard 8453 Diode Array Spectrometer in a 0.5 mL quartz fluorescence cell with a path length of 1.0 cm (Hellma GmbH & Co KG, Müllheim, Germany) at ambient temperature (21℃). Steady state fluorescence experiments were carried out at ambient temperature (21℃) in a 0.5 mL quartz fluorescence cell with a path length of 1.0 cm (Hellma GmbH & Co KG, Müllheim, Germany) on a Jobin Yvon Horiba FluoroMax-3 luminescence spectrometer with excitation and emission slit-widths of 5 nm. The $E_T(30)$ values of solvents were determined experimentally by taking the long wavelength absorption maximum of the dissolved Reichardt's dye.

All emission maxima in cm^{-1} were determined after correction of the intensity according:

$$\text{Intensity } [\upsilon] = \lambda^2 \times \text{Intensity } [\lambda].$$

Curve fits were generated using OriginPro 8. All reported standard deviations were calculated using STDEVP in Microsoft Excel.

Quantum yield for nucleoside **2** (Φ_F = 0.42±0.04) on its own and in the single strand RNA (Φ_F = 0.04) relative to the coumarin standard was determined using the following equation.[S1]

$$\Phi F(x) = (As/Ax)(Fx/Fs)(nx/ns)^2 \Phi F(s)$$

Where s is the standard, x is the nucleoside, A is the absorbance at excitation wavelength, F is the area under the emission curve, *n* is the refractive index of the solvent and ΦF is the quantum yield.[S1] In a similar fashion, the quantum yield for nucleoside **4** was determined to be 0.37±0.03.

Table A3.1: Photophysical properties of nucleoside **2**.

Solvent	$E_T(30)$	λ_{abs} (nm)	λ_{em} (nm)	Stokes Shift (cm^{-1})	ε_{350nm} (M^{-1} cm^{-1})
Water	63.1	349	445	6181	4239
Methanol	55.4	352	432	5261	4896
Acetonitrile	45.5	350	412	4300	5014
Dichloromethane	40.6	350	414	4417	4849
Dioxane	36.1	350	407	4001	5052

Table A3.2: Photophysical properties of nucleoside **4**.

Solvent	$E_T(30)$	λ_{abs} (nm)	λ_{em} (nm)	Stokes Shift (cm^{-1})	ε_{330nm} (M^{-1} cm^{-1})
Water	63.1	330	406	5672	2166
Methanol	55.4	331	396	4959	2300
Dioxane	36.1	333	385	4056	2247

A3.3 – Oligonucleotide Synthesis and Purification

The unmodified oligonucleotide was purchased from Integrated DNA Technologies. The modified oligonucleotide was synthesized on a Biosearch Cyclone Plus DNA synthesizer using a 0.2 µmole scale 500 Å CPG column. Phosphoramidite **3** was site specifically incorporated into the oligonucleotide by trityl-off synthesis of the base oligonucleotide, followed by manual coupling of phosphoramidite **3**. Typically, the modified phosphoramidite was dissolved in 100 µL of anhydrous acetonitrile to give a final concentration of 0.1M. The phosphoramidite solution was pushed into the CPG column via syringe and then 200 µL of 0.45M 1*H*-tetrazole was pushed into the other end of the column via syringe. Coupling reactions, performed twice, were allowed to proceed for 5 minutes (97% coupling efficiency) and were subsequently followed by standard oxidation and capping steps. The rest of the oligonucleotide was synthesized via the standard trityl-off procedure. Upon completion of the oligonucleotide synthesis, the CPG column was dried completely. The beads from the column were transferred into a 2.5 mL conical glass vial. 1mL of $MeNH_2$ in water and 1mL of $MeNH_2$ in ethanol were added. The vial was capped tightly and allowed to react for 15 h at room temperature. The supernatant from the reaction vial was transferred into Eppendorf tubes. The remaining beads were

washed with 3x500 µL of 33% ethanol in water. The supernatant was evaporated in speed vac. The solid residue was dissolved in 1 mL of 1M TBAF in THF and warmed to 50 ℃ for 5min. The deprotection took place overnight at 25 ℃. The reaction was quenched by adding 1 mL of Tris buffer (1M, pH 7.4). The volume was reduced to half by speed vac. The residue was desalted on a G10 sephadex column. The residue was loaded onto the column in 1 mL of water and eluted with 10 mL of water. The fractions were collected and analyzed by UV (260 nm). Fractions containing RNA were evaporated and desalted again on a G10 sephadex column. The desalted RNA was pooled together and evaporated in speed vac. The RNA was purified by 20% polyacrylamide gel electrophoresis. The oligonucleotide was visualized by UV shadowing; bands were excised from the gel and extracted with 0.3M sodium acetate buffer overnight. The resulting solution was filtered (Bio Rad poly-prep chromatography column) and desalted using a Sep-Pak cartridge (Waters Corporation, MA). The following 260 nm extinction coefficients were used to determine the concentration of oligonucleotides: rG = 11,700, rC = 7,300, rA = 15,400, rU = 10,100, and **2** = 10300.

A3.4 –Oligonucleotide MALDI-TOF MS

The MW and sequencing of the modified oligonucleotide was determined via MALDI-TOF MS. 1 µL of a ~200 µM stock solution of the synthesized RNA was combined with 1 µL of 100 mM ammonium citrate buffer (PE Biosystems), 1 µL of a 75 µM DNA standard (25-mer) and 4 µL of saturated 3-hydroxypicolinic acid. The samples were desalted with an ionexchange resin (PE Biosystems) and spotted onto a gold-coated plate where they were air dried. The resulting spectra were calibrated relative to the +1 ion of the internal DNA standard (7693.32). MALDI-TOF MS calc. for the +1 ions: 11088.87; found 11091.17.

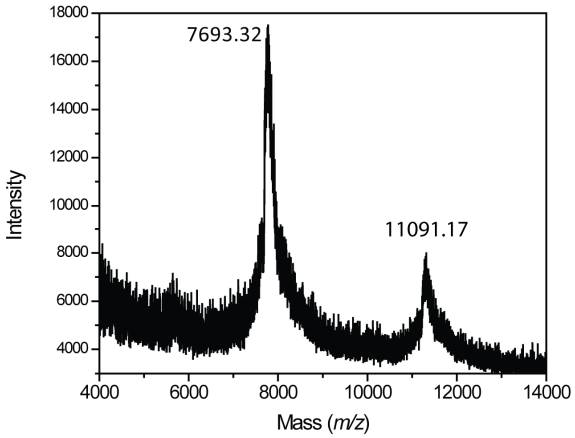

Figure A3.1: MALDI-TOF MS spectrum of the modified RNA calibrated relative to the +1 ion of an internal 25-mer DNA standard (m/z: 7693.32). Calculated mass = 11088.87; observed mass = 11091.17.

A3.5 – Photophysical Studies of Oligonucleotides

Steady state fluorescence experiments were carried out at 21°C in a 150 µL quartz fluorescence cell with a path length of 1.0 cm (Hellma GmbH & Co KG, Müllheim, Germany) on a Jobin Yvon Horiba FluoroMax-3 luminescence spectrometer with excitation and emission slit-widths of 8 nm. Anisotropy measurements were carried out at 21°C in a 150 µL quartz fluorescence cell with a path length of 1.0 cm (Hellma GmbH & Co KG, Müllheim, Germany) on a Jobin Yvon Horiba FluoroMax-4 luminescence spectrometer with excitation and emission slit-widths of 8 nm. RNA samples were hybridized by heating to 75 ºC for 5 min and subsequently allowed to cool to room temperature over 2 h prior to measurements. RNA samples were measured at 5×10^{-6} M concentration in 20 mM cacodylate buffer (pH 7.0, 100 mM NaCl, 0.5 mM EDTA).

For FRET binding experiments, labeled RRE was titrated into 10 µM Rev peptide in 20 mM cacodylate buffer (pH 7.0, 100 mM NaCl, 0.5 mM EDTA). The samples were excited at 280 nm, and emission intensities were observed at 350 nm and 445 nm. Fitting for K_D^{S2} values were conducted for three different sets of experiments to generate error bars. For displacement experiments, a saturated sample of labeled RRE and 10 µM Rev peptide was made. RSG peptide was titrated into the solution and emission intensity changes were recorded upon excitation at 280 nm. Emission spectra were normalized. Fitting for IC_{50}^{S3} values were conducted for three different sets of experiments to generate error bars.

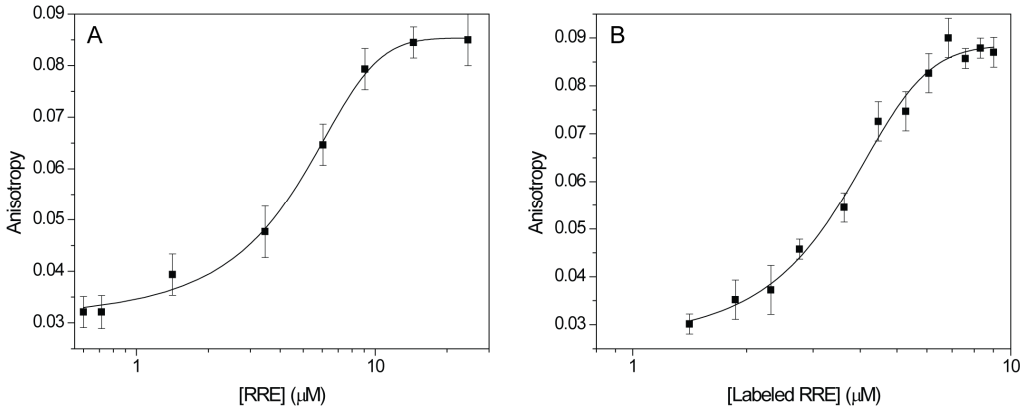

Figure A3.2: Anisotropy response of tryptophan (■) in Rev in the following experiments: (A) titration of the RRE into Rev; (B) titration of labeled RRE into Rev. Conditions: Rev (1.0×10^{-5} M), cacodylate buffer pH 7.0 (2.0×10^{-2} M), NaCl (1.0×10^{-1} M).

A3.6 – Thermal Denaturation Measurements

All hybridizations and UV melting experiments were carried out at 1×10^{-6} M concentration in 20 mM cacodylate buffer (pH 7.0, 100 mM NaCl, 0.5 mM EDTA), using a Beckman-Coulter DU® 640 spectrometer with a high performance

temperature controller and micro auto six holder. Samples were heated to 75 ºC for 5 min, cooled to room temperature over 2 h, and placed on ice for 30 min prior to measurements. Samples were placed in a stoppered 1.0 cm path length cell (Beckman-Coulter) and a background spectrum (buffer) was subtracted from each sample. Denaturation runs were performed between 25 and 90 ºC at a scan rate of 1.0 ºC min^{-1} with optical monitoring every ºC at 260 nm. Beckman-Coulter software (provided with T_m Analysis Accessory for DU® Series 600 Spectrometers) determined the melting temperatures utilizing the first derivative from the melting profile.

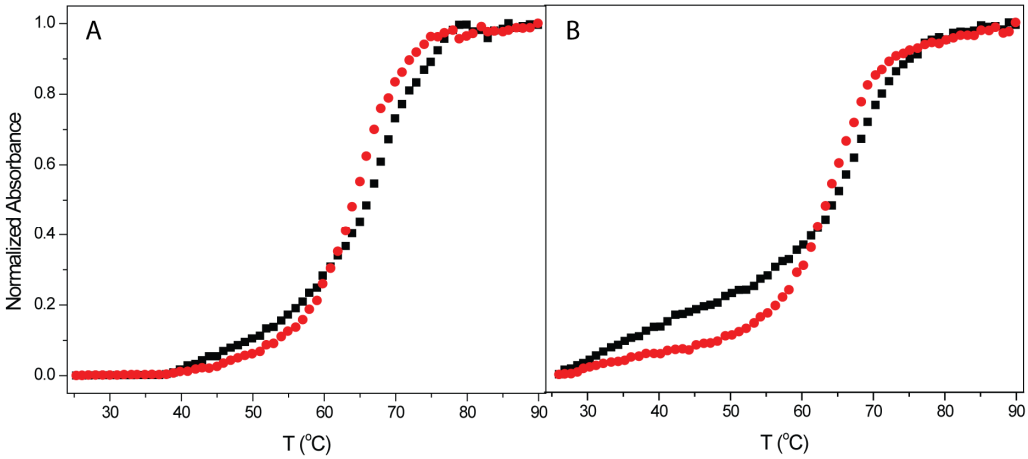

Figure A3.3: (A) Thermal denaturation curves of unlabeled RRE (■) and labeled RRE* (●). (B) Reverse thermal denaturation curves of unlabeled RRE (■) and labeled RRE* (●).

A3.7 – References

(A1) Lavabre, D.; Fery-Forgues, S. *J. Chem. Educ.*, **1999**, *76*, 1260–1264.

(A2) Lacourciere, K. A.; Stivers, J. T.; Marino, J. P. *Biochemistry* **2000**, *39*, 5630–5641.

(A3) Xie, Y.; Dix, A. V.; Tor, Y. *J. Am. Chem. Soc.* **2009**, *131*, 17605–17614.

Appendix 4: Supporting Information for Chapter 4

Supporting Information

- **A4.1** Synthetic Procedures and Experimental Data.
  - **Scheme A4.1.** Synthetic scheme for **3**.
- **A4.2** Crystal structure of **2**.
  - **Figure A4.1.** Crystal structure image of **2**.
  - **Table A4.1.** Crystal data and structure refinement for **2**.
- **A4.3** Oligonucleotide Synthesis and Purification.
- **A4.4** MALDI-TOF MS of Oligonucleotide **4**.
  - **Figure A4.2.** MALDI-TOF MS Spectrum of Oligonucleotide **4**.
- **A4.5** Photophysical Studies of Oligonucleotides.
- **A4.6** Thermal Denaturation Studies.
  - **Figure A4.3.** Oligonucleotides used for Thermal Denaturation Experiments.
  - **Figure A4.4.** Thermal Denaturation Plots of Duplexes.
- **Abbreviations Used.**
  - DMSO = dimethylsulfoxide
  - PAGE = polyacrylamide gel electrophoresis
  - DMTr = 4,4′-dimethoxytrityl chloride

A4.1 – Synthetic Procedures and Experimental Data

General Procedures

NMR spectra were recorded on a Varian Mercury 400 MHz spectrometer. Mass spectra were recorded at the UCSD Chemistry and Biochemistry Mass Spectrometry Facility, utilizing either a LCQDECA (Finnigan) ESI with a quadrapole ion trap or a MAT900XL (ThermoFinnigan) FAB double focusing mass spectrometer. UV-Vis spectra were recorded on either a Hewlett Packard 8452A or 8453 Diode Array Spectrometer.

Unless otherwise specified, materials obtained from commercial suppliers were used without further purification. 2-D-3,5-di-*O*-p-toluoyl-α-L-erythro-pentofuranosyl chloride was purchased from Berry & Associates, Inc. Anhydrous pyridine, dichloroethane and acetonitrile were obtained from Fluka. Anhydrous *N,N*-diisopropylethylamine and triethylamine were obtained from Acros. The unmodified oligonucleotides were purchased from Integrated DNA Technologies. Standard phosphoramidites and solutions necessary for solid phase RNA synthesis were purchased from Glen Research. Oligonucleotides were purified by gel electrophoresis and desalted on a Sep-Pak (Waters Corporation). Chemicals for preparing buffer solutions were purchased from Fisher Biotech (enzyme grade). Autoclaved water was used in all fluorescence titrations. NMR solvents were purchased from Cambridge Isotope Laboratories (Andover, MA).

Synthetic Schemes

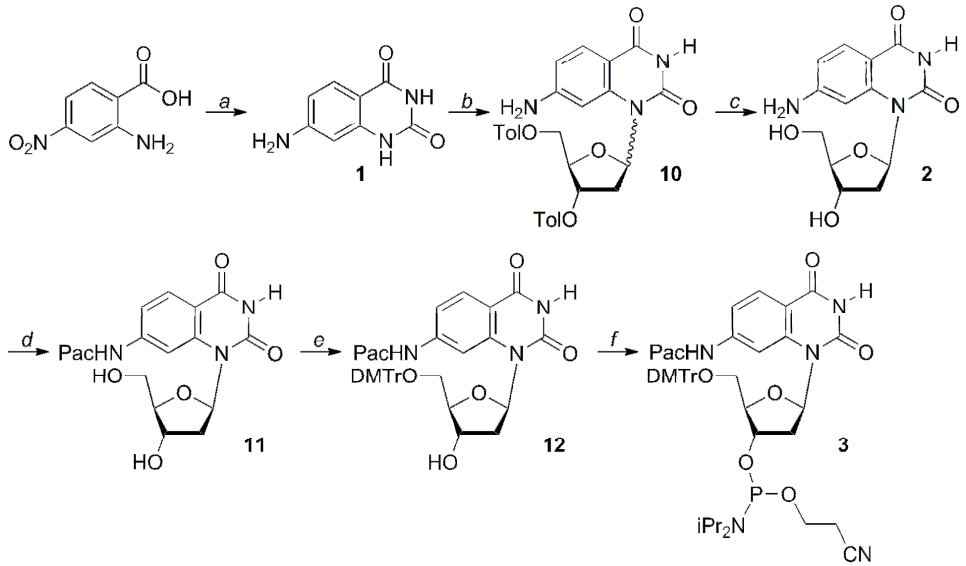

Scheme A4.1: Synthesis of **3**. (a) (i) Urea; (ii) $SnCl_2$, conc. HCl, 40%. (b) $(NH_4)_2SO_4$, *N,O*-bis(trimethylsilyl)acetamide, $CF_3SO_3Si(CH_3)_3$, 2-D-3,5-di-*O*-p-toluoyl-α-L-erythro-petofuranosyl chloride, CH_3CN, 80%. (c) conc. NH_4OH, 50%. (d) $(CH_3)_3SiCl$, phenoxyacetic anhydride, H_2O, conc. NH_4OH, pyridine, 75%. (e) DMTrCl, Et_3N, pyridine, 85%. (f) *i*Pr_2NEt, (*i*Pr_2N)P(Cl)O-CH_2CH_2CN, $ClCH_2CH_2Cl$, 65%.

7-Aminoquinazoline-2,4(1*H*,3*H*)-dione (1). Urea (10.0 g, 166.5 mmol) was mixed with 2-amino-4-nitrobenzoic acid (10.0 g, 54.9 mmol). The powder was heated to 200 ℃ for 4 h. The reaction was cooled to room temperature. Using a coarse frit, the solid was washed with water (250 mL), 5% sodium bicarbonate (200 mL), 10% sodium carbonate (400 mL), dilute sulfuric acid (250 mL), and boiling methanol (300 mL). The solid was stirred in boiling 50% acetic acid (800 mL) for 1 h. The remaining solid was filtered off and the solution was brought back to boiling. The solution was allowed to cool to room temperature and crystals were collected by filtration. The crystals were redissolved in boiling 50% acetic acid. Activated carbon was added to the solution and boiled for 10 min. The solution was filtered hot and allowed to crystallize. The clear yellow crystals, 7-nitroquinazoline-2,4(1*H*,3*H*)-dione, were used without further purification. A suspension of tin chloride (8.20 g, 43.2 mmol) in concentrated HCl (100 mL) was brought to boiling. 7-Nitroquinazoline-2,4(1*H*,3*H*)-dione (2.20 g, 10.6 mmol) was added, and the suspension was refluxed for 5 h. The boiling suspension was filtered with a coarse frit, and the solid was washed with water (500 mL). Product: white solid (3.9 g, 22 mmol, 40 % yield over two steps). ^{1}HNMR (400 MHz, DMSO-d_6): δ 10.88 (s, NH, 1H), 10.82 (s, NH, 1H), 7.62 (d, J = 8.4 Hz, 1H), 6.52 (d, J = 8.4 Hz, 1H), 6.39 (s, 1H); ^{13}CNMR (100 MHz, DMSO-d_6): δ 166.04, 152.84, 151.46, 143.30, 129.12, 111.93, 105.25, 98.90; ESI-MS calculated for $C_8H_7N_3O_3$ $[M+H]^+$ 178.06, found 178.15; m.p. > 300 ºC.

7-Aminoquinazoline-2,4(1*H*,3*H*)-dione deoxyribonucleoside (2). To a suspension of **1** (1.50 g, 8.47 mmol) and ammonium sulfate (0.56 g, 4.2 mmol) in anhydrous acetonitrile (100 mL), *N,O*-bis(trimethylsilyl)acetamide (10.5 mL, 42.3 mmol) was added dropwise under argon. The reaction was stirred at 25 ℃ for 30 min. 2-D-3,5-di-*O*-p-toluoyl-α-L-erythro-petofuranosyl chloride (3.29 g, 8.46 mmol) was added to the reaction over ice and under argon. TMSOTf (0.77 mL, 4.2 mmol) was dissolved in 1mL of anhydrous acetonitrile and added dropwise over ice. The reaction temperature was raised to room temperature and stirred for 4 h. The reaction was concentrated to an oil, and diluted with dichloromethane (100 mL). The solution was washed with saturated sodium bicarbonate and brine. The organic layer was dried over sodium sulfate. The solvent was removed under reduced pressure, and the crude product was isolated by flash chromatography (0.4-0.8% methanol in dichloromethane). Dioxane (30 mL) was added to **10** (2.00 g, 3.78 mmol) in a pressure tube. Ammonium hydroxide (30%, 70 mL) was added to the tube. The reaction was stirred at 80 ℃ for 24 h. The solvent was removed under reduced pressure, and the product was isolated by flash chromatography (10% methanol in ethyl acetate). Product: white solid (0.554 g, 1.89 mmol, 40 % over two steps). ^{1}HNMR (400 MHz, DMSO-d_6): δ 11.03 (s, NH, 1H), 7.62 (d, J = 8.4 Hz, 1H), 6.66 (m, 1H), 6.48 (t, J = 7.6 Hz, 1H), 6.42 (d, J_1 = 6.8 Hz, J_2 = 2.0 Hz, 1H), 6.12 (s, NH_2, 2H), 5.21 (d, J = 5.2 Hz, 1H), 4.83 (t, J = 5.2 Hz, 1H), 4.31 (m, 1H), 3.64 (m, 3H), 2.67 (m, 1H), 1.87 (m, 1H); ^{13}CNMR (100 MHz, DMSO-d_6): δ 161.80, 155.23, 151.16, 142.15, 129.82, 110.62, 105.16, 99.03, 87.14, 83.94, 70.70, 62.33, 36.59; ESI-MS calculated

for $C_{13}H_{15}N_3O_5$ $[M+H]^+$ 294.11 and $[M+Na]^+$ 316.09, found 293.82 and 316.00, respectively.

7-phenoxyacetylaminoquinazoline-2,4(1*H*,3*H*)-dione deoxyribonucleoside (11). To a suspension of **2** (0.50 g, 1.7 mmol) in anhydrous pyridine (16 mL), chloro trimethylsilane (0.52 mL, 4.1 mmol) was added dropwise under argon. The reaction was stirred at 25 ℃ for 1 h. Phenoxyacetic anhydride (0.63 g, 2.2 mmol) was added under argon. The reaction was stirred at 25 ℃ for 18 h. The reaction was cooled on ice, and cold water (10 mL) was added. The reaction was stirred at 0 ℃ for 15 min. Cold aqueous ammonium hydroxide (10 mL) was added, and the reaction was stirred at 0 ℃ for 15 min. The solvent was removed under reduced pressure, and the product was isolated by flash chromatography (2-5% methanol in dichloromethane). Product: white solid (0.547 g, 1.28 mmol, 75 %). ^{1}HNMR (400 MHz, DMSO-d_6): δ 11.51 (s, 1H), 10.39 (s, 1H), 8.104 (s, 1H), 7.94 (d, J = 8.4 Hz, 1H), 7.40 (d, J = 8.8 Hz, 1H), 7.31 (t, J = 7.2 Hz, 2H), 6.99 (m, 3H), 6.59 (t, J = 8.0 Hz, 1H), 5.24 (d, J = 5.2 Hz, 1H), 4.80 (m, 1H), 4.74 (s, 2H), 4.38 (m, 1H), 3.65 (m, 3H), 2.72 (m, 1H), 1.90 (m, 1H); ^{13}CNMR (100 MHz, DMSO-d_6): δ 167.21, 161.68, 158.97, 150.68, 143.34, 136.57, 128.00, 123.25, 113.83, 113.46, 107.52, 87.01, 84.98, 84.55, 72.72, 67.96, 65.02, 61.14, 37.22; ESI-MS calculated for $C_{21}H_{21}N_3O_7$ $[M+K]^+$ 466.10, found 466.04.

5′-Dimethoxytrityl-7*N*-phenoxyacetylaminoquinazoline-2,4(1*H*,3*H*)-dione deoxyriboribonucleoside (12). Anhydrous pyridine (7.5 mL), anhydrous triethylamine (237 µL, 1.7 mmol) and 4,4′-dimethoxytrityl chloride (0.58 g, 1.7 mmol) were added to **11** (0.50 g, 1.2 mmol) over argon. The reaction was stirred at room temperature for 16 hours and quenched with methanol (1.0 mL). The solvent was removed under reduced pressure, and the product was isolated by flash chromatography (1% triethylamine, 5% methanol, 94 % dichloromethane). Product: off-white solid (0.73 g, 0.96 mmol, 85 % yield). ^{1}HNMR (400 MHz, $CDCl_3$): δ 8.54 (s, 1H), 8.33 (s, 1H), 8.13 (d, J = 8.4 Hz, 1H), 7.42 (d, J = 8.4 Hz, 1H), 7.35–7.30 (m, 12H), 7.19–7.05 (m, 6H), 6.95 (d, J = 7.6 Hz, 1H), 6.84 (t, J = 8.0 Hz, 1H), 6.71 (dd, J_1 = 8.8 Hz, J_2 = 3.2 Hz, 2H), 4.74 (m, 1H), 4.41 (d, J = 14.8 Hz, 1H), 4.24 (d, J = 15.2 Hz, 1H), 4.11 (dd, J_1 = 7.2 Hz, J_2 = 6.8 Hz, 1H), 4.02 (m, 1H), 3.69 (s, 6H), 3.49 (q, J = 7.2 Hz, 1H), 3.42 (dd, J_1 = 5.6 Hz, J_2 = 4.4 Hz, 1H), 3.03 (d, J = 7.2 Hz, 1H); ^{13}CNMR (100 MHz, $CDCl_3$): δ 166.76, 161.29, 158.59, 158.56, 156.98, 150.34, 145.09, 142.80, 141.00, 136.26, 136.23, 130.42, 130.40, 129.82, 128.49, 127.93, 126.91, 122.84, 115.09, 115.05, 113.24, 112.94, 106.99, 86.50, 84.43, 84.00, 72.20, 67.45, 64.52, 60.64, 55.38, 55.36, 53.08, 46.03, 36.64, 29.92; ESI-MS calculated for $C_{42}H_{39}N_3O_9$ $[M+Na]^+$ 752.26, found 752.23.

3′-2-Cyanoethyldiisopropylphosphoramidite-7*N*-phenoxyacetylaminoquinazoline-2,4(1*H*, 3*H*)-dione deoxyribonucleoside (3). Anhydrous dichloroethane (2.0 mL) and *N,N*-diisopropylethylamine (0.28 mL, 1.6 mmol) were added to **12** (0.10 g, 0.14 mmol). The reaction was cooled on ice, and 2-cyanoethyl *N,N*-diisopropylchlorophosphoramidite (38 µL, 0.17 mmol) was added.

The reaction was stirred at room temperature for 18 h. The solvent was removed under reduced pressure, and the product was isolated by flash chromatography (1% triethylamine, 15–40% ethyl acetate in hexanes). Product: white foam (0.083 g, 0.088 mmol, 65 % yield). ^{1}HNMR (300 MHz, $CDCl_3$): δ 9.02 (b, 1H), 8.39 (s, 1H), 8.29 (d, *J* = 11.2 Hz, 1H), 8.19 (d, *J* = 8.4 Hz, 1H), 7.43–7.31 (m, 12H), 7.20–7.08 (m, 6H), 6.94 (d, *J* = 7.2 Hz, 1H), 6.89 (d, *J* = 7.2 Hz, 1H), 6.71 (m, 2H), 4.67 (m, 1H), 4.34 (m, 1H), 4.17 (m, 1H), 3.79 (m, 1H), 3.67 (s, 6H), 3.54 (m, 2H), 3.57 (m, 1H), 2.97 (m, 2H), 2.58 (t, *J* = 6.0 Hz, 2H), 2.38 (m, 1H), 1.16−1.00 (m, 12H); ^{31}PNMR (162 MHz, $CDCl_3$): δ 150.13, 149.91; ESI-MS calculated for $C_{51}H_{56}N_5O_{10}P$ $[M+Na]^+$ 952.37 and $[M+K]^+$ 968.34, found 952.27 and 968.22, respectively.

A4.2 – Crystal Structure of 2

A colorless needle 0.15 × 0.02 × 0.02 mm in size was mounted on a Cryoloop with Paratone oil. Data were collected in a nitrogen gas stream at 100(2) K using phi and omega scans. Crystal-to-detector distance was 60 mm and exposure time was 10 seconds per frame using a scan width of 0.5°. Data collection was 98.1% complete to 67.00° in θ. A total of 6001 reflections were collected covering the indices, –7<=*h*<=8, –9<=*k*<=12, –22<=*l*<=21. 2269 reflections were found to be symmetry independent, with a R_{int} of 0.0245. Indexing and unit cell refinement indicated a primitive, orthorhombic lattice. The space group was found to be P2(1)2(1)2(1). The data were integrated using the Bruker SMART software program and scaled using the SADABS software program. Solution by direct methods (SIR-2004) produced a complete heavy-atom phasing model consistent with the proposed structure. All non-hydrogen atoms were refined anisotropically by full-matrix least-squares (SHELXL-97). All hydrogen atoms were placed using a riding model. Their positions were constrained relative to their parent atom using the appropriate HFIX command in SHELXL-97. The absolute stereochemistry was unambiguously determined to be *R*, *S*, and *R* at C9, C11, and C12 respectively.

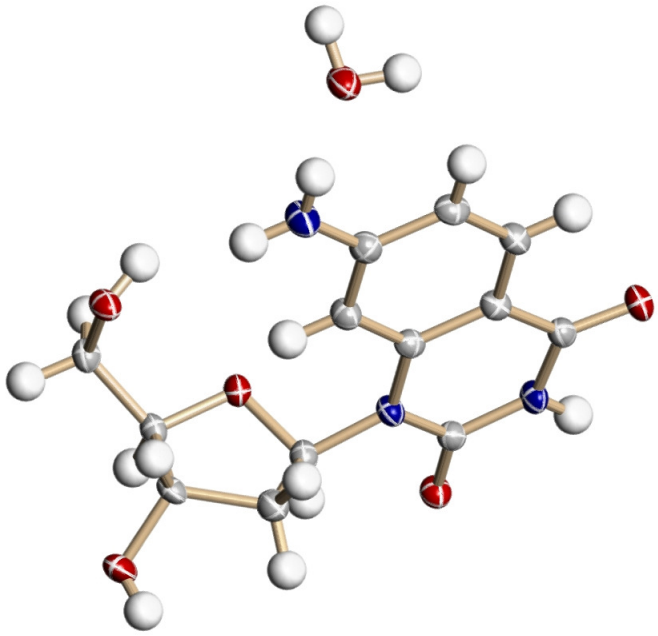

Figure A4.1: Crystal structure image of **2**.

Table A4.1: Crystal data and structure refinement for **2**.

X-ray ID	tor41	
Sample/notebook ID	ADDTop	
Empirical formula	C13 H17 N3 O6	
Formula weight	311.30	
Temperature	100(2) K	
Wavelength	1.54178 Å	
Crystal system	Orthorhombic	
Space group	P2(1)2(1)2(1)	
Unit cell dimensions	a = 6.837(2) Å	α= 90°.
	b = 10.470(5) Å	β= 90°.
	c = 18.506(6) Å	γ = 90°.
Volume	1324.7(9) $Å^3$	
Z	4	
Density (calculated)	1.561 Mg/m^3	
Absorption coefficient	1.064 mm^{-1}	
F(000)	656	
Crystal size	0.15 x 0.02 x 0.02 mm^3	
Crystal color/habit	colorless needle	
Theta range for data collection	4.78 to 68.50°.	
Index ranges	–7<=h<=8, –9<=k<=12, –22<=l<=21	
Reflections collected	6001	
Independent reflections	2269 [R(int) = 0.0245]	
Completeness to theta = 67.00°	98.1 %	
Absorption correction	Semi-empirical from equivalents	
Max. and min. transmission	0.9790 and 0.8567	
Refinement method	Full-matrix least-squares on F^2	
Data / restraints / parameters	2269 / 0 / 208	
Goodness-of-fit on F^2	1.059	
Final R indices [I>2sigma(I)]	R1 = 0.0358, wR2 = 0.0882	
R indices (all data)	R1 = 0.0409, wR2 = 0.0910	
Absolute structure parameter	-0.2(2)	
Extinction coefficient	0.0033(5)	
Largest diff. peak and hole	0.256 and -0.204 $e.Å^{-3}$	

A4.3 – Oligonucleotide Synthesis and Purification

The unmodified oligonucleotide was purchased from Thermo Scientific. The modified oligonucleotide was synthesized on a Biosearch Cyclone Plus DNA synthesizer using a 1 μmole scale 500 Å CPG column. Phosphoramidite **3** was site specifically incorporated into the oligonucleotide by trityl-off synthesis of the base oligonucleotide, followed by manual coupling of phosphoramidite **3**. Typically, the modified phosphoramidite was dissolved in 100 μL of anhydrous acetonitrile to give a

final concentration of 0.1M. The phosphoramidite solution was pushed into the CPG column via syringe and then 200 µL of 0.45M 1*H*-tetrazole was pushed into the other end of the column via syringe. Coupling reactions, performed twice, were allowed to proceed for 5 minutes (99% coupling efficiency) and were subsequently followed by standard oxidation and capping steps. The rest of the oligonucleotide was synthesized via the standard trityl-off procedure. Upon completion of the oligonucleotide synthesis, the CPG column was treated with 3 mL of 30% aqueous ammonium hydroxide for 2 h at room temperature, mixing via syringe every 1 h. The resulting solution was removed and the CPG column was treated with 1 mL of 30% aqueous ammonium hydroxide at room temperature for 15 min, mixing via syringe every 5 min. The resulting aqueous ammonium hydroxide solutions were consolidated and incubated at 55 ºC for 96 h. The aqueous ammonium hydroxide solution was freeze-dried. The DNA was purified by 20% polyacrylamide gel electrophoresis. The oligonucleotide was visualized by UV shadowing; bands were excised from the gel and extracted with 0.5M sodium acetate buffer (pH 7.0) overnight. The resulting solution was filtered (Bio Rad poly-prep chromatography column) and desalted using a Sep-Pak cartridge (Waters Corporation, MA). The following 260 nm extinction coefficients were used to determine the concentration of oligonucleotides: dG = 11,700, dC = 7,300, dA = 15,400, dU = 10,100, and **2** = 6,000.

A4.4 –MALDI-TOF MS of Oligonucleotide

The MW of the modified oligonucleotide was determined via MALDI-TOF MS. 1 µL of a ~200 µM stock solution of the synthesized DNA was combined with 1 µL of 100 mM ammonium citrate buffer (PE Biosystems), 1 µL of a 75 µM DNA standard (5′-GCTGAATACATAAGACG-3′) and 4 µL of saturated 3-hydroxypicolinic acid. The samples were desalted with an ionexchange resin (PE Biosystems) and spotted onto a gold-coated plate where they were air dried. The resulting spectra were calibrated relative to the +1 and +2 ions of the internal DNA standard (m/z: 5225.79 and 2613.40). MALDI-TOF MS calc. for the +1 ion: 4081.65; found 4079.84.

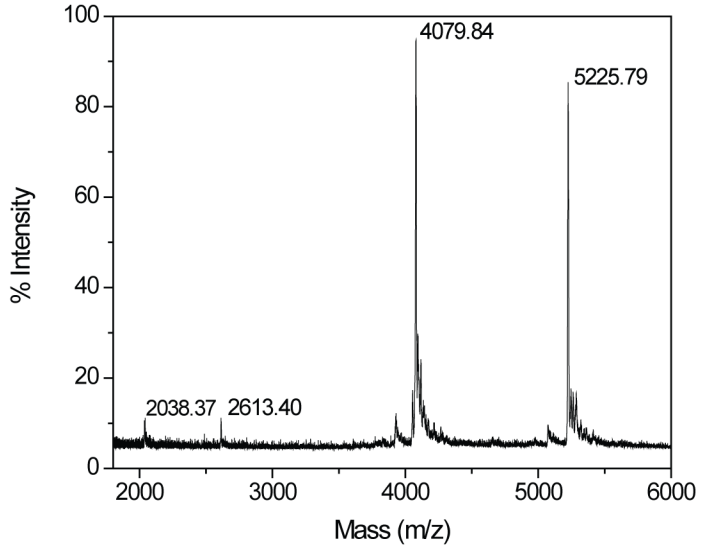

Figure A4.2: MALDI-TOF MS spectrum of the modified DNA calibrated relative to the +1 and +2 ions of an internal 17-mer DNA standard (m/z: 5225.79 and 2613.40). Calculated mass = 4081.65; observed mass = 4079.84.

A4.5 – Photophysical Studies of Oligonucleotides

Steady state fluorescence experiments were carried out at 21°C in a 150 µL quartz fluorescence cell with a path length of 1.0 cm (Hellma GmbH & Co KG, Müllheim, Germany) on a Jobin Yvon Horiba FluoroMax-3 luminescence spectrometer with excitation and emission slit-widths of 8 nm. DNA samples were hybridized by heating to 90 ºC for 5 min and subsequently allowed to cool to room temperature over 2 h prior to measurements. DNA samples were measured at 5 × 10^{-6} M concentration in 20 mM sodium phosphate buffer (pH 7.0, 500 mM NaCl).

A4.6 – Thermal Denaturation Measurements

All hybridizations and UV melting experiments were carried out at 5 × 10^{-6} M concentration in 20 mM sodium phosphate buffer (pH 7.0, 500 mM NaCl), using a Beckman-Coulter DU® 640 spectrometer with a high performance temperature controller and micro auto six holder. Samples were heated to 90 ºC for 5 min, cooled to room temperature over 2 h, and placed on ice for 30 min prior to measurements. Samples were placed in a stoppered 1.0-cm path length cell (Beckman-Coulter) and a background spectrum (buffer) was subtracted from each sample. Denaturation runs were performed between 25 and 90 ºC at a scan rate of 1.0 ºC min^{-1} with optical monitoring every ºC at 260 nm. Beckman-Coulter software (provided with T_m Analysis Accessory for DU® Series 600 Spectrometers) determined the melting temperatures utilizing the first derivative from the melting profile.

4 5'-GCG ATG **2** GTA GCG-3'
5 3'-CGC TAC **G** CAT CGC-5'
6 3'-CGC TAC **T** CAT CGC-5'
7 3'-CGC TAC **A** CAT CGC-5'
8 3'-CGC TAC **C** CAT CGC-5'
9 5'-GCG ATG **A** GTA GCG-3'

Figure A4.3: Oligonucleotides used in thermal denaturation experiments.

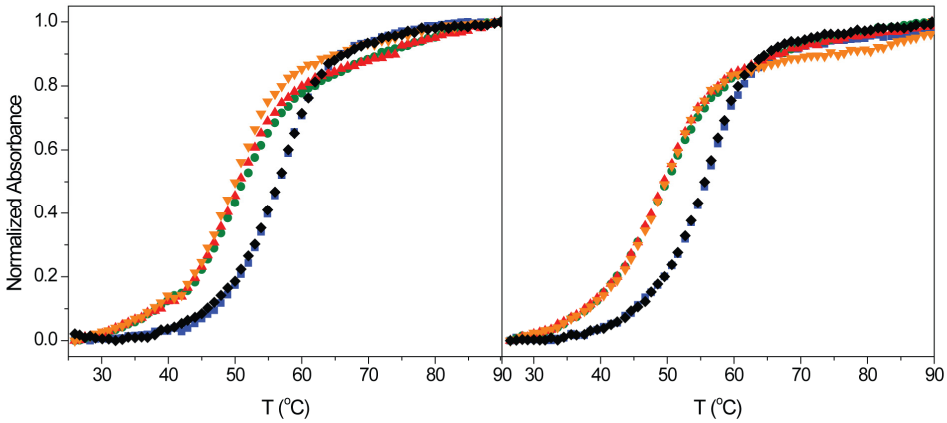

Figure A4.4: (A) Thermal denaturation curves of **4 • 5** (green), **4 • 6** (orange), **4 •7** (blue), **4 • 8** (red), and **6 • 9** (black). (B) Reverse thermal denaturation curves of **4 • 5** (green), **4 • 6** (orange), **4 •7** (blue), **4 • 8** (red), and **6 • 9** (black).

Appendix 5: Supporting Information for Chapter 5

Supporting Information

- **A5.1** Crystal structure of **4** and **8**.
  - **Figure A5.1.** Crystal structure image of **4**.
  - **Table A5.1.** Crystal data and structure refinement for **4**.
  - **Figure A5.2.** Crystal structure image of **8**.
  - **Table A5.2.** Crystal data and structure refinement for **8.**
- **A5.2** Oligonucleotide Synthesis and Purification.
- **A5.3** MALDI-TOF MS of Oligonucleotide **4**.
  - **Figure A5.3.** MALDI-TOF MS Spectra of Oligonucleotide **4**.
- **A5.4** Thermal Denaturation Studies.
  - **Figure A5.4.** Thermal Denaturation Plots of Duplexes.
- **Abbreviations Used.**
  - DMSO = dimethylsulfoxide
  - PAGE = polyacrylamide gel electrophoresis
  - DMTr = 4,4′-dimethoxytrityl chloride

A5.1 – Crystal Structure of 4 and 8.

Crystals were mounted on a Cryoloop with Paratone oil. Data were collected in a nitrogen gas stream at 100(2) K using phi and omega scans. The data were integrated using the Bruker SMART software program and scaled using the SADABS software program. Solution by direct methods (SIR-2004) produced a complete heavy-atom phasing model consistent with the proposed structure. All non-hydrogen atoms were refined anisotropically by full-matrix least-squares (SHELXL-97). All hydrogen atoms were placed using a riding model. Their positions were constrained relative to their parent atom using the appropriate HFIX command in SHELXL-97.

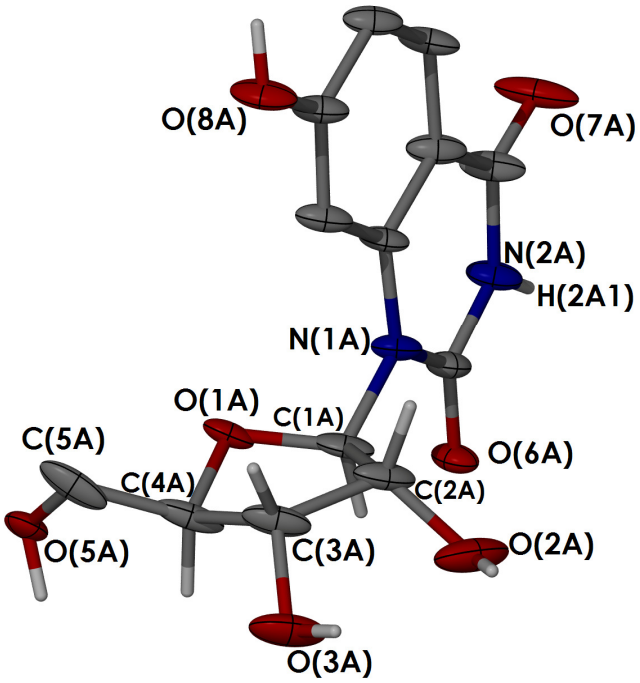

Figure A5.1: Crystal structure image of **4**.

Table A5.1: Crystal data and structure refinement for **4**.

Identification code	TOR29	
Empirical formula	C13 H14 N2 O7	
Formula weight	310.26	
Temperature	123(2) K	
Wavelength	0.71073 Å	
Crystal system	Monoclinic	
Space group	P21	
Unit cell dimensions	a = 13.942 Å	α= 90°.
	b = 7.104 Å	β= 107.73°.
	c = 15.018 Å	γ = 90°.
Volume	1416.8 $Å^3$	
Z	4	
Density (calculated)	1.455 Mg/m^3	
Absorption coefficient	0.120 mm^{-1}	
F(000)	648	
Crystal size	0.21 x 0.20 x 0.10 mm^3	
Theta range for data collection	2.39 to 25.00°.	
Index ranges	–16<=h<=16, –8<=k<=8, –17<=l<=17	
Reflections collected	10149	
Independent reflections	2711 [R(int) = 0.0288]	
Completeness to theta = 25.00°	99.4 %	
Absorption correction	Empirical	
Max. and min. transmission	0.9881 and 0.9752	
Refinement method	Full-matrix least-squares on F^2	
Data / restraints / parameters	2711 / 1 / 409	
Goodness-of-fit on F^2	1.080	
Final R indices [I>2sigma(I)]	R1 = 0.0682, wR2 = 0.1703	
R indices (all data)	R1 = 0.0714, wR2 = 0.1728	
Absolute structure parameter	0(10)	
Largest diff. peak and hole	0.551 and -0.422 $e.Å^{-3}$	

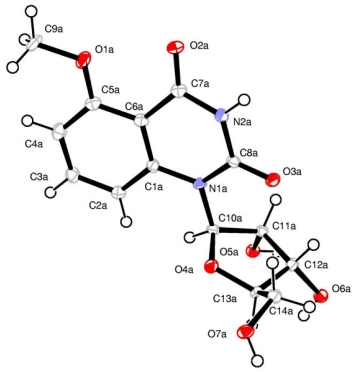

Figure A5.2: Crystal structure image of **8**.

Table A5.2: Crystal data and structure refinement for **8**.

X-ray ID	tor47	
Sample/notebook ID	OMeRiboFu	
Empirical formula	C28 H34 N4 O15	
Formula weight	666.59	
Temperature	100(2) K	
Wavelength	1.54178 Å	
Crystal system	Orthorhombic	
Space group	P2(1)2(1)2(1)	
Unit cell dimensions	a = 7.4705(2) Å	α= 90°.
	b = 17.9489(5) Å	β= 90°.
	c = 20.7876(6) Å	γ = 90°.
Volume	2787.35(13) $Å^3$	
Z	4	
Density (calculated)	1.588 Mg/m^3	
Absorption coefficient	1.118 mm^{-1}	
F(000)	1400	
Crystal size	0.15 x 0.06 x 0.04 mm^3	
Crystal color/habit	colorless needle	
Theta range for data collection	3.25 to 68.18°.	
Index ranges	–7<=h<=8, –19<=k<=21, –24<=l<=24	
Reflections collected	11714	
Independent reflections	4921 [R(int) = 0.0471]	
Completeness to theta = 67.00°	98.8 %	
Absorption correction	Semi-empirical from equivalents	
Max. and min. transmission	0.9566 and 0.8502	
Refinement method	Full-matrix least-squares on F^2	
Data / restraints / parameters	4921 / 0 / 438	
Goodness-of-fit on F^2	1.018	
Final R indices [I>2sigma(I)]	R1 = 0.0402, wR2 = 0.0860	
R indices (all data)	R1 = 0.0523, wR2 = 0.0915	
Absolute structure parameter	–0.02(17)	
Largest diff. peak and hole	0.196 and -0.211 $e.Å^{-3}$	

A5.2 – Oligonucleotide Synthesis and Purification

The unmodified oligonucleotide was purchased from Thermo Scientific. The modified oligonucleotide was synthesized on a Biosearch Cyclone Plus DNA synthesizer using a 1 µmole scale 500 Å CPG column. Phosphoramidite of **9** was site specifically incorporated into the oligonucleotide by trityl-off synthesis of the base oligonucleotide, followed by manual coupling of phosphoramidite of **9**. Typically, the modified phosphoramidite was dissolved in 100 µL of anhydrous acetonitrile to give a final concentration of 0.1M. The phosphoramidite solution was pushed into the CPG

column via syringe and then 200 µL of 0.45M 1*H*-tetrazole was pushed into the other end of the column via syringe. Coupling reactions, performed twice, were allowed to proceed for 5 minutes (98% coupling efficiency) and were subsequently followed by standard oxidation and capping steps. The rest of the oligonucleotide was synthesized via the standard trityl-off procedure. Upon completion of the oligonucleotide synthesis, the CPG column was treated with 3 mL of 30% aqueous ammonium hydroxide for 2 h at room temperature, mixing via syringe every 1 h. The resulting solution was removed and the CPG column was treated with 1 mL of 30% aqueous ammonium hydroxide at room temperature for 15 min, mixing via syringe every 5 min. The resulting aqueous ammonium hydroxide solutions were consolidated and incubated at 55 ºC for 96 h. The aqueous ammonium hydroxide solution was freeze-dried. The DNA was purified by 20% polyacrylamide gel electrophoresis. The oligonucleotide was visualized by UV shadowing; bands were excised from the gel and extracted with 0.5M sodium acetate buffer (pH 7.0) overnight. The resulting solution was filtered (Bio Rad poly-prep chromatography column) and desalted using a Sep-Pak cartridge (Waters Corporation, MA). The following 260 nm extinction coefficients were used to determine the concentration of oligonucleotides.

A5.3 –MALDI-TOF MS of Oligonucleotide

The MW of the modified oligonucleotide was determined via MALDI-TOF MS. 1 µL of a ~200 µM stock solution of the synthesized RNA was combined with 1 µL of 100 mM ammonium citrate buffer (PE Biosystems), 1 µL of a 75 µM DNA standard (5′-GCTGAATACATAAGACG-3′) and 4 µL of saturated 3-hydroxypicolinic acid. The samples were desalted with an ionexchange resin (PE Biosystems) and spotted onto a gold-coated plate where they were air dried. The resulting spectra were calibrated relative to the +1 ion of the internal DNA standard (m/z: 5225.79). MALDI-TOF MS calc. for the +1 ion: 4261.63; found 4079.84.

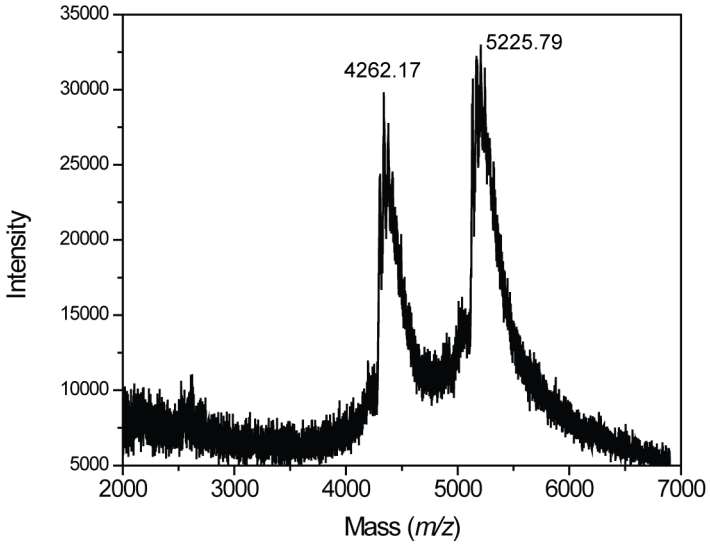

Figure A5.3: MALDI-TOF MS spectrum of the modified RNA calibrated relative to the +1 ion of an internal 17-mer DNA standard (m/z: 5225.79). Calculated mass = 4261.63; observed mass = 4262.17.

A5.4 – Thermal Denaturation Measurements

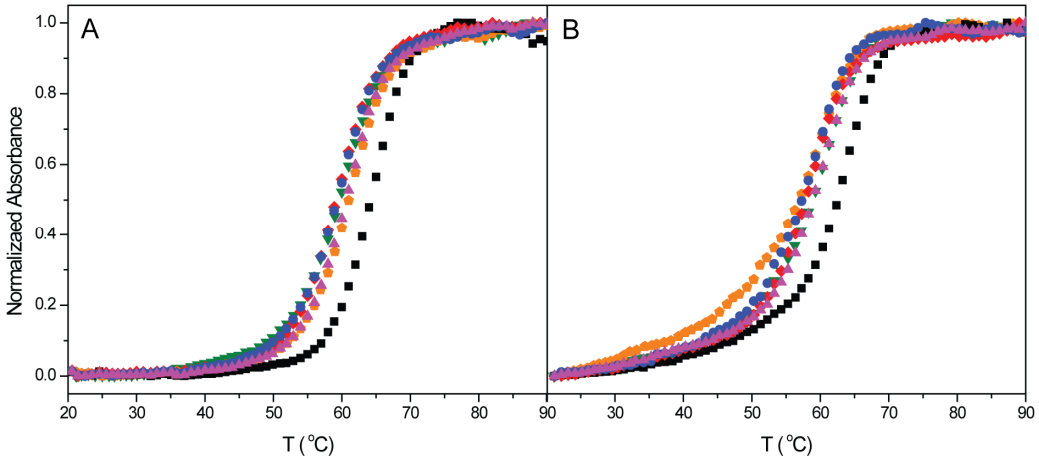

Figure A5.4: (A) Thermal denaturation curves and (B) reverse thermal denaturation curves of **15•16** (black), **15•17** (blue), **15•18** (orange), **15•19** (red), **15•20** (green), **15•21** (yellow), and **15•22** (purple).